DAVID W. TAYLOR NAVAL SHIP RESEARCH AND DEVELOPMENT CENTER

Bethesda, Md. 20084

EXPERIMENTAL EVALUATION OF THE PERFORMANCE OF THE TAP-1 SUPERCAVITATING HYDROFOIL MODEL AT 80 KNOTS

by

Henry Holling, Elwyn Baker and Edwin Rood

SHIP PERFORMANCE DEPARTMENT
RESEARCH AND DEVELOPMENT REPORT

July 1975

Report 4681

MAJOR DTNSRDC ORGANIZATIONAL COMPONENTS

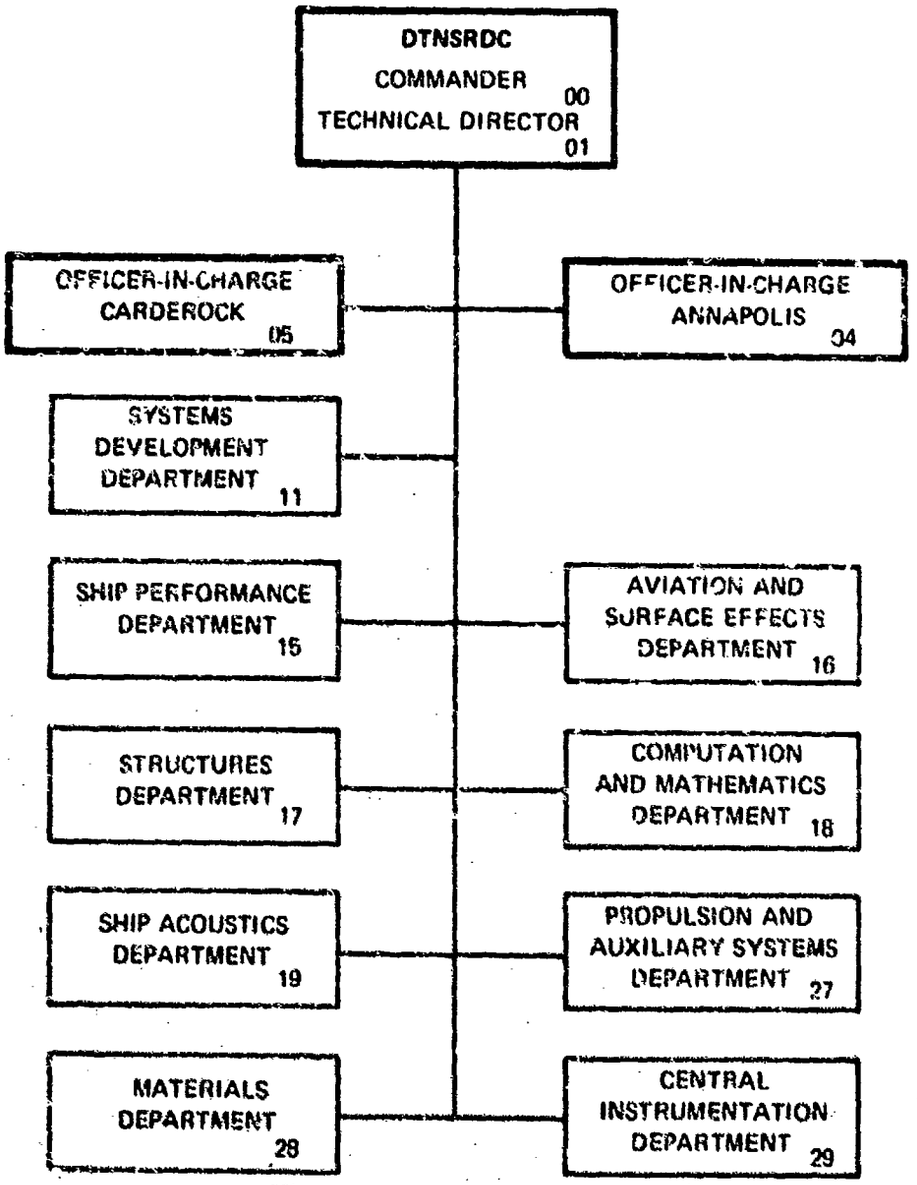

DTNSRDC ISSUES THREE TYPES OF REPORTS

(1) DTNSRDC REPORTS, A FORMAL SERIES PUBLISHING INFORMATION OF PERMANENT TECHNICAL VALUE, DESIGNATED BY A SERIAL REPORT NUMBER.

(2) DEPARTMENTAL REPORTS, A SEMIFORMAL SERIES, RECORDING INFORMATION OF A PRELIMINARY OR TEMPORARY NATURE, OR OF LIMITED INTEREST OR SIGNIFICANCE, CARRYING A DEPARTMENTAL ALPHANUMERIC IDENTIFICATION.

(3) TECHNICAL MEMORANDA, AN INFORMAL SERIES, USUALLY INTERNAL WORKING PAPERS OR DIRECT REPORTS TO SPONSORS, NUMBERED AS TM SERIES REPORTS; NOT FOR GENERAL DISTRIBUTION.

UNCLASSIFIED

SECURITY CLASSIFICATION OF THIS PAGE (When Data Entered)

REPORT DOCUMENTATION PAGE

READ INSTRUCTIONS BEFORE COMPLETING FORM

1. REPORT NUMBER: 4681 (14) DTNSRDC-4681
2. GOVT ACCESSION NO.
3. RECIPIENT'S CATALOG NUMBER

4. TITLE (and Subtitle): (6) EXPERIMENTAL EVALUATION OF THE PERFORMANCE OF THE TAP-1 SUPERCAVITATING HYDROFOIL MODEL AT 80 KNOTS
5. TYPE OF REPORT & PERIOD COVERED: (9) Final rept.
6. PERFORMING ORG. REPORT NUMBER

7. AUTHOR(s): (10) Henry/Holling, Elwyn/Baker, Edwin/Rood
8. CONTRACT OR GRANT NUMBER(s)

9. PERFORMING ORGANIZATION NAME AND ADDRESS
David W. Taylor Naval Ship Research and Development Center
Bethesda, Maryland 20084

10. PROGRAM ELEMENT, PROJECT, TASK AREA & WORK UNIT NUMBERS
(See reverse side)

11. CONTROLLING OFFICE NAME AND ADDRESS
Naval Material Command
Washington, D.C. 20362

(12) 92p.

12. REPORT DATE: (11) Jul[redacted]75
13. NUMBER OF PAGES: 92

14. MONITORING AGENCY NAME & ADDRESS (if different from Controlling Office)

15. SECURITY CLASS. (of this report): UNCLASSIFIED
15a. DECLASSIFICATION/DOWNGRADING SCHEDULE

16. DISTRIBUTION STATEMENT (of this Report)

APPROVED FOR PUBLIC RELEASE: DISTRIBUTION UNLIMITED

17. DISTRIBUTION STATEMENT (of the abstract entered in Block 20, if different from Report)

18. SUPPLEMENTARY NOTES

19. KEY WORDS (Continue on reverse side if necessary and identify by block number)

supercavitating hydrofoil
high speed
ventilation
spray wedges

20. ABSTRACT (Continue on reverse side if necessary and identify by block number)

Experimental results are presented for a model of the TAP-1 supercavitating hydrofoil system in its high-speed mode of operation. To realistically simulate the ventilation air demand of the prototype craft, the model was examined at full water speeds using cavitation number scaling. The experiments were conducted in the NASA Aircraft Landing Dynamics Facility, an outdoor free-running towing carriage. Unsteady loads in lift, drag, side

(Continued on reverse side)

DD FORM 1 JAN 73 1473 EDITION OF 1 NOV 65 IS OBSOLETE
S/N 0102-014-6601

UNCLASSIFIED

SECURITY CLASSIFICATION OF THIS PAGE (When Data Entered)

387 682

(Block 10)

Program Element 62754N
Task Area ZF43421001
Work Unit 1-1520-001

(Block 20 continued)

force, and pitching moment were continuously recorded on analog tape and were then time averaged. The foil (chordline) angle of attack ranged from 2.4 to 10.4 degrees at 80 knots. The strut side force in yaw developed by the foil system and by the basic parabolic strut only was recorded for speeds of 50, 70, and 80 knots.

The maximum strut sideslip angle at 80 knots before sudden side ventilation was 3 1/4 degrees. The cavity air demand increased linearly with water speed (or Froude number) over the range of speeds examined. While the strut spray wedges were absolutely necessary to achieve full ventilation, their presence added only about 10 percent to the drag. The spanwise twist of the model was successful in maintaining the cavity out to the wing tips at low angles of attack, but failed to recreate the sectional loading. The maximum lift-to-drag ratio measured in full cavity flow was 6.6. No vortex shedding or leading edge vibrations were observed.

TABLE OF CONTENTS

LIST OF FIGURES

LIST OF FIGURES (cont.)

LIST OF FIGURES (con't)

LIST OF FIGURES (con't)

LIST OF TABLES

NOTATION

A	Foil plan area	L^2
C_D	Drag coefficient of strut and foil assembly, $C_D = D/[(1/2)\rho V^2 A]$	
C_L	Lift coefficient of strut and foil assembly, $C_L = L/[(1/2)\rho V^2 A]$	
C_M	Pitching moment coefficient of strut and foil assembly, $C_M = M/[(1/2)\rho V^2 Ac]$	
C_y	Side force coefficient, $C_y = Y/[(1/2)\rho V^2 A]$	
$C_{y\beta}$	Side force slope, $C_{y\beta} = \partial C_y/\partial\beta$	
$C_{y_{max}}$	Maximum side force coefficient before ventilation, $C_{y_{max}} = C_y$ at $\beta=\beta_{vent}$	
c	Mean foil chord (average of centerline and tip chord)	L
D	Drag of strut and foil assembly	MLT^{-2}
d	Foil depth from water surface	L
d/c	Depth-to-Chord ratio of foil	
g	Acceleration due to gravity	LT^{-2}
L	Lift of strut and foil assembly	MLT^{-2}
ℓ	Strut chord length	L
L/D	Lift-to-Drag ratio of strut and foil assembly	
M	Pitching moment of strut and foil assembly; positive for pitch up of leading edge	ML^1T^{-2}
P_c	Measured cavity pressure	$ML^{-1}T^{-2}$

P_v	Facility water vapor pressure	$ML^{-1}T^{-2}$
P_∞	Free stream static pressure	$ML^{-1}T^{-2}$
t	Maximum strut section thickness	L
t/ℓ	Strut thickness-to-chord ratio	
Q_v	Volumetric airflow rate	L^3T^{-1}
V	Velocity	LT^{-1}
Y	Side force	MLT^{-2}
α	Foil incidence angle (angle between the untwisted section chordline and the horizontal)	
β	Yaw angle of strut	
β_{vent}	Yaw angle of strut at ventilation inception	
ρ	Water density	ML^{-3}
σ	Cavitation number based on vapor pressure of water, $\sigma = [p_\infty - p_v]/[(1/2)\rho V^2]$	
σ_c	Cavitation number based on cavity pressure of foil, $\sigma_c = [p_\infty - p_c]/[(1/2)\rho V^2]$	
σ_{vent}	Vapor cavitation number at ventilation inception	

ABSTRACT

Experimental results are presented for a model of the TAP-1 supercavitating hydrofoil system in its high-speed mode of operation. To realistically simulate the ventilation air demand of the prototype craft, the model was examined at full water speeds using cavitation number scaling. The experiments were conducted in the NASA Aircraft Landing Dynamics Facility, an outdoor free-running towing carriage. Unsteady loads in lift, drag, side force, and pitching moment were continuously recorded on analog tape and were then time averaged. The foil (chordline) angle of attack ranged from 2.4 to 10.4 degrees at 80 knots. The strut side force in yaw developed by the foil system and by the basic parabolic strut only was recorded for speeds of 50, 70, and 80 knots.

The maximum strut sideslip angle at 80 knots before sudden side ventilation was 3 1/4 degrees. The cavity air demand increased linearly with water speed (or Froude number) over the range of speeds examined. While the strut spray wedges were absolutely necessary to achieve full ventilation, their presence added only about 10 percent to the drag. The spanwise twist of the model was successful in maintaining the cavity out to the wing tips at low angles of attack, but failed to recreate the sectional loading. The maximum lift-to-drag ratio measured in full cavity flow was 6.6. No vortex shedding or leading edge vibrations were observed.

ADMINISTRATIVE INFORMATION

This project was supported by the Naval Material Command under the High Speed Struts and Foils Direct Laboratory Funded Project,

Program Element 62754N, Task Area ZF 43421001, Work Unit Number 1-1520-001.

INTRODUCTION

In September 1972, the Naval Material Command tasked the Naval Ship Research and Development Center (NSRDC) to develop a data base and design criteria for high-speed struts and foils in general, and the Developmental Fast Hydrofoil (DFH) in particular. The procedures selected to accomplish the primary objectives have been to:

1. Select a strut/foil configuration for 80-knot operation,

2. Determine the hydrodynamic loads for a strut/foil system associated with the various operational modes,

3. Determine methods of controlling these hydrodynamic forces, and

4. Determine the impact of hydrodynamic loading on structures and materials.

As part of this program, hydrofoil cruise (80 knots) experiments were conducted at the NASA Aircraft Landing Dynamics Facility, Langley Field, Virginia. This facility has a carriage capable of towing models in a tank at high speeds (up to 150 knots). The foil used for the experiments was of a supercavitating design. The foil section designated as "TAP-1" was designed using Wu's[1] nonlinear analysis of a two-dimensional supercavitating hydrofoil section. The design

[1]Wu, T. Y., "A Free Streamline Theory for Two-Dimensional Fully Cavitating Hydrofoils," Journal Mat. Phys. Vol. 35, No. 3, 1956 pp. 236-265

phase of the program is described in Reference 2. Two parabolic struts of different t/ℓ ratios (thickness-to-chord) were examined with the foil. Attachable spanwise wedges were designed to be fitted on the trailing edge of each strut at various positions above the foil in order to ensure an air path behind the strut for ventilation of the foil. The purpose of these experiments was to measure quantities on the foil which could not adequately be measured or represented in a simulated speed facility (lift, drag, pitch moment, and cavity pressure). Also, the two struts were examined to determine the effects of speed, submergence depth, foil flow (superventilated or wetted), and trailing edge wedges.

DESCRIPTION OF THE MODEL

DESIGN OF STRUT AND FOIL

Photographs of the TAP-1 strut/foil model are shown in Figure 1, and the foil geometry is described in Table 1. The channel shown on the back of the strut was not used for these experiments. The TAP-1 foil section design was based on Wu's 1955 analytical method for designing supercavitating section shapes. The method is adopted for low cavitation numbers and involves a nonlinear computation of cambered two-term section properties in an infinite stream medium. The foil design was based on a section having a nearly circular arc camber and a forward center of pressure. Spanwise sections were twisted about the trailing edge. The section twist axis is defined in Figure 2, and the degree of twist of each section is defined relative to the "untwisted" section at 40 percent of the span from the strut center plane. Two-dimensional section design criteria for the foil are:

[2]Dobay, G. F. and E. S. Baker, "Special Problems in the Design of Supercavitating Hydrofoils," AIAA Paper No. 74-309 presented at the AIAA/SNAME Advanced Marine Vehicles Conference, February 1974

α = 4.616 degrees	Chord inclination angle
C_L = 0.136	Lift coefficient
L/D = 12.95	Lift-to-drag ratio
C_M = 0.049	Moment coefficient about LE

The hydrofoil was designed to be fully cavitating over the upper surface at cavitation numbers below σ_v = 0.05.

TABLE 1 - TAP-1 DESIGN CHARACTERISTICS

Area	75 sq. inches
Aspect Ratio	2.4
Centerline Chord Length	7.5 inches
Tip Chord	3.75 inches
Span	13.33 inches
Annex Percentage of Wetted Chord	33 percent
Design Cavitation Number	$\leq$ 0.05

Each section for the TAP-1 foil has a 33-percent (of wetted chord) annex. The function of the annex (shown in Figure 3) was to increase the wetted lifting area during takeoff and to increase the foil's structural integrity.

The struts used in the TAP-1 configuration had a parabolic section chosen to avoid any cavitation formation ahead of the strut base at zero or small yaw angles. The section of both struts was uniform over their span with a 6-inch chord and 12- and 18-percent thickness-to-chord ratio (t/ℓ = 0.12 and 0.18). The struts had a span of 15.6 inches and a sweepback angle of 12 degrees.

Figure 1 - Photographs of TAP-1 Strut-Foil Model

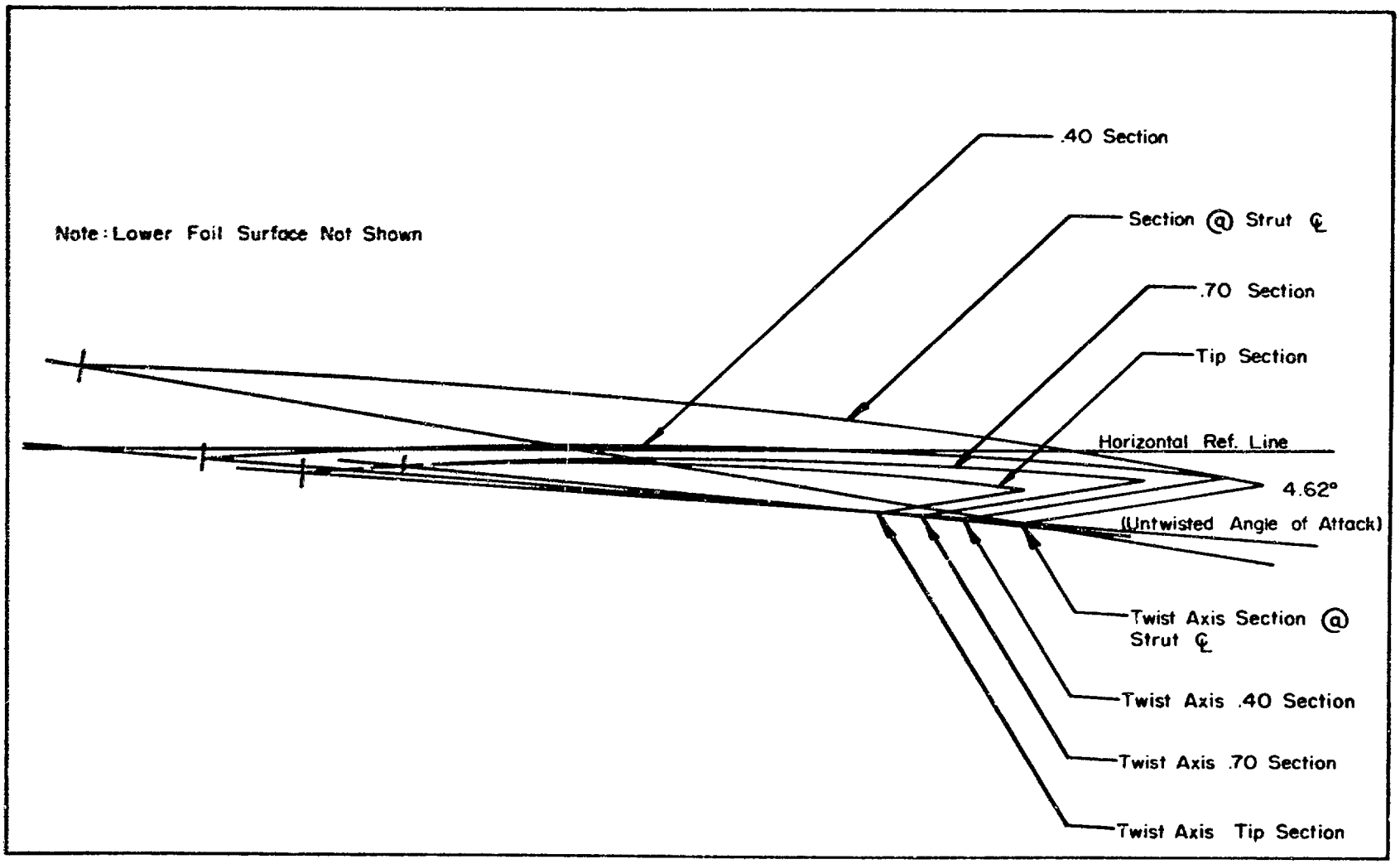

Figure 2 - Definition of TAP-1 Hydrofoil Twist Axis

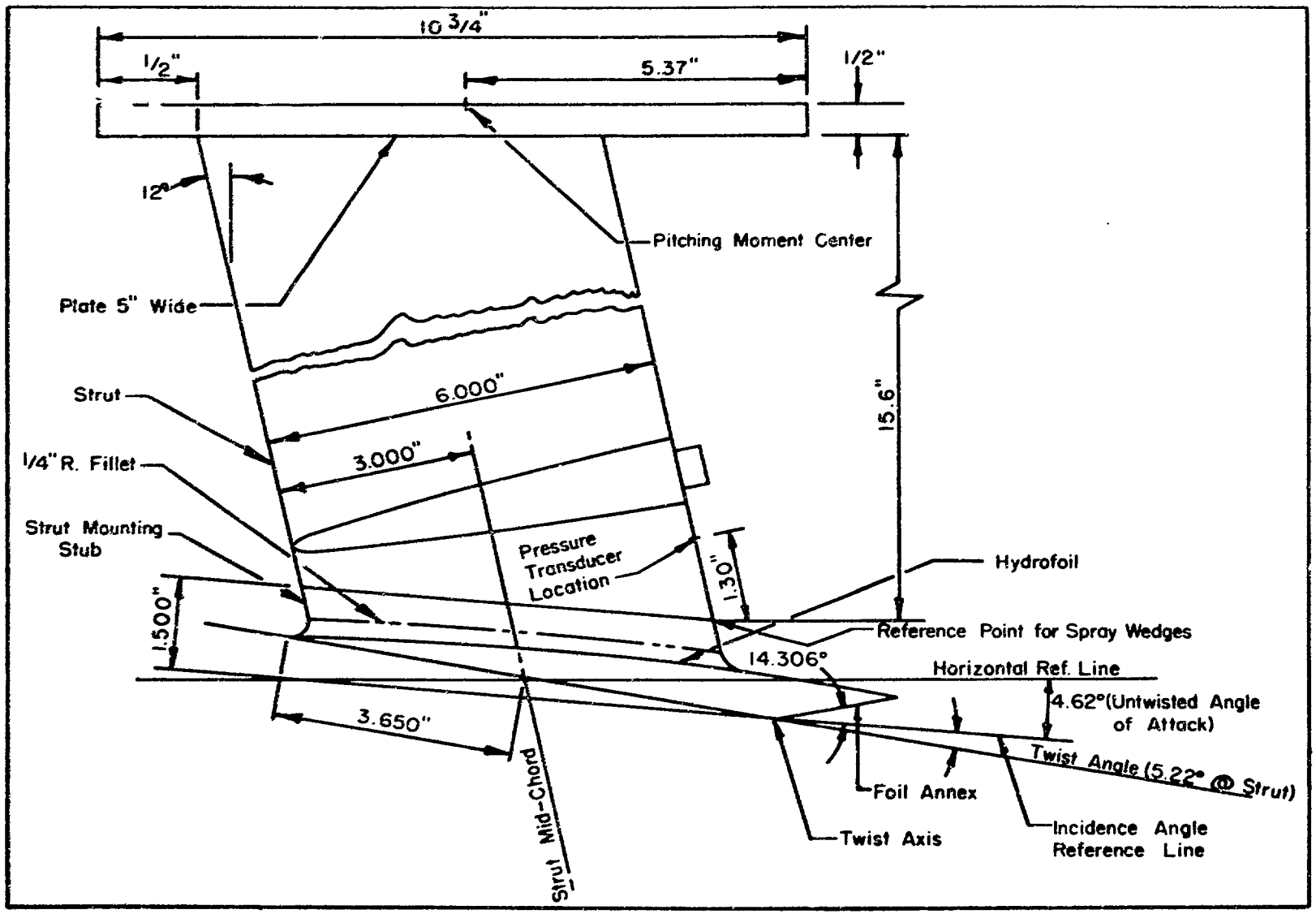

Figure 3 - Section View of TAP-1 Foil and Strut

DESIGN OF VENTILATION DOORS

As is well known, the air supply required to maintain a ventilated condition of a hydrofoil increases quite drastically with physical water speed (see for example, Reference 3), and the mere presence of a blunt-based, parabolic strut above the foil is generally not enough to insure a cavitation number in the ventilation range (say $\sigma < 0.01$) at high actual water speeds. For example, Johnson's high-speed tests failed to fully ventilate an aspect ratio three hydrofoil at a depth-to-chord ratio of 0.8 (Reference 4), or a base-ventilated hydrofoil (Reference 5) even though both had parabolic struts. High-speed tests of the BuShips parent hydrofoil[6] also showed a failure to ventilate below a depth-to-chord ratio of 0.5 above a certain speed (approximately 60 knots). This problem was addressed by Wadlin[7] near the end of the NASA high-speed hydrofoil program, who solved it by adding vent wings to the side of the strut to enlarge the strut cavity. The cavitation number could not be brought to zero by this method but could be reduced to the range $0.01 < \sigma < 0.03$, which would correspond to a ventilated flow.

---

[3]Schiebe, F. R. and J. M. Wetzel, "Ventilated Cavities on Submerged Three-Dimensional Hydrofoils," University of Minnesota, St. Anthony Falls Hydraulic Laboratory, Technical Paper No. 36, Series B, Dec 1961

[4]Christopher, K. W. and V. E. Johnson, Jr., "Experimental Investigation of Two Low-Drag Supercavitating Hydrofoils at Speeds up to 200 Feet per Second," NASA TN D-436, Aug 1960

[5]Johnson, V. E., Jr. and T. A. Rasnick, "Investigation of a High-Speed Hydrofoil with Parabolic Thickness Distribution," NASA TN D-119, Nov 1959

[6]Spangler, P. K., "Performance and Correlation Studies of the BuShips Parent Hydrofoil at Speeds from 40 to 75 Knots," NSRDC Report 2353 Dec 1966

[7]Wadlin, K. L., "Ventilated Flows with Hydrofoils," Presented at the 12th General Meeting of American Towing Tank Conference, University of California, Aug 1959

Subsequently, vent wings were included in the design of the Boeing annex foil. Although they doubled the strut drag, most of the cavity pressure measurements reported at high water speed (80 knots) included their use.[8] The design used appears from the report to be effective down to a depth-to-chord ratio of 2.2.

For the ventilated TAP-1 foil, it was intended that the foil be tested both with an 18- and a 12-percent thick strut, which presumably would provide two different air ventilation rates from the atmosphere. Since vent wings provide no structural strength while adding to the strut drag, it was hoped that the 18-percent strut could ventilate the foil through its own thickness, without ventilation wedges, and thereby provide more structural strength and power transmission space while supporting the larger cavity.

The vent wings designed for both the 18- and 12-percent parabolic struts were meant to be identical. However, as finally developed, there is a difference in the section shape of the wedges. Each has an untapered length of 4 inches joined to a tapered length of 5 inches, for a total wedge length of 9 inches (see Figure 4). Both are mounted at the rear (base) of the strut in such a way that their vertical elevation along the strut base above the foil can be adjusted in 2-inch increments. At their lowest position, the tapered section was down below the static waterline and the straight section above it.

The purpose of the wedges was both to enlarge the strut cavity and to deflect the spray sheet, which rises up the sides of the strut away from the strut cavity opening. The opening angle of the

[8]Gornstein, R. J. and T. A. Holgate, "Depth Effects on Hydrodynamic Characteristics of the Annex Foil at 80 Knots," Boeing Company Report Number D2-82505-1, Feb 1965

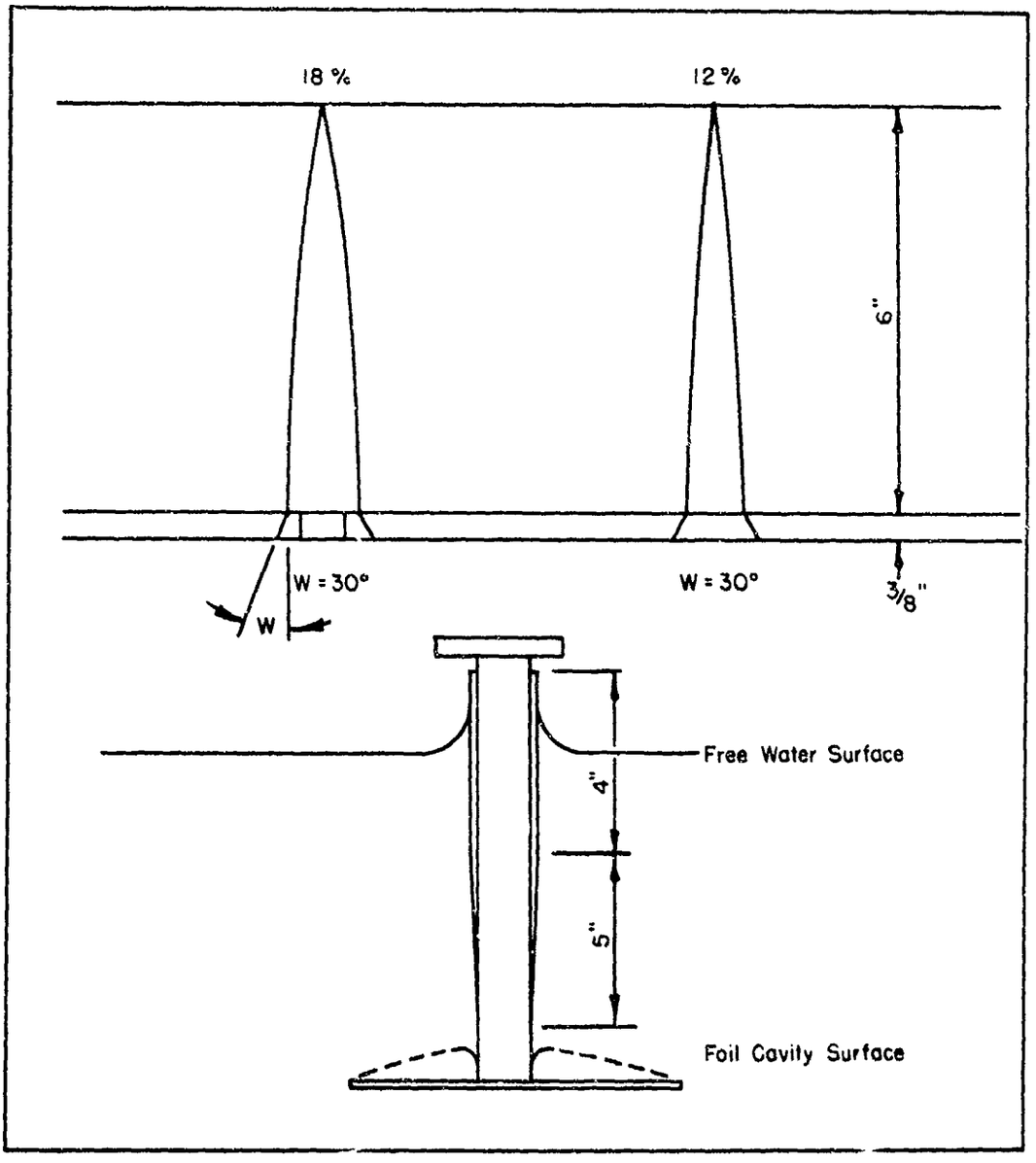

Figure 4 - Strut Spray Wedges and Boundary Layer

wedges was 30 degrees. The wedge opening angle tapers to zero at the bottom for the 18-percent strut, while for the 12-percent strut, the wedge angle remains constant at 30 degrees and the chord of the wedge is constant, but the thickness of the wedge base is reduced by filing it flat, tapering down to zero thickness at the bottom near the foil. The chord of each wedge is 3/8 inch. Prior to the main set of experiments, a series of runs was made to determine the minimum submergence position, and hence drag, of the spray wedges in order to consistently ventilate the hydrofoil to $\sigma_c \leq 0.01$. For both strut cases, this position was found to be 2 1/2 inches up from the top of the foil, a position which was used for the remainder of the program with each strut. In this position it appeared that their sole function was to deflect the strut spray sheet away from the cavity opening, and the added drag due to their presence was minor.

It might be noted here that since the initial acceleration of the test carriage used is approximately 4 to 5 g's, there should not be any problem in establishing an initially ventilated cavity, since water can only fill in the cavity with a maximum acceleration of 1 g. This is contrary to ordinary towing basin practice where, with an initial towing carriage acceleration of 0.5 g, supercavitating hydrofoils consistently refuse to ventilate at a depth-to-chord ratio of 1.0 unless special techniques are used to trigger the initially ventilated condition.[9] This might explain the discrepancy in data between Spangler's report of high-speed towing tests of the BuShips parent foil[6] and the indoor towing test of the exact same foil[10] where, for identical towing speeds, depth of submersion and angle of attack, the foil ventilated at a depth-to-chord ratio of 1.5 during the outdoor test and at a depth-to-chord ratio of 0.5 during the indoor tests.

[9]McGehee, J. R. and V. E. Johnson, Jr., "Hydrodynamic Characteristics of Two Low-Drag Supercavitating Hydrofoils," NASA Memo 5-9-59L, Jun 1959

[10]Dobay, G. F., "Performance Characteristics of the BuShips Parent Foil," NSRDC Report 2084, Aug 1965

DESCRIPTION OF THE EXPERIMENTS

EXPERIMENTAL APPARATUS

The present experiments were conducted on the small (30-ton) carriage at the NASA Aircraft Landing Dynamics Facility. The carriage is propelled by a waterjet that impinges on a reversing bucket fixed to the rear of the carriage. The carriage is accelerated at 4 to 5 g's over the first 400 feet or less of each experimental run, then decelerates while coasting through the test section and is brought to a stop by an arresting gear. Because of the large accelerations inherent in its operation, personnel do not ride the carriage.

The towing tank is rectangular in cross section, and is 2200 feet long, 8 feet wide, and has a maximum water depth of 5 feet. For these experiments the water depth was set at 32 inches. This was the maximum depth which would allow the foil to be completely raised from the water. The tank was cleaned and filled with fresh water prior to the experiments. Since the facility is outdoors, chlorine was added periodically to control algae and other growths in the water.

The supporting strut was attached to the dynamometer shown in Figure 5 as specified in DTMB Drawing Number E-1156. Eight NSRDC differential reluctance modular force gages were used for measuring lift, drag, and side force. Three 500-pound gages were used for measuring drag, three 500-pound gages were used for side force, and two 1000-pound gages were used for measuring lift. Pitching moment was computed from the lift gages. The supporting strut was mounted directly to the lift gages. The dynamometer allows pitch adjustments of $\pm$13 degrees and yaw adjustments of $\pm$10 degrees. The lift gages were attached under the mounting table which was adjustable in pitch. Lift was therefore measured along an axis normal to the pitch table.

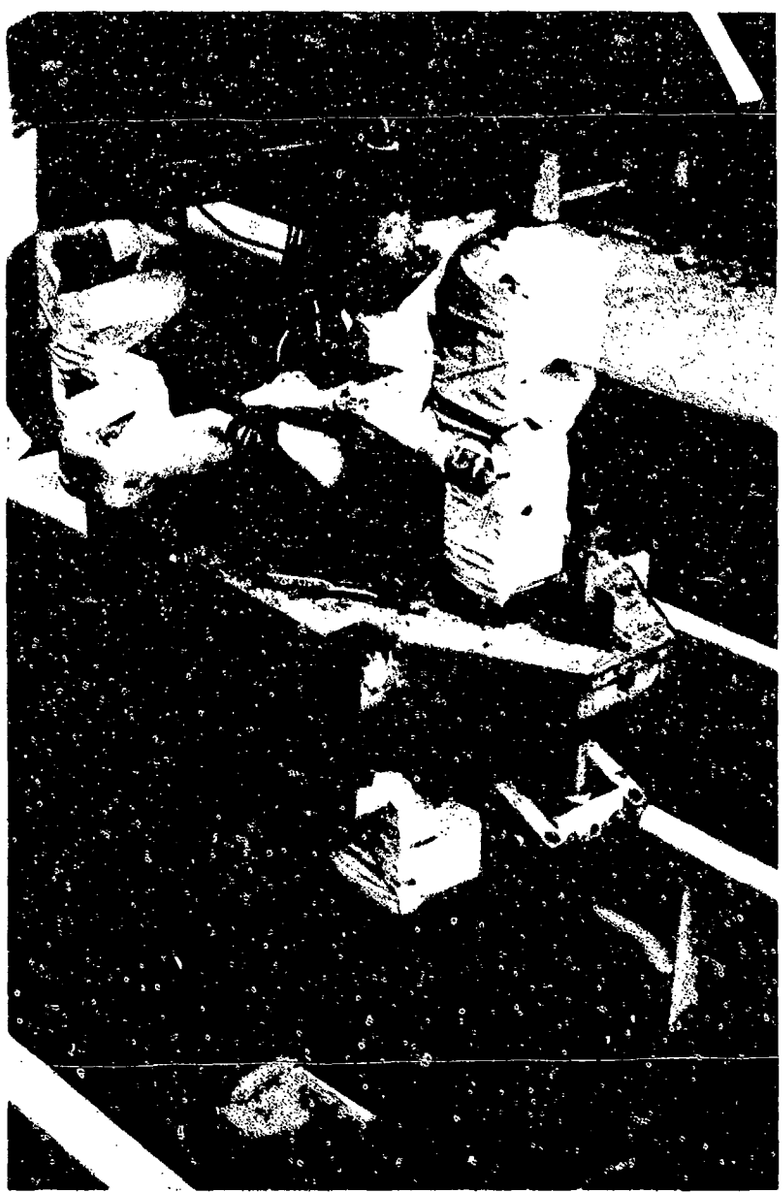

Figure 5 - Dynamometer Used for TAP-1 High-Speed Experiments

Pressure gages were mounted flush with the suction side of each wing of the foil and at the base of each of the interchangeable struts. The location of all gages is shown in Figures 3 and 6. The pressure gages were built at NSRDC in accordance with NSRDC Drawing No. E-307601 and have a range of -14 to +50 psi gage. The gage internal pressure was close to atmospheric. The recorded pressures for these experiments were referenced to the static pressure at the experimental water depth.

EXPERIMENTAL PROCEDURE

Each of the two support struts of different thickness-to-chord ratios (0.12 and 0.18) were used at times during these experiments. Because each strut had adjustable wedges attached to its trailing edge, several initial runs were made with each strut without the wedges and with the wedges at various distances above the foil. Figure 3 locates the point on the foil to which wedge location is referenced. From these runs, an optimum location was determined which gave realistic ventilation and drag characteristics. This optimum wedge location was used during the remainder of the experimental program except for the side force studies where most runs were made without the wedges.

Model experiments were conducted over a speed range of 40 to 90 knots at various depth-to-chord ratios, incidence angles, trailing edge wedge positions, and with various yaw angles for the strut side force studies. A complete outline of the conditions set before each run is given in Tables 2 and 3. The incidence angles were chosen to match those of the parent foil high-speed experiments described in Reference 6.

The model depth which was set and checked before each run was referenced to a point on the leading edge of the untwisted (40 percent wing span) foil section. Incidence angle is defined as the geometric

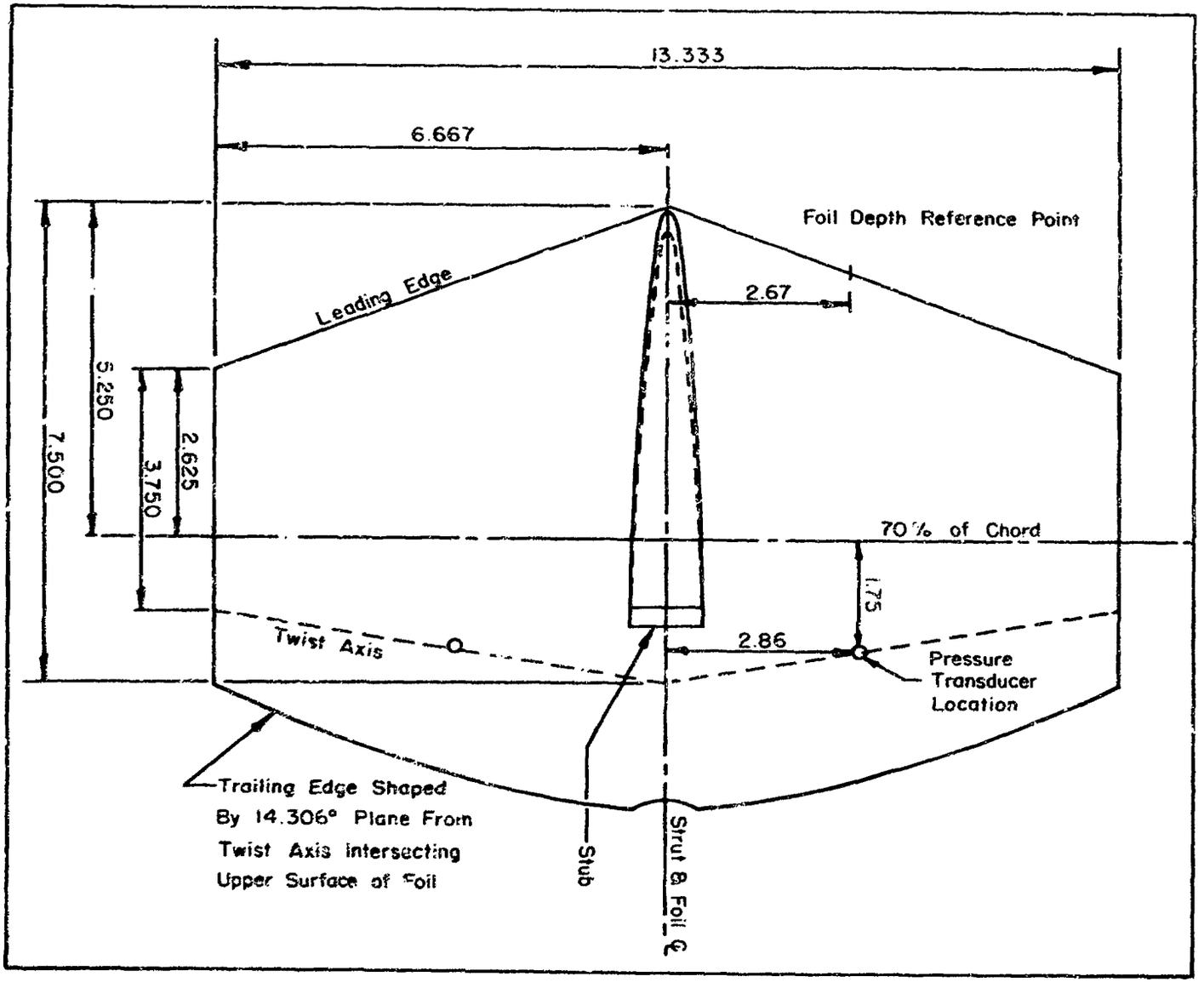

Figure 6 - Plan View of TAP-1 Foil

TABLE 2 - FOIL EXPERIMENTAL CONDITIONS AND OPERATIONAL CHARACTERISTICS

V Knots	τ deg	β deg	d/c	Wedge Position in.	Strut t/l	Lift lb	Drag lb	Mass X Acceleration	C_L	C_D	L/D	C_M
80	2.44	0	1.0	4	.18	663	111	41	.072	.012	5.97	.035
80	3.44	0	1.0	4	.18	1126	168	51	.122	.018	6.70	.040
80	4.44	0	1.0	4	.18	1058	172	54	.115	.019	6.15	.033
80	4.90	0	1.0	4	.18	848	---	--	.092	---	----	.027
80	5.44	0	1.0	4	.18	966	199	65	.105	.022	4.85	.030
80	6.44	0	1.0	4	.18	1154	252	60	.126	.027	4.58	.035
80	7.44	0	1.0	4	.18	1306	292	50	.142	.032	4.47	.039
80	8.44	0	1.0	4	.18	1442	342	45	.157	.037	4.21	.042
80	9.44	0	1.0	4	.18	1575	381	51	.171	.041	4.13	.046
80	10.44	0	1.0	4	.18	1673	445	51	.182	.048	3.76	.050
80	8.44	0	1.0	0	.18	1437	429	67	.156	.047	3.35	
80	8.44	0	1.0	2	.18	1447	364	62	.157	.040	3.96	
80	8.44	0	1.0	4	.18	1442	342	45	.157	.037	4.21	
40	8.44	0	1.0	-	.18	372	83	8	.162	.036	4.48	
50	8.44	0	1.0	-	.18	627	---	--	.174	---	----	
60	8.44	0	1.0	-	.18	881	---	--	.170	---	----	
70	8.44	0	1.0	-	.18	1217	275	30	.173	.039	4.43	
80	8.44	0	1.0	-	.18	1636	377	43	.178	.041	4.34	
50	8.44	0	1.0	0	.18	567	178	16	.158	.050	3.18	
70	8.44	0	1.0	0	.18	1108	329	45	.157	.047	3.37	
80	8.44	0	1.0	0	.18	1437	429	67	.156	.047	3.35	
85	8.44	0	1.0	0	.18	1644	471	50	.158	.045	3.49	
90	8.44	0	1.0	0	.18	1827	---	--	.157	---	----	
80	7.44	0	.25	4	.18	1438	253	53	.156	.028	5.68	
80	7.44	0	.50	4	.18	1361	251	49	.148	.027	5.42	
80	7.44	0	.75	4	.18	1338	257	52	.145	.028	5.21	

TABLE 2 (Continued)

V Knots	α deg	β deg	d/c	Wedge Position in.	Strut t/l	Lift lb	Drag lb	Mass X Acceleration	C_L	C_D	L/D	C_M
80	2.44	0	.5	4	.18	1022	130	46	.111	.014	7.86	
80	3.44	0	.5	4	.18	1252	143	48	.136	.016	8.76	
80	5.44	0	.5	4	.18	1006	158	40	.109	.017	6.37	
80	7.44	0	.5	4	.18	1361	251	49	.148	.027	5.42	
80	9.44	0	.5	4	.18	1621	346	46	.176	.038	4.68	
80	4.44	0	1.0	4	.12	907	139	54	.099	.015	6.53	.032
80	4.70	0	1.0	4	.12	927	140	48	.101	.015	6.62	.033
80	4.90	0	1.0	4	.12	866	162	65	.094	.018	5.35	.032
80	5.44	0	1.0	4	.12	963	194	57	.105	.021	4.96	.035
80	8.44	0	1.0	4	.12	1428	324	57	.155	.035	4.41	.048
80	8.44	0	1.0	2	.12	1438	362	66	.156	.039	3.97	
80	8.44	0	1.0	4	.12	1428	324	57	.155	.035	4.41	
80	8.44	0	1.0	6	.12	1435	306	57	.156	.033	4.70	
80	8.44	0	1.0	8	.12	1636	347	53	.178	.038	4.71	
40	8.44	0	1.0	-	.12	457	102	13	.199	.044	4.48	
50	8.44	0	1.0	-	.12	639	133	14	.178	.037	4.80	
60	8.44	0	1.0	-	.12	927	209	44	.179	.040	4.44	
70	8.44	0	1.0	-	.12	1262	281	46	.179	.040	4.49	
80	8.44	0	1.0	-	.12	1627	355	60	.177	.039	4.58	
90	8.44	0	1.0	-	.12	2039	431	76	.175	.037	4.73	
80	5.44	0	1.0	-	.12	1112	191	49	.121	.021	5.86	
80	4.90	0	1.0	-	.12	1068	173	56	.116	.019	6.17	
80	5.44	0	.5	4	.12	1198	177	48	.130	.019	6.77	
80	4.90	0	.5	4	.12	1060	151	50	.115	.016	7.02	

TABLE 2 (Continued)

V Knots	α deg	β deg	d/c	Wedge Position in.	Strut t/l	σ_{strut}	σ_{wing}
40	8.44	0	1.0	-	.18	.0294	.0150
50	8.44	0	1.0	-	.18	.0415	.0236
60	8.44	0	1.0	-	.18	.0475	.0435
70	8.44	0	1.0	-	.18	.0500	.0380
80	8.44	0	1.0	-	.18	.0485	.0422
50	8.44	0	1.0	0	.18	.0120	.0460
70	8.44	0	1.0	0	.18	.0065	.0004
80	8.44	0	1.0	0	.18	.0064	.0001
90	8.44	0	1.0	0	.18	.0065	.0004
80	8.44	0	1.0	0	.18	.0064	.00007
80	8.44	0	1.0	2	.18	.0065	.0009
80	8.44	0	1.0	4	.18	.0074	.00168
40	8.44	0	1.0	-	.12	.0627	.0620
50	8.44	0	1.0	-	.12	.0637	.0618
60	8.44	0	1.0	-	.12	.0640	.0607
70	8.44	0	1.0	-	.12	.0607	.0573
80	8.44	0	1.0	-	.12	.0550	.0517
90	8.44	0	1.0	-	.12	.0515	.0485

TABLE 3 - STRUT SIDEFORCE EXPERIMENTAL CONDITIONS

V Knots	α deg	β deg	d/c	Wedge Position in.	Strut t/l
80	7.44	1.0	1.0	-	.18
80	7.44	2.0	1.0	-	.18
80	7.44	3.0	1.0	-	.18
80	7.44	4.0	1.0	-	.18
80	7.44	0.5	1.0	-	.18
80	7.44	1.0	1.0	-	.18
80	7.44	2.0	1.0	-	.18
80	7.44	3.0	1.0	-	.18
80	7.44	3.5	1.0	-	.18
80	7.44	5.0	1.0	-	.18
70	7.44	3.5	1.0	-	.18
70	7.44	4.5	1.0	-	.18
70	7.44	5.0	1.0	-	.18
70	7.44	5.5	1.0	-	.18
70	7.44	6.5	1.0	-	.18
80	7.44	1.0	2.0	-	.18
80	7.44	2.0	2.0	-	.18
80	7.44	2.5	2.0	-	.18
80	7.44	3.0	2.0	-	.18
80	7.44	3.5	2.0	-	.18
80	7.44	2.0	0.5	-	.18
80	7.44	3.0	0.5	-	.18
80	7.44	3.5	0.5	-	.18
80	7.44	4.0	0.5	-	.18
80	7.44	5.0	0.5	-	.18
80	7.44	7.0	0.5	-	.18

TABLE 3 (Continued)

V Knots	α deg	β deg	d/c	Wedge Position in.	Strut t/l
50	7.44	2.0	1.0	-	.18
50	7.44	4.0	1.0	-	.18
50	7.44	5.0	1.0	-	.18
50	7.44	5.5	1.0	-	.18
50	7.44	6.0	1.0	-	.18
50	7.44	8.0	1.0	-	.18
80	1.44	1.0	1.0	-	.18
80	1.44	2.0	1.0	-	.18
80	1.44	3.0	1.0	-	.18
80	1.44	3.5	1.0	-	.18
80	1.44	4.0	1.0	-	.18
80	1.44	5.0	1.0	-	.18
80	7.44	1.0	1.0	4	.18
80	7.44	2.0	1.0	4	.18
80	7.44	3.0	1.0	4	.18
80	7.44	0.0	2.0	-	.18
80	7.44	2.0	1.0	-	.12
80	7.44	4.0	1.0	-	.12
80	7.44	5.0	1.0	-	.12
80	7.44	5.5	1.0	-	.12
80	7.44	6.0	1.0	-	.12

angle of attack between the untwisted section chordline and the horizontal reference plane. Yaw angle is defined as the angle between the strut centerline and velocity axis.

Lift, drag, side force, strut base pressure, starboard, and port wing pressures and speed were recorded on a 14-channel Honeywell 5600C Analog Tape Recorder. Speed was measured with a police radar unit. The transponder was mounted on the carriage front and aimed toward a building at the end of the tank. The instruments were switched on approximately 3 seconds before each run and stopped by trip wires before the carriage engaged the arresting cables. Measurement system calibrations were checked and zeros taken before the start of each run and at the end of each run.

Motion pictures and still photographs were used for recording observed flow characteristics during the experiments. The cameras were mounted above and to the starboard side of the model. High speed movies were taken from a pit in the side of the tank, but were of little value due to murky water.

DATA REDUCTION

All forces were measured or resolved to horizontal and vertical coordinates. Pitching moment was computed from the output of the lift force block gages and was referenced to a point at the top of the strut (Figure 3). The reported wing pressure was obtained by averaging the output of the port and starboard wing gages. The analog data were digitized at a rate of 100 data points per second for each channel except the side force channels which were digitized at a rate of 50 data points per second. Several sampling rates were tried for the side force channels; however, no appreciable difference was found in the digitized data. Each half second of data points

was averaged and printed out in final form. The analog tapes of a few selected runs were examined by oscilloscope and were found to have oscillations of 8 and 13 Hz imposed on the output of the drag block gages of a magnitude on the order of the output signal. During the strut side force experiments, the natural frequency of the dynamometer assembly was measured, including the effect of the 532-pound mounting table which hung beneath the drag and sideforce gages. It was found to be 12 to 13 Hz, mostly due to the mounting table swinging beneath the force gages, which act like springs with a very high spring constant (500-pound force over .005 inch travel). A short calculation shows that for linear characteristics of the block gages the output reading of average force is undisturbed by the superimposed oscillations of whatever magnitude. Oscillations of 13 Hz were also found imposed on the output of the lift gages but were small enough to be considered insignificant. These selected runs were digitized again as previously described using a 6 Hz low-pass filter. There was no appreciable difference between the filtered and unfiltered data.

The drag data were corrected for air drag and for carriage deceleration including the effects of the 532-pound mounting table and the foil weight. Air drag values, which were measured in dry runs with the dynamometer only without the foil attached, are given in Table 4 for each experimental speed.

TABLE 4 - AIR DRAG OF DYNAMOMETER FOR THE TAP-1 HIGH-SPEED EXPERIMENTS

Velocity (knots)	Air Drag (pounds)
40	24
50	38
60	55
70	75
80	97
85	109
90	123

The carriage deceleration for each run was determined by plotting carriage speed against half-second time intervals. A sample plot is shown in Figure 7. The force, pressure, and moment data for each individual carriage run were plotted against carriage speed, and a value at the nominal speeds interpolated for each run. A sample plot of lift and drag is shown in Figure 8.

DATA ACCURACY

The six modular force gages used in the dynamometer for these experiments to measure drag and side force were arranged in a triangular array above the mounting table. The two modular force gages for measuring lift were mounted on the bottom surface of the mounting table in a fore and aft position. Calibration of the assembled dynamometer indicated the accuracy of the three 500-pound gages for measuring drag was within 2 percent of full scale, the three 500-pound gages for measuring side force were within 5 percent of full scale, and the two 1000-pound gages for measuring lift were within 2 percent of full scale. Calibration also showed no interaction between lift and drag; however, there was a 5 percent error in side force with 957 pounds of lift applied. There was no interaction between drag and lift or drag and side force. The method used for reducing the drag data, i.e., interpolation of deceleration and the actual drag output, has a cumulative possible error of around 5 percent. The dynamometer had a natural frequency of 12 Hz which was excited by the strut side forces. The effect was large oscillations in the side force which may have accounted for as much as 0.3 degrees of the effective side slip angle of the strut to the apparent flow. In addition, the yaw angle was accurate to only ± 0.4 degrees due to errors in setting the angle and clearances required in the forward block gage assembly. The cumulative maximum possible error in the side force is 20 percent; however, the data reduction "arranged" the

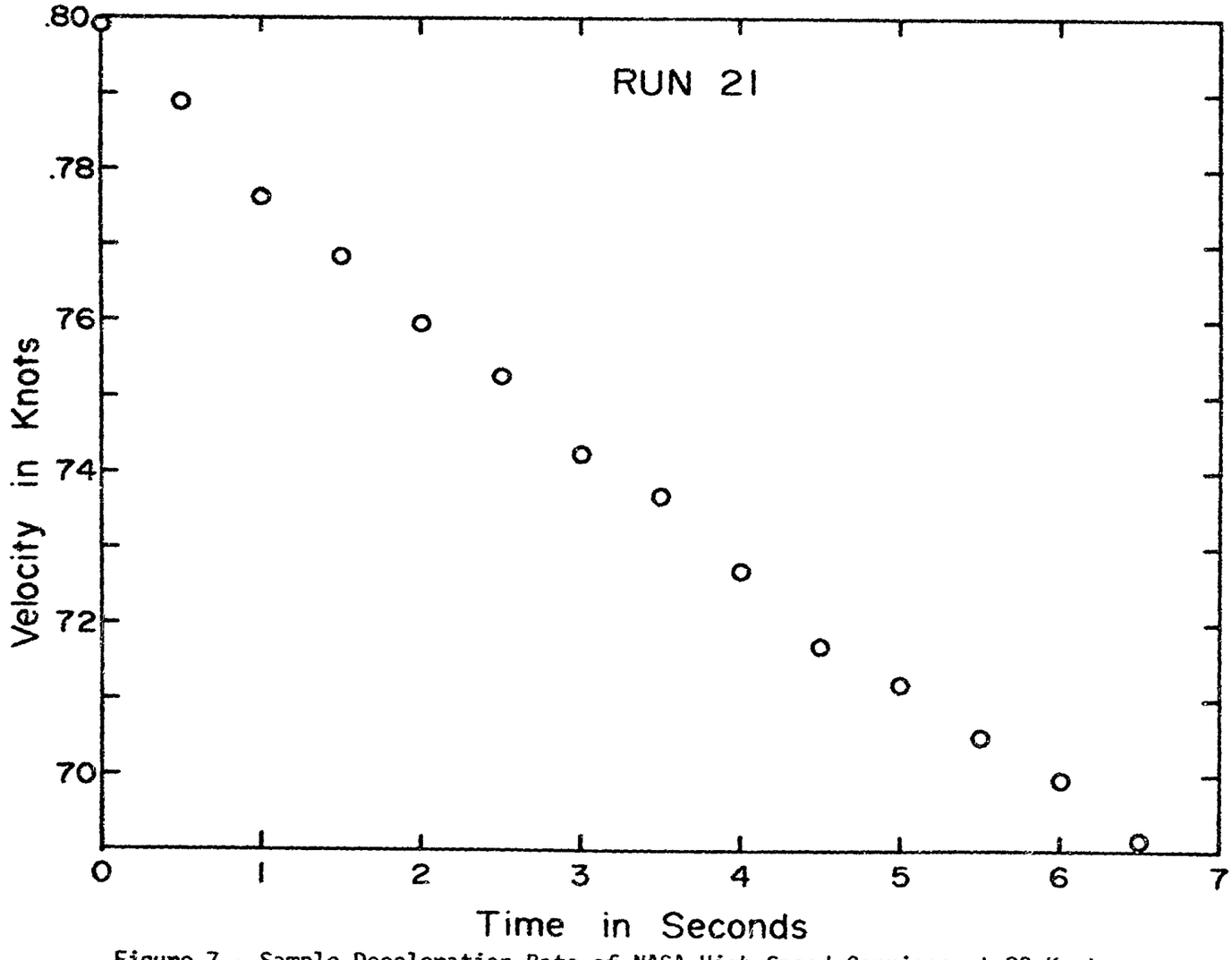

Figure 7 - Sample Deceleration Rate of NASA High-Speed Carriage at 80 Knots

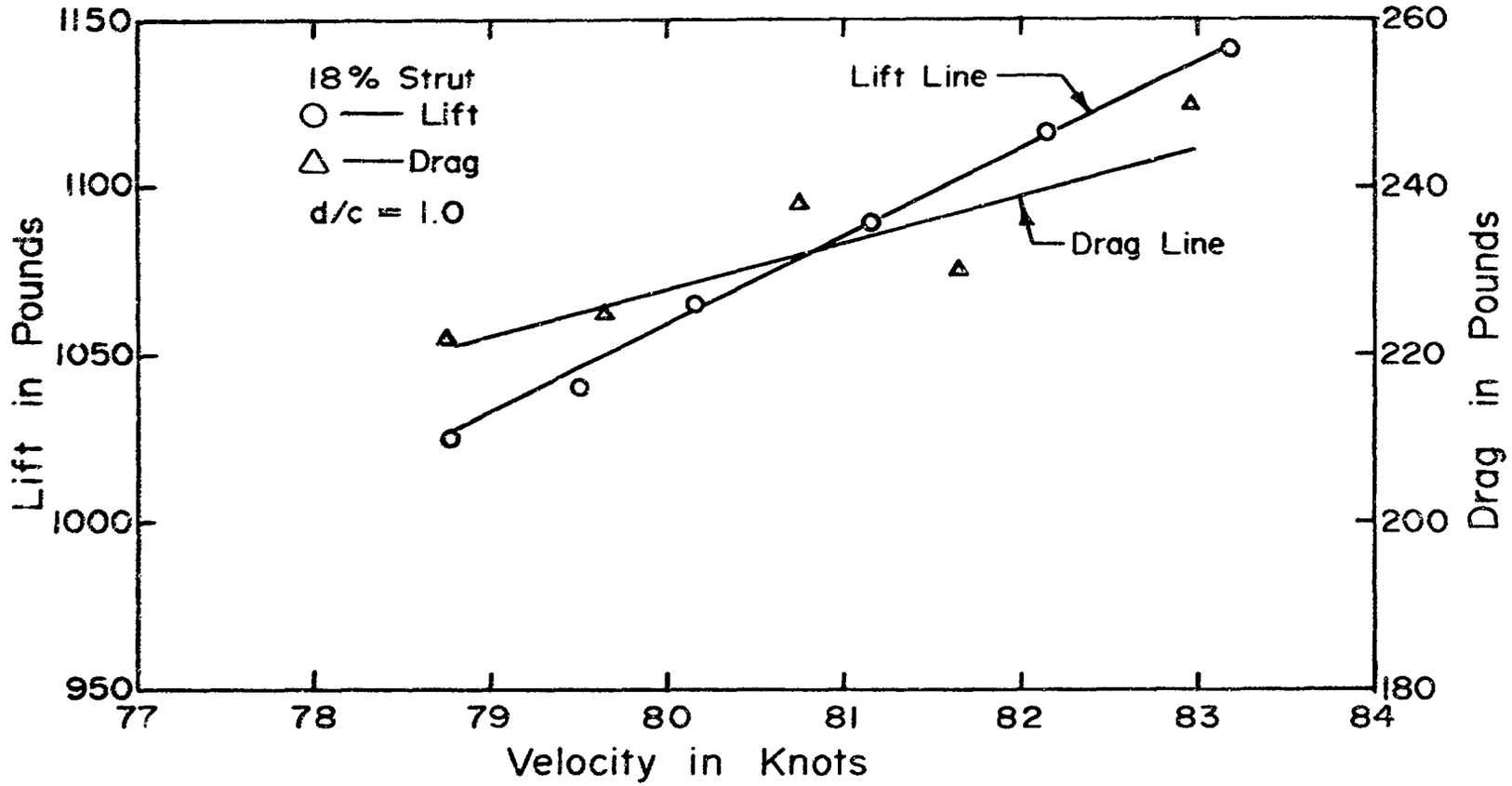

Figure 8 - Sample Plot of Lift and Drag during Deceleration from 83 Knots

results in a manner that probably reduces the error to 10 percent. The foil incidence angle and yaw angle were set to within ±0.1 degree. The foil angle of attack was adjusted by pitching the entire strut and foil assembly from the mounting table. Therefore, comparisons of data from fully ventilated and wetted foil conditions must take into account a 6-degree difference in the strut sweep angle between the two conditions. The strut sweep angle difference would change the side force by approximately 1 percent, and is therefore insignificant.

Pressure transducers installed in the foil wings and strut base were rated at +50 to -14 psig. The transducers are accurate to ±0.17 psi. The speed was measured by radar and is accurate to within 0.1 knot.

The submergence depth was set before each run by raising or lowering the dynamometer foil assembly with a hydraulic piston until the marked point on the 40 percent spanwise section was level with the static waterline. Variation in the piston setting due to foil lift was nil as determined by placing grease marks on the piston. The water surface was affected by wind, and therefore, the accuracy of setting the submergence depth varied between 0.1 and 0.5 inches depending on wind velocity.

The average water temperature was 67 degrees Fahrenheit and was within ±3.0 degrees of that value for the period of experimentation.

EXPERIMENTAL RESULTS

The experimental data are presented in two sections. The first section concerns forces, moments, and cavity pressures on the foil. The second section examines side force characteristics of the two struts.

The data are presented in tabular form (see Table 2) and graphical form for the foil force section, and in graphical form only for the strut side force section.

FOIL FORCES AND PRESSURES

Plots of measured data at zero yaw are presented in Figures 9 through 28. Except as noted, the spray wedge location was 4 inches above the strut mounting stub for all runs, or 4 1/2 inches above the foil itself. This position insured full ventilation at any speed.

The measured forces and moments on the TAP-1 foil system are shown in Figures 9 through 14. Here the pitching moment is reported about a point at the top of the strut, see Figure 3. The angles of attack refer to the chordline incidence of the 40 percent spanwise, untwisted section. With full ventilation force data plots against vapor cavitation number are unvarying, and the incidence angle is used as the independent variable.

The minimum angle of attack for which full cavity flow was observed was α = 4.9 degrees, which agrees very well with the two-dimensional design value of α = 4.6 degrees. However at that angle the measured lift coefficient was only C_L = 0.092, which compares unfavorably with the two-dimensional section design value of 0.136. Apparently the wing twist was more successful in maintaining the cavity out to the wing tips than in maintaining the loading. Consequently the lift-to-drag ratio also suffers in comparison to that of the parent foil (6.6 versus 6.9), although the two foils are not directly comparable because the design lift and stress levels differ between them. Also the peak fully cavitating lift-to-drag values for the untwisted parent foil occur at incidence angles where the curvature of the L/D versus α curve was negative, which would

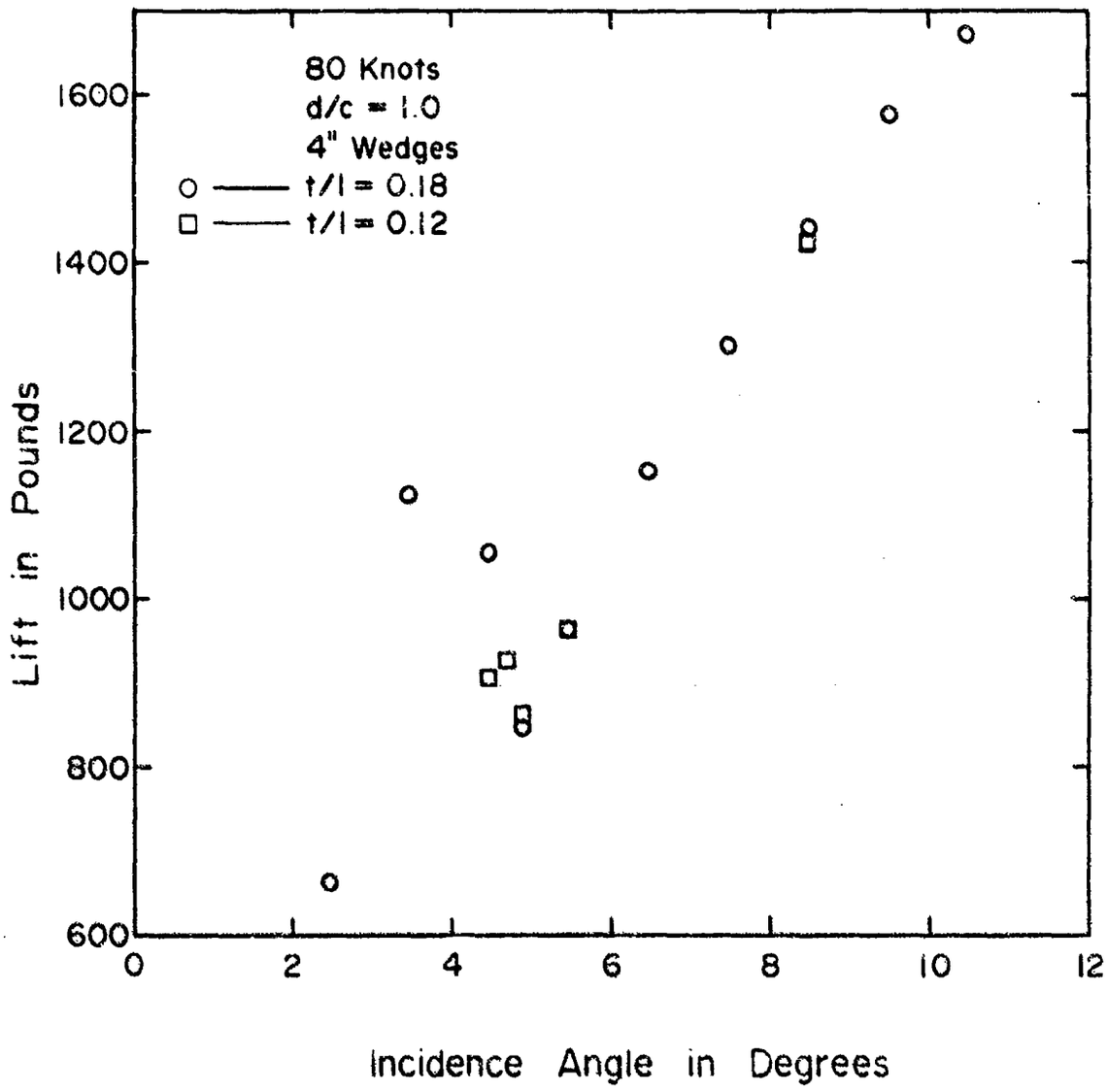

Figure 9 - Lift in Pounds versus Incidence Angle,
V = 80 Knots, d/c = 1.0

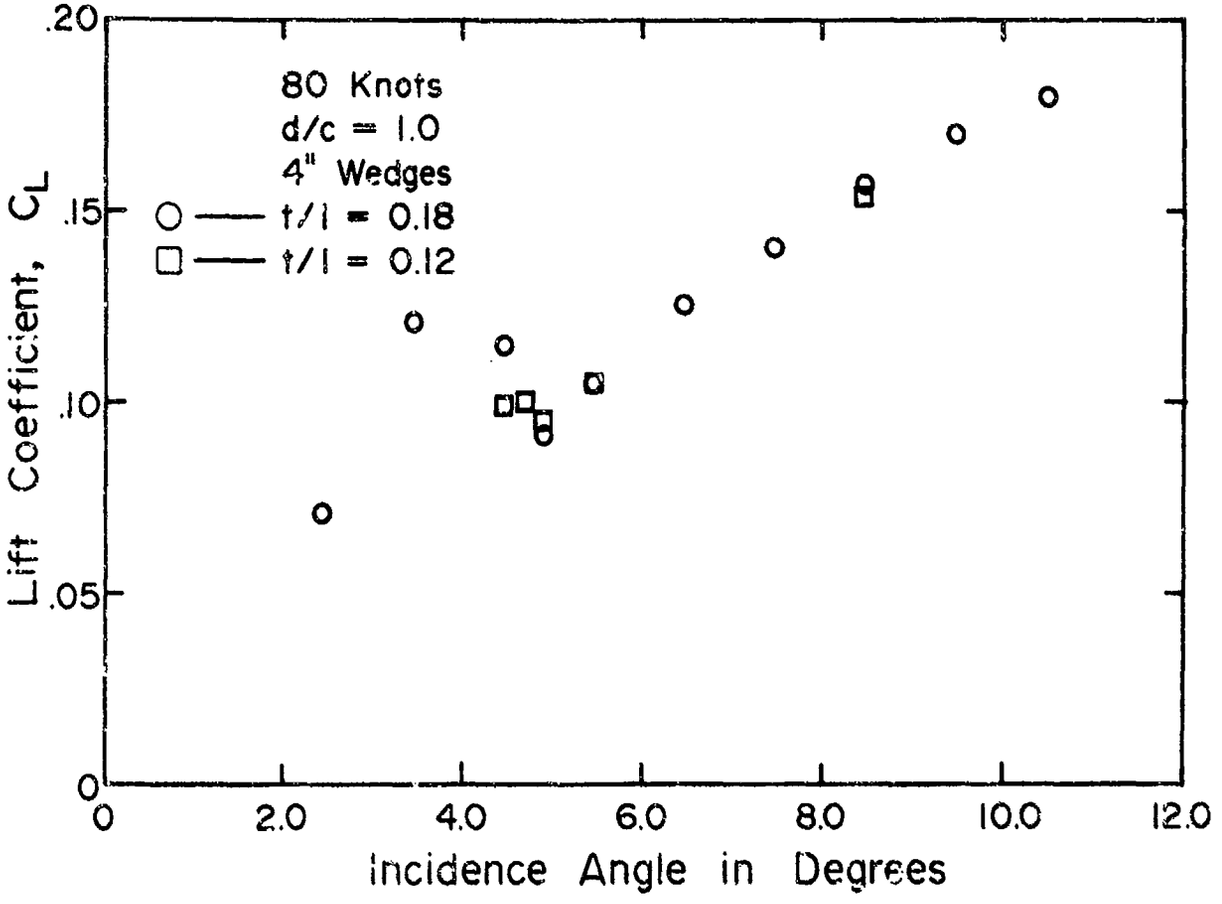

Figure 10 - Lift Coefficient versus Incidence Angle, d/c = 1.0

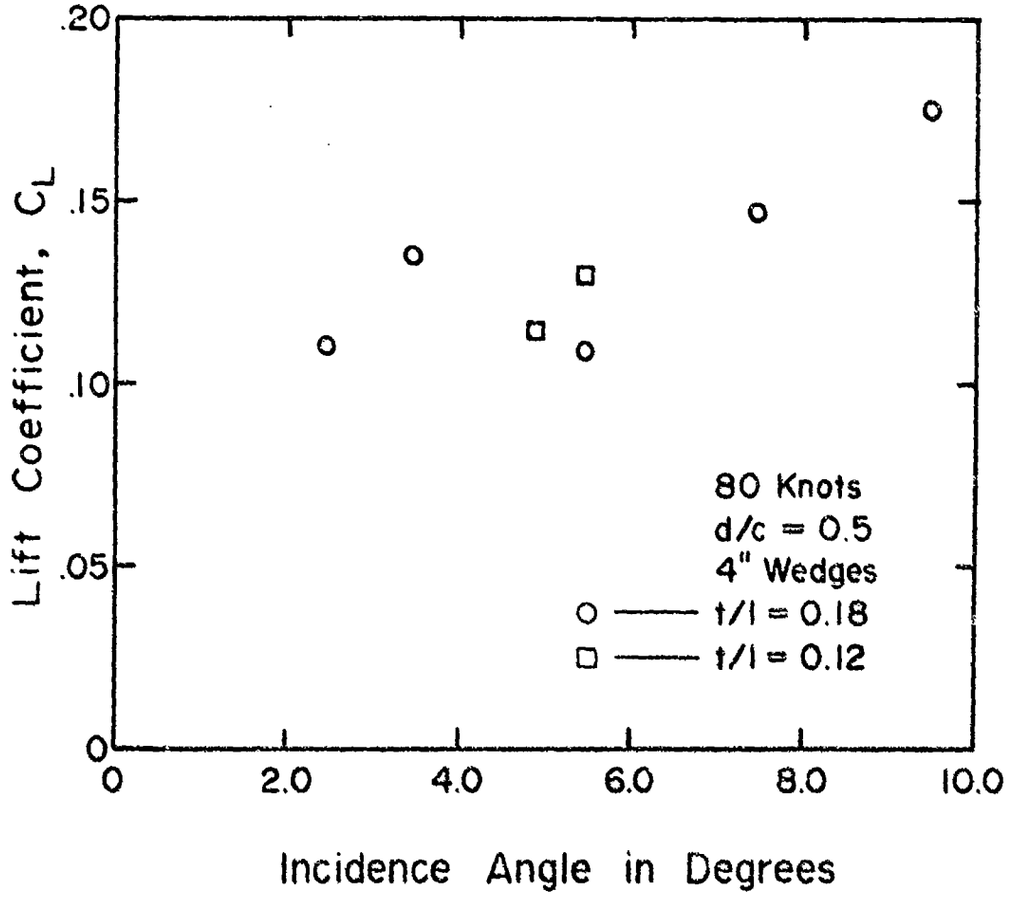

Figure 11 - Lift Coefficient versus Incidence Angle, d/c = 0.5

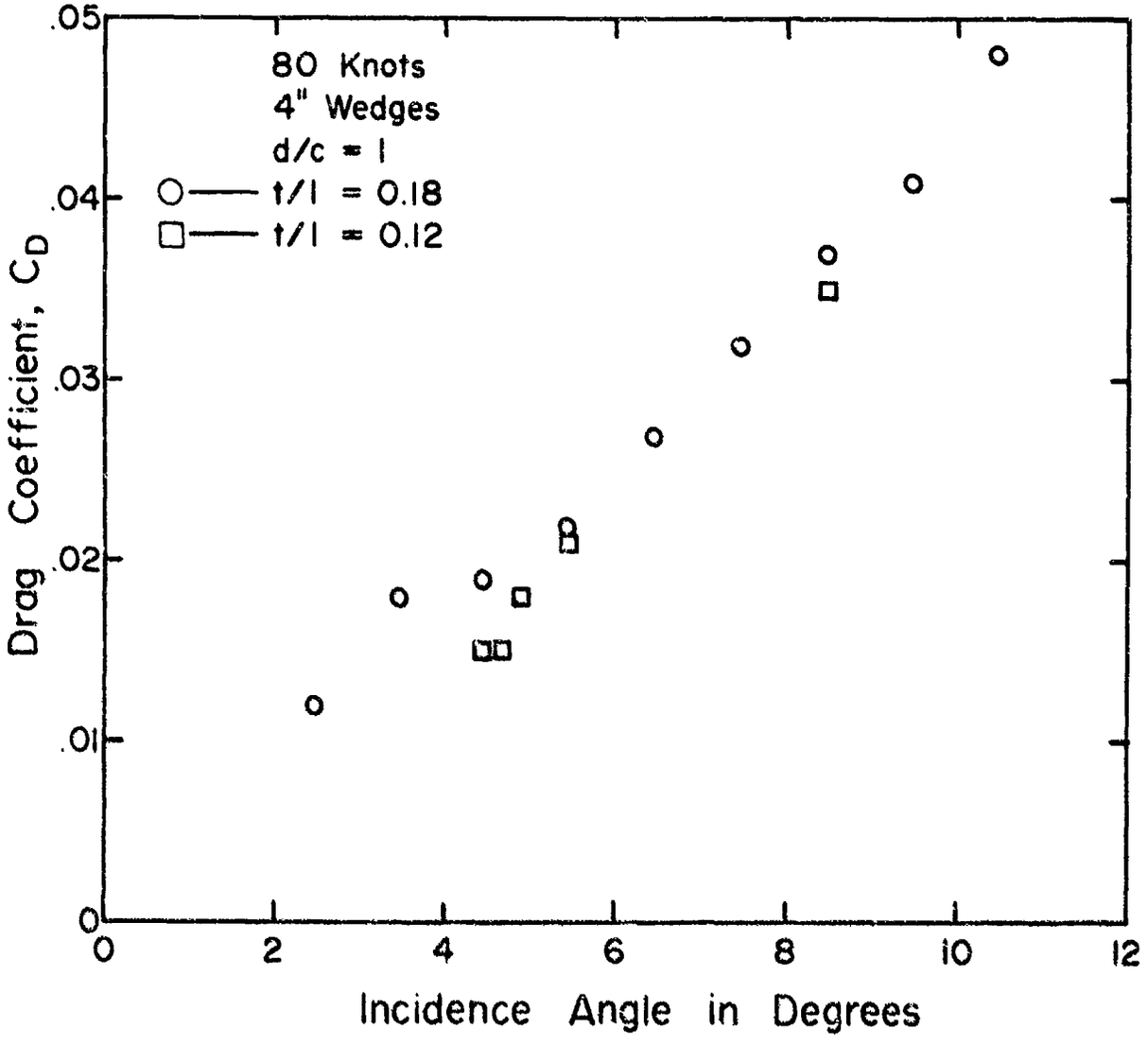

Figure 12 - Drag Coefficient versus Incidence Angle, d/c = 1.0

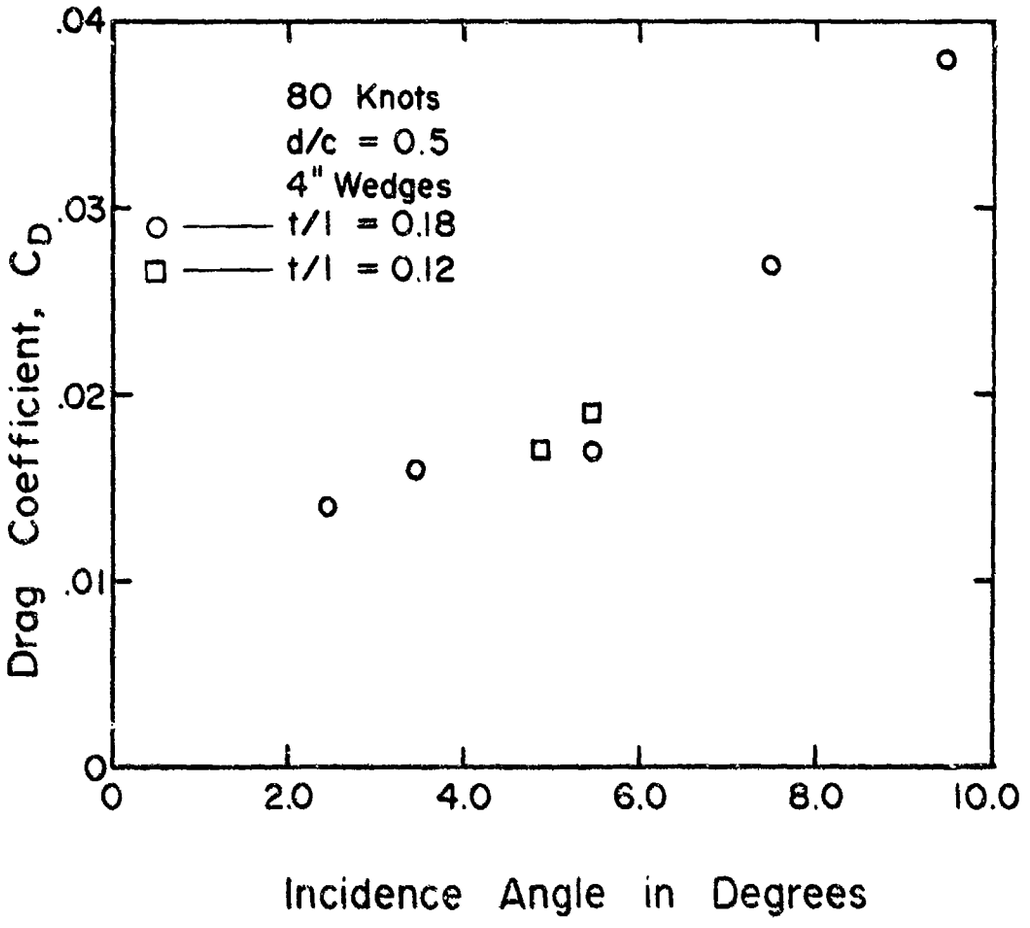

Figure 13 - Drag Coefficient versus Incidence Angle, d/c = 0.5

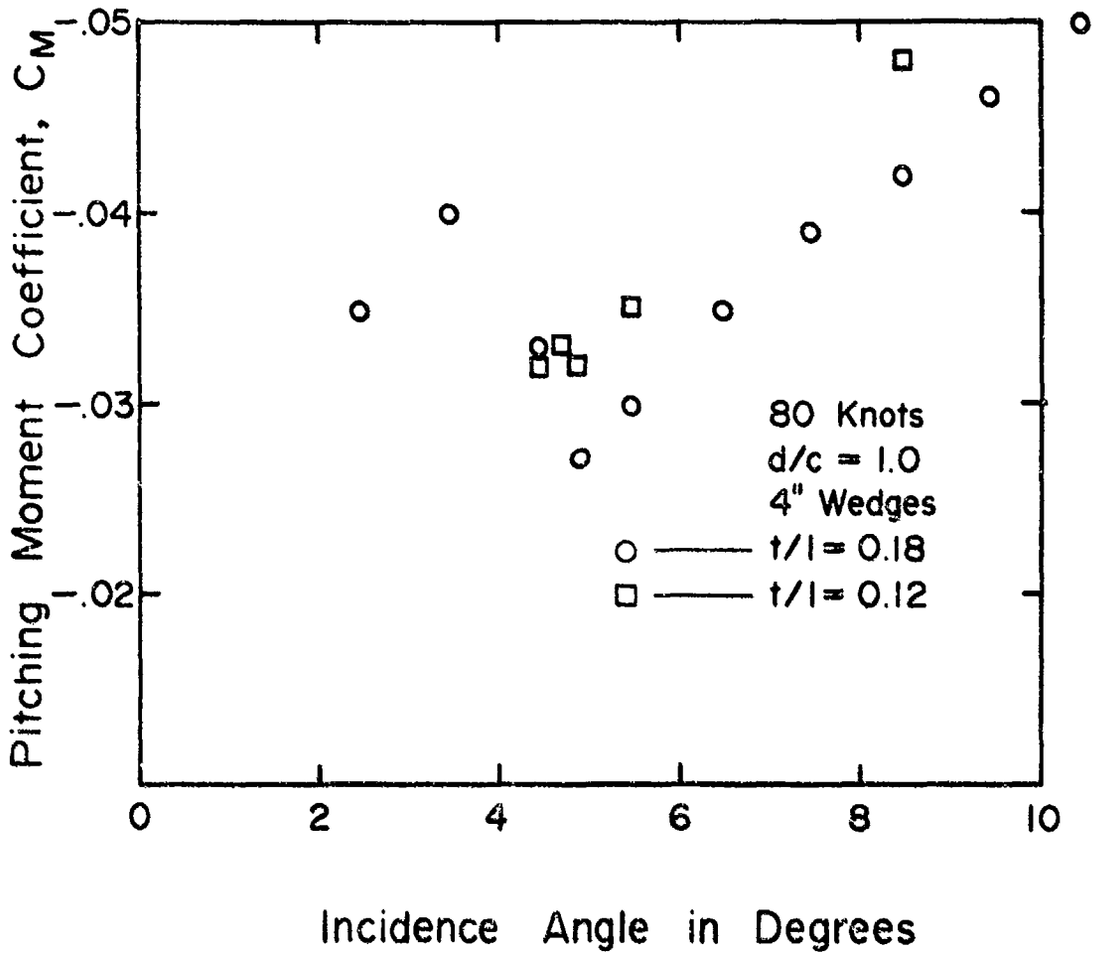

Figure 14 - Pitching Moment Coefficient about Top of Strut versus Foil Incidence Angle

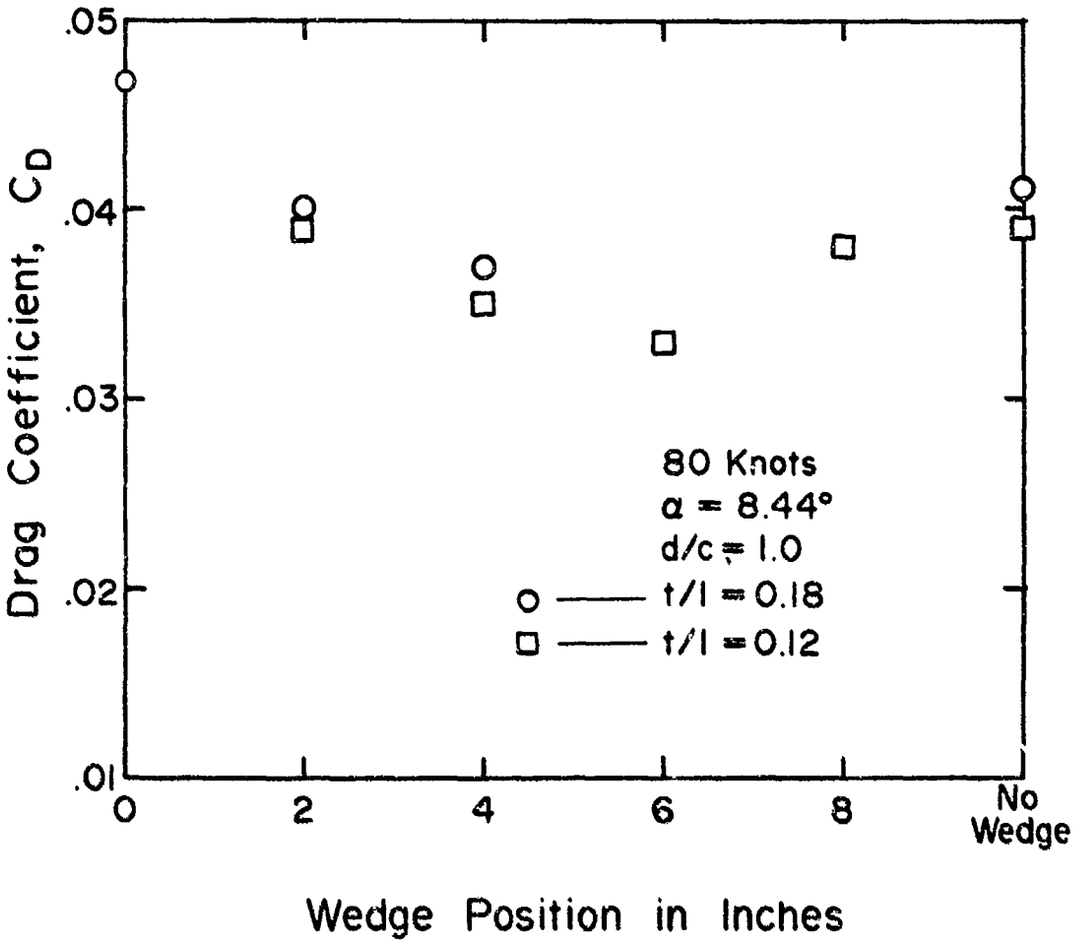

Figure 15 - Drag Coefficient as a Function of Wedge Position at V = 80 Knots, α = 8.44 Degrees, and d/c = 1.0

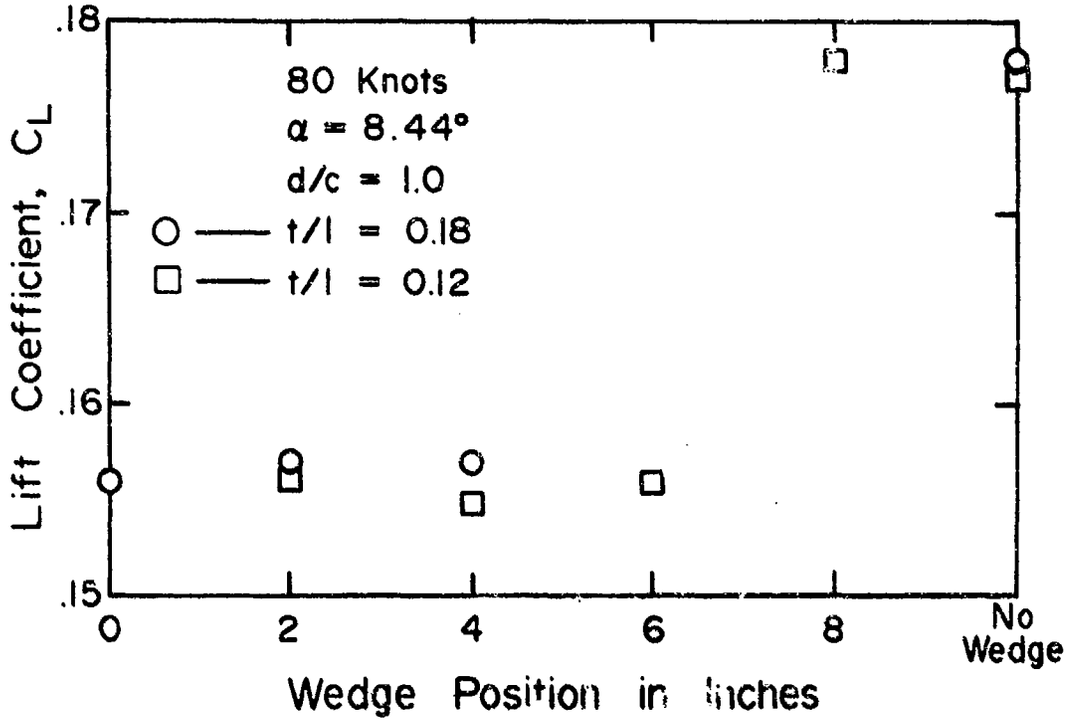

Figure 16 - Lift Coefficient as a Function of Wedge Position at V = 80 Knots, α = 8.44 Degrees, and d/c = 1.0

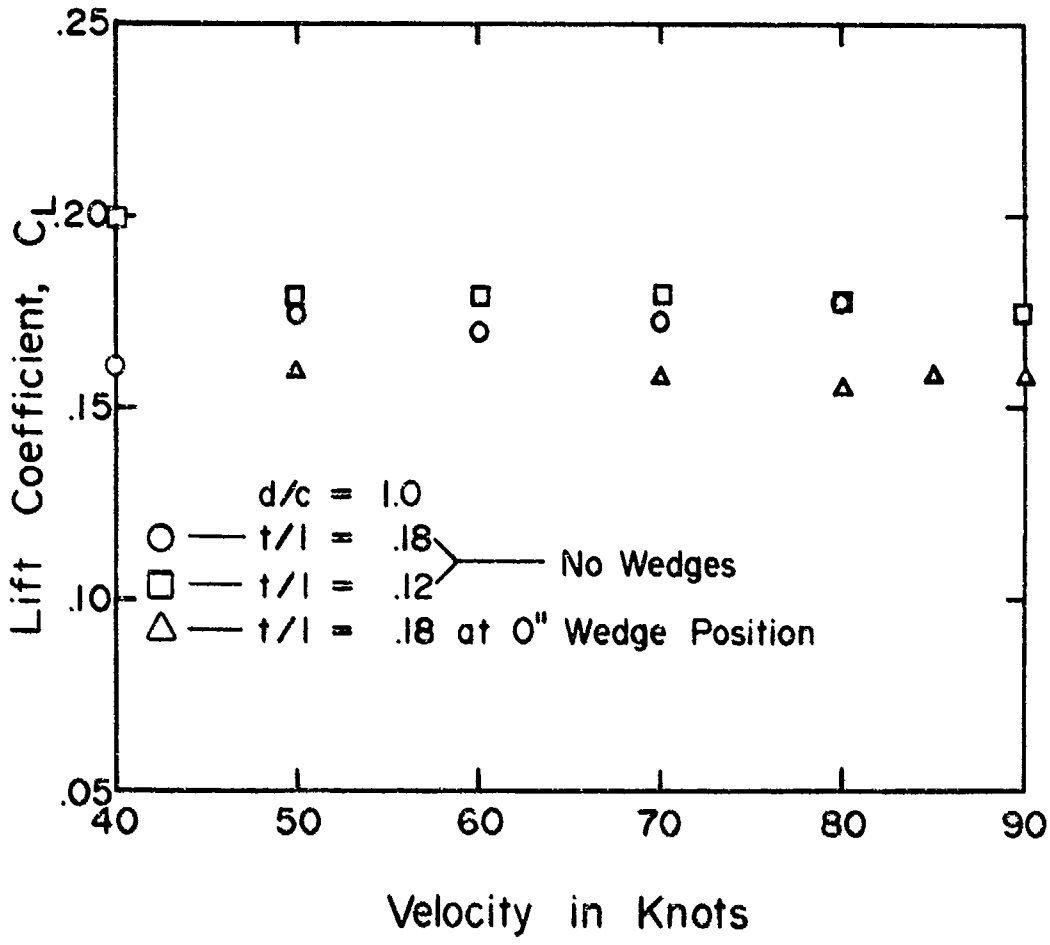

Figure 17 - Lift Coefficient as a Function of Velocity at α = 8.44 Degrees, d/c = 1.0

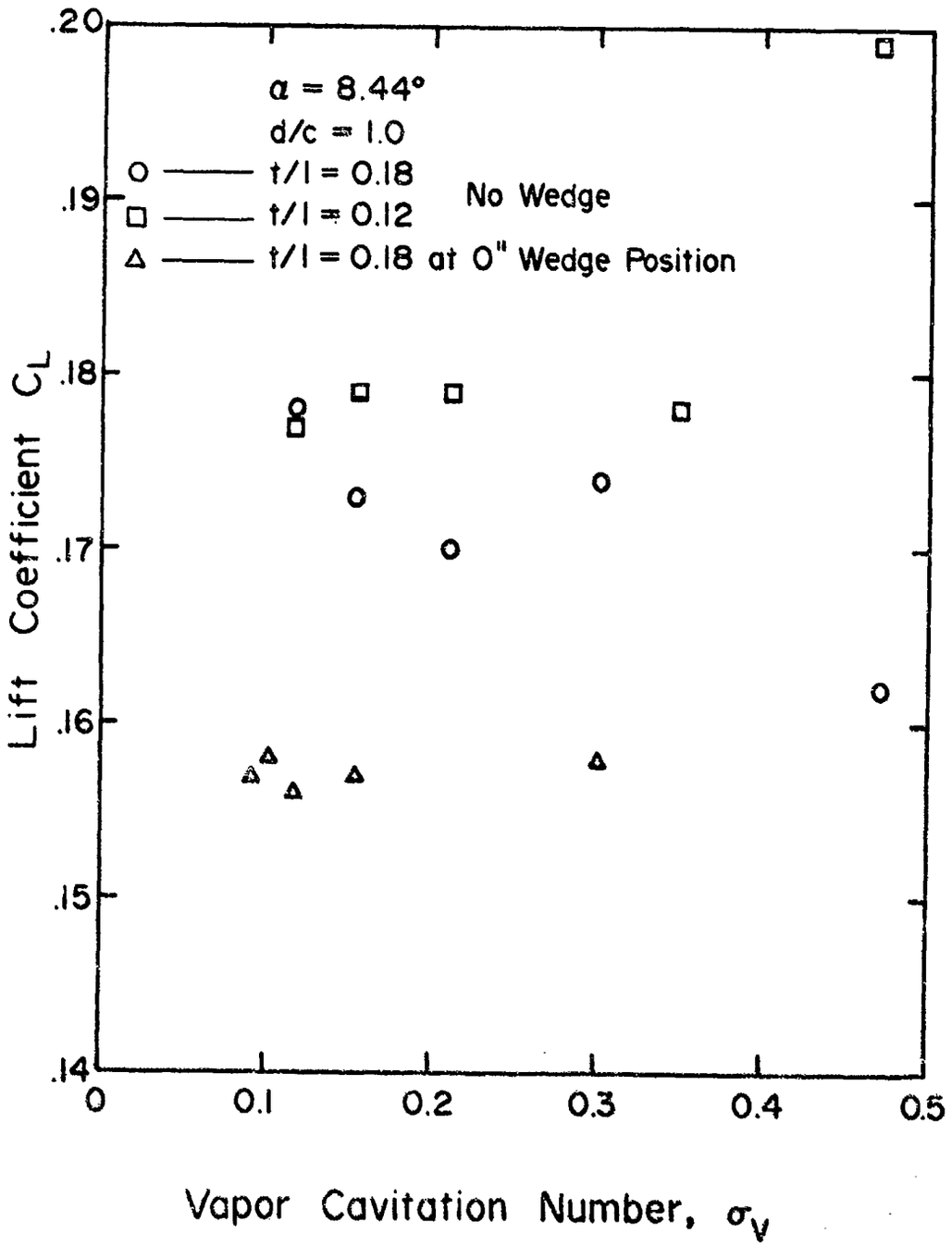

Figure 18 - Lift Coefficient as a Function of σ_v at α = 8.44 Degrees, d/c = 1.0

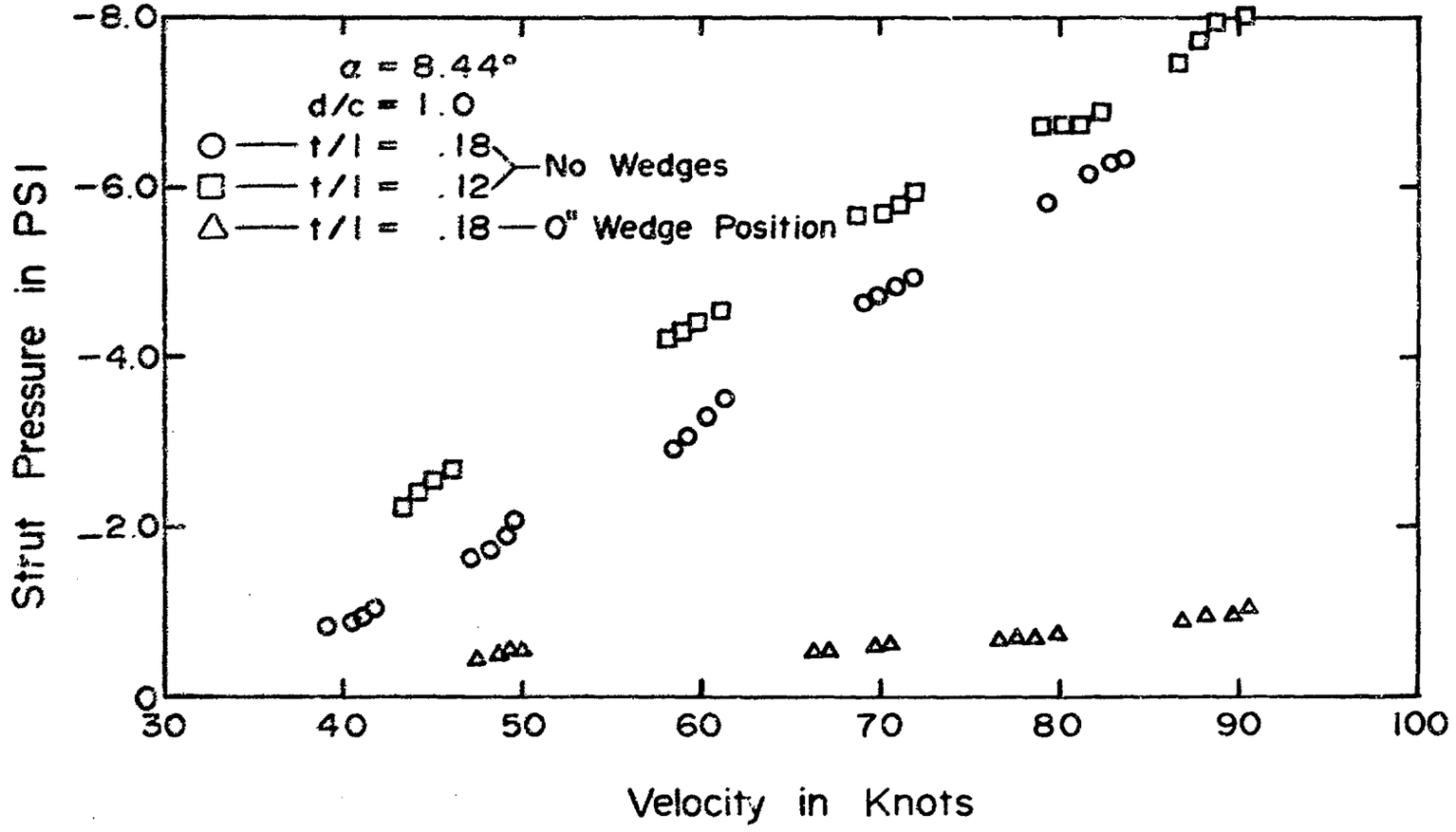

Figure 19 - Strut Base Pressure as a Function of Velocity at α = 8.44 Degrees, d/c = 1.0

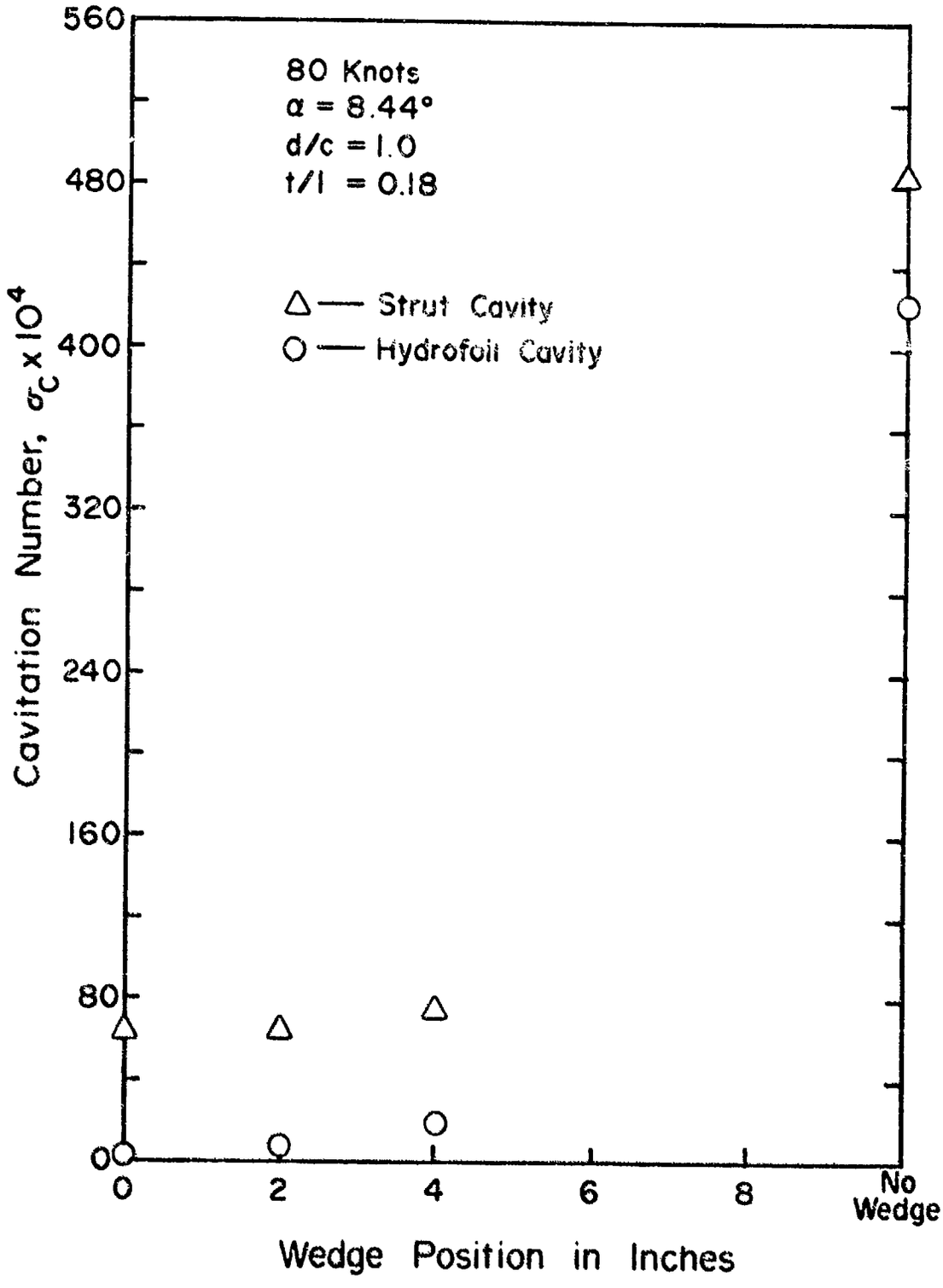

Figure 20 - Measured Cavitation Numbers versus Spray Wedge Mounting Position

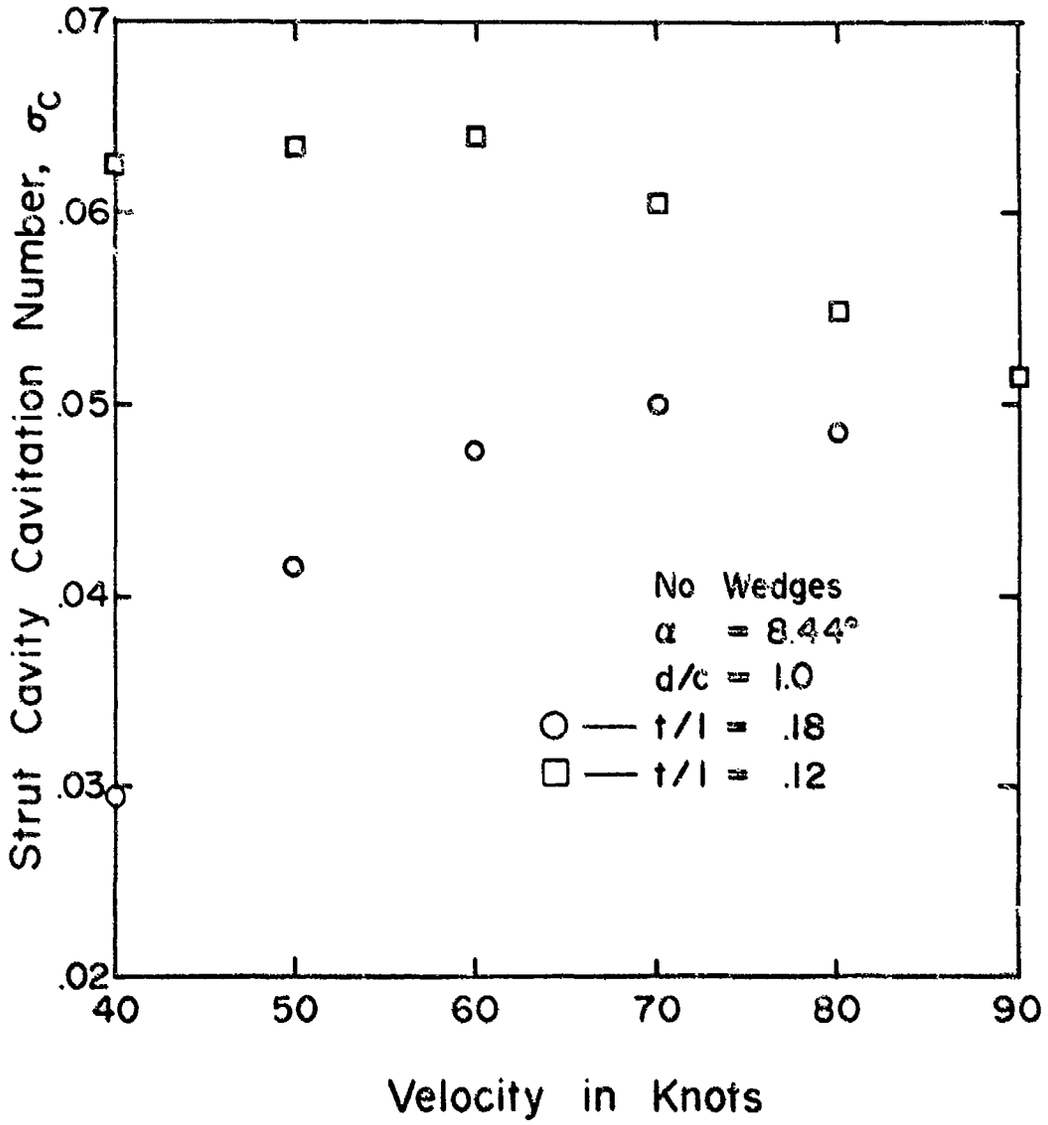

Figure 21 - Measured Cavitation Numbers at Strut Base versus Velocity, No Spray Wedges

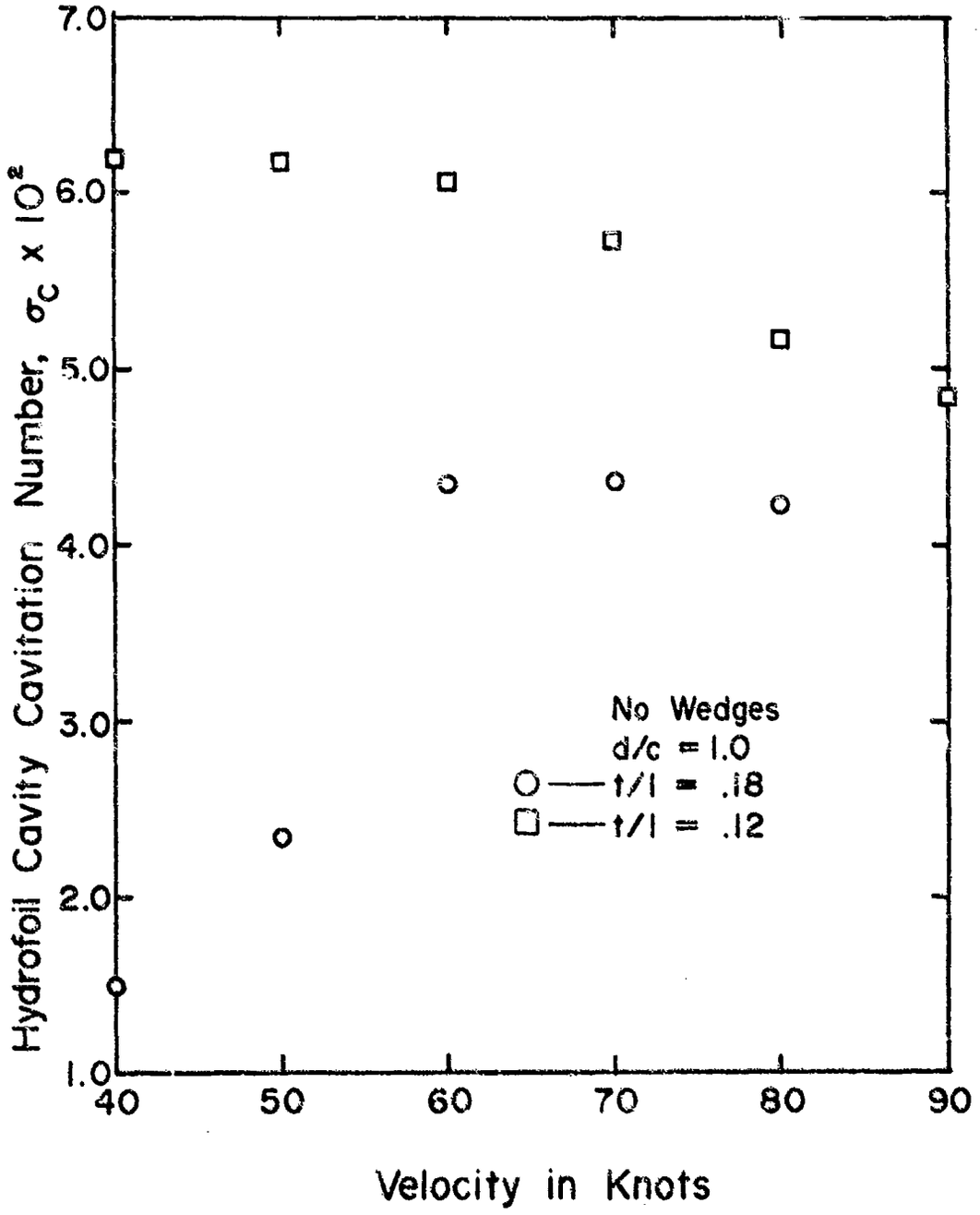

Figure 22 - Measured Cavitation Numbers at Wing versus Velocity, No Spray Wedges

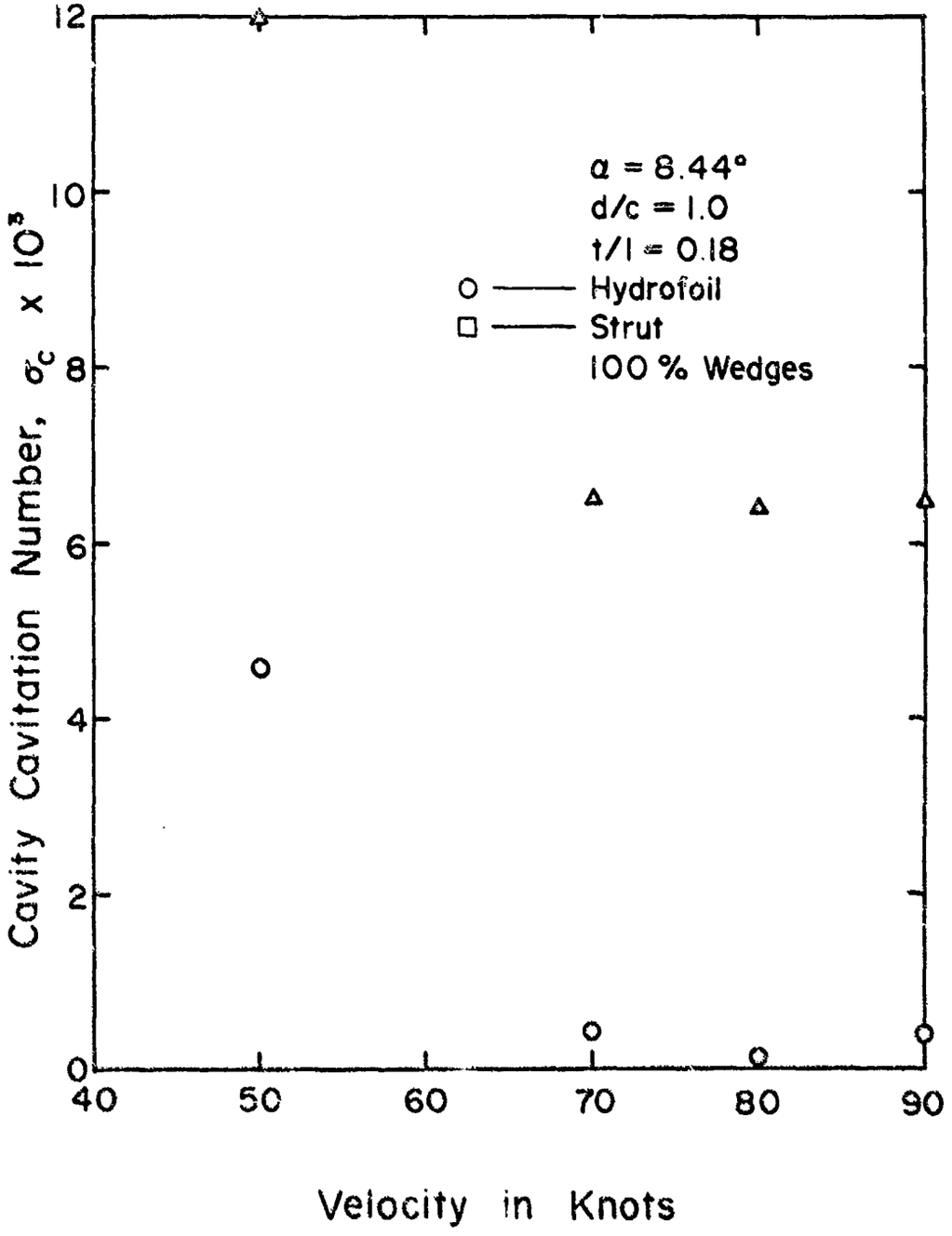

Figure 23 - Measured Cavitation Numbers versus Velocity with Wedges

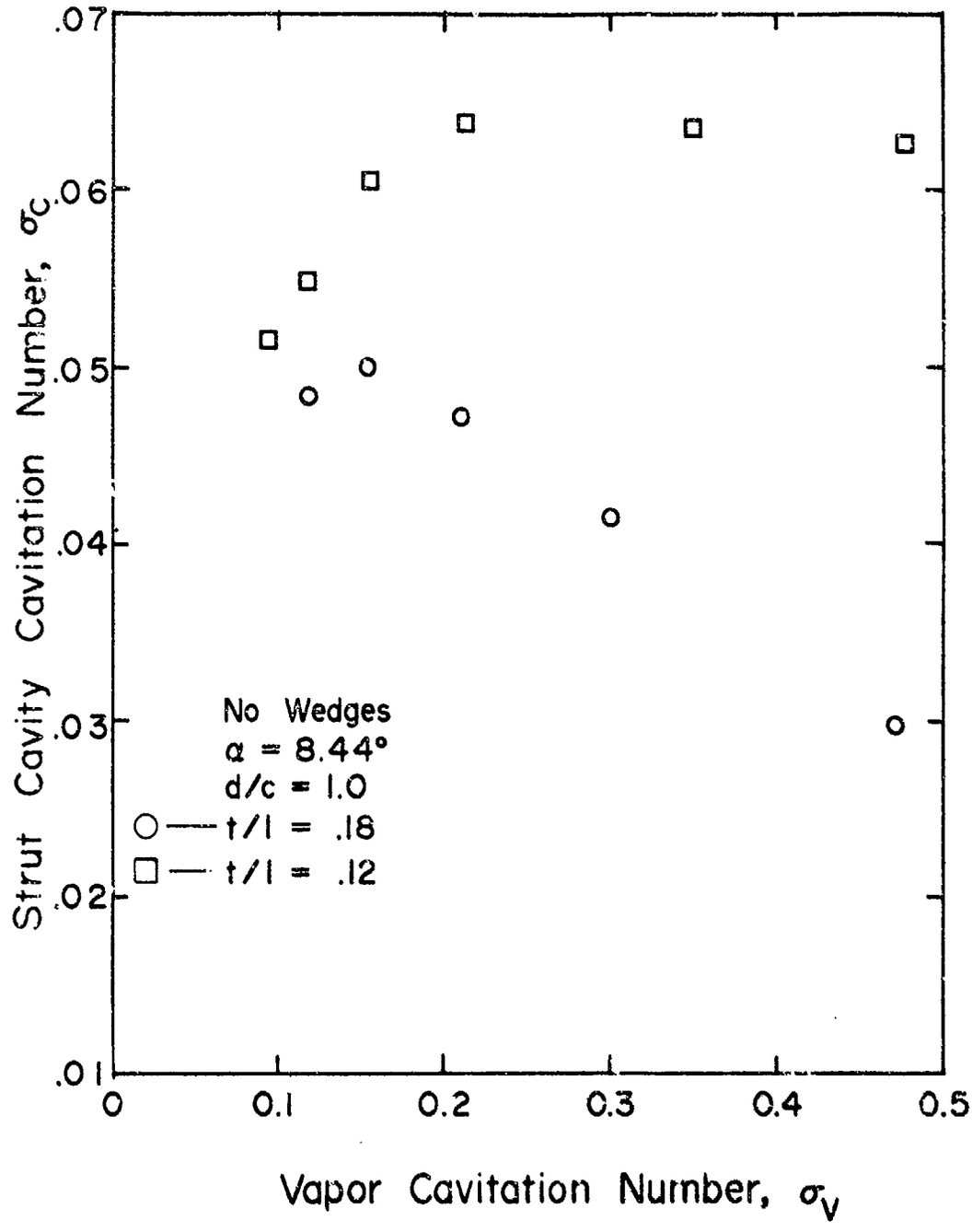

Figure 24 - Measured Cavitation Number at Strut Base versus Vapor Cavitation Number, No Spray Wedges

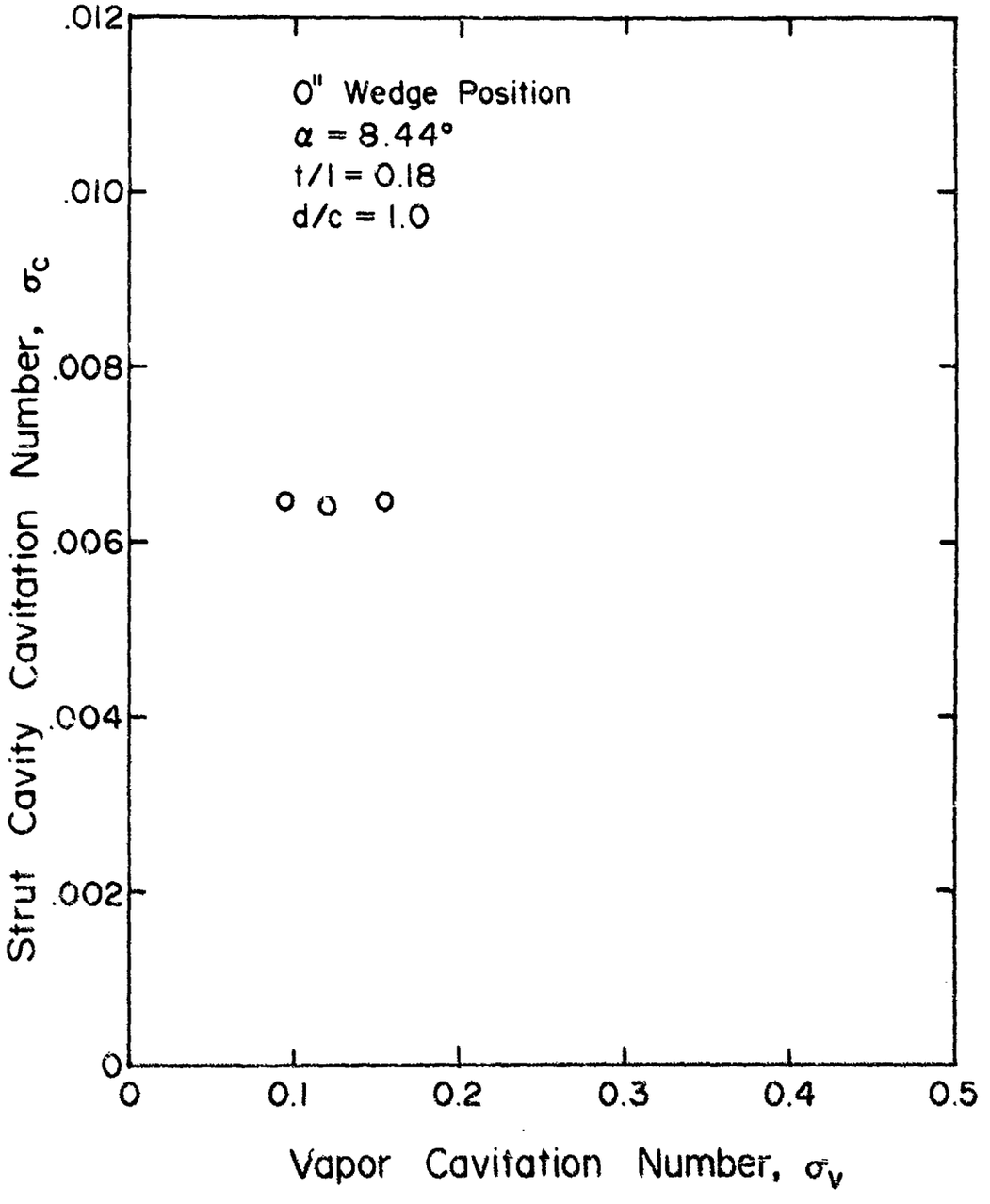

Figure 25 - Measured Cavitation Number at Strut Base versus Vapor Cavitation Number with Spray Wedges

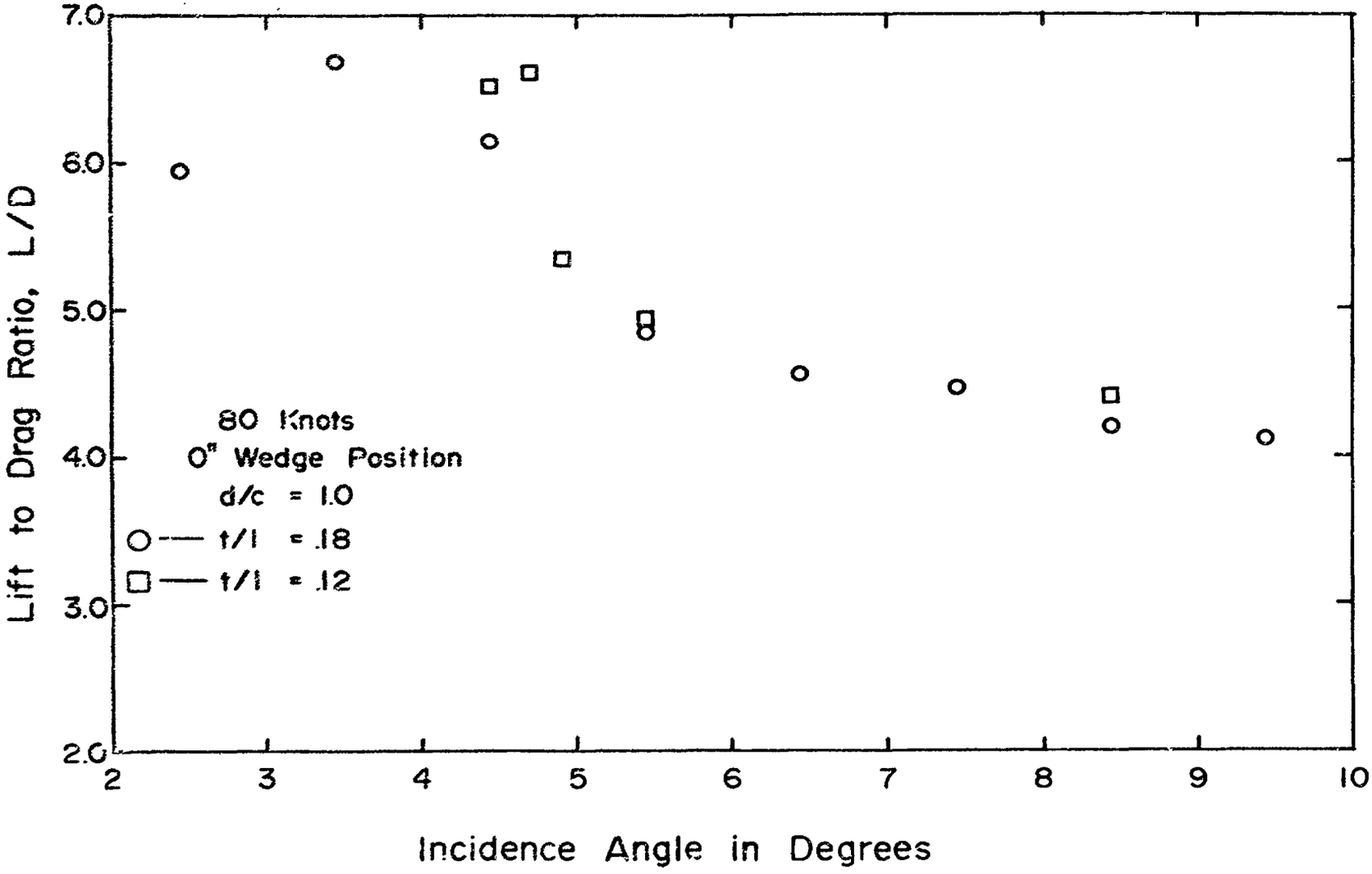

Figure 26 - Lift-to-Drag Ratio versus Incidence Angle,
d/c = 1.0, V = 80 Knots

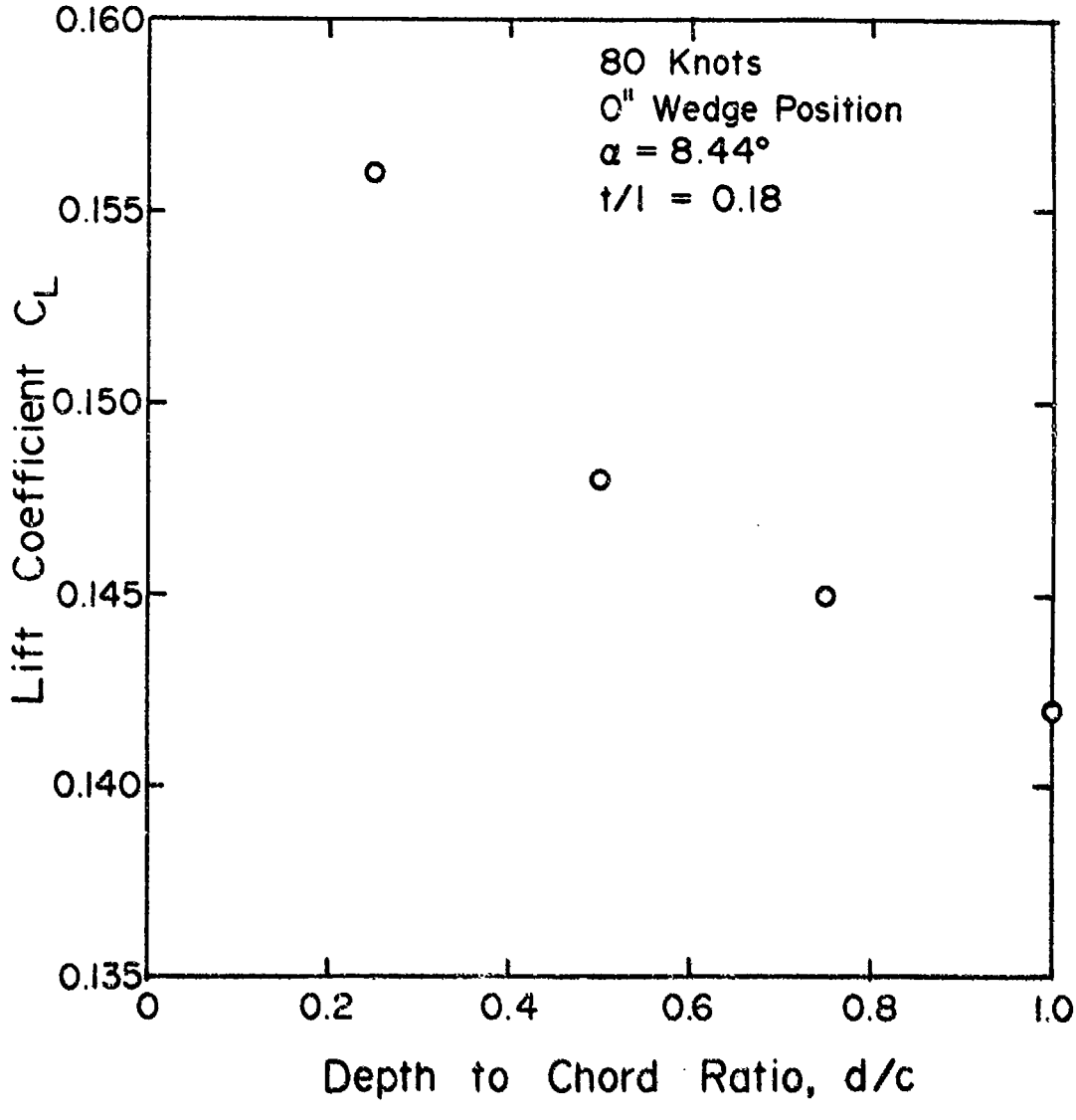

Figure 27 - Lift Coefficient versus Depth of Submergence, V = 80 Knots

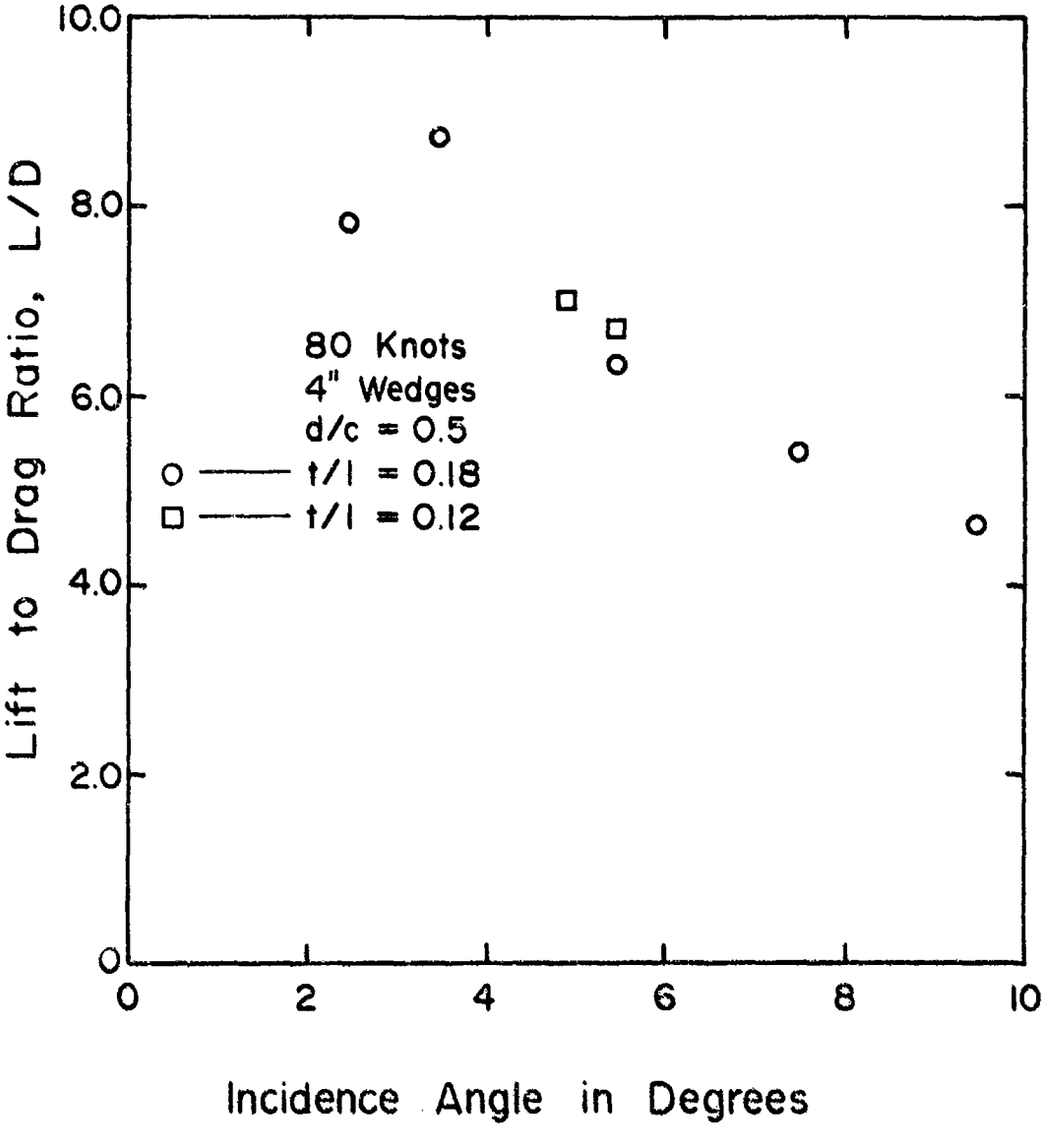

Figure 28 - Lift-to-Drag Ratio versus Incidence Angle, d/c = 0.5, V = 80 Knots

imply that portions of its upper surface, presumably the root and tip sections, were partially wetted. It is unclear whether this is a possible operating mode.

The measured C_L versus α curve (Figure 10) shows a break in slope at $\alpha \approx 8$ degrees. Presumably this is caused by the foil annex intersecting the lower cavity wall, which separates from the wetted trailing edge.

Underwater photographs of the TAP-1 foil at 40 knots (taken in an indoor basin) showed the lower surface flow clearing the annex at $\alpha \approx 5$ to 7 degrees. Underwater photographs during the high-speed experiments were not possible due to murky water conditions.

The Boeing annex foil, whose length of annex was 100 percent of the wetted chord, also showed a break in $dC_L/d\alpha$ at larger α, but lift-curve slope increased at larger α values. Presumably the longer annex on this foil showed a positive lift increment by actually deflecting the lower streamline downward when it intersected the flow.

The TAP-1 hydrofoil, whose lower annex surface is tilted up quite sharply with respect to the foil chord (a length 30 percent of wetted chord), may have developed an underside cavitation bubble instead at that juncture, which would reduce the effective camber of the foil and reduce the slope of the lift curve. Presumably there is some length of annex where these two effects cancel out one another.

The additional drag and lift on the foil due to spray strips is shown in Figures 15 through 18, where the proximity of the wedges to the strut mounting stub is shown as a variable. Zero distance corresponds to full down position of the wedges. The lift changes because the ventilation air path to the foil is affected.

VENTILATION

Because of the unusual ventilation behavior of the parent foil at high speed, a series of runs was made with the TAP-1 foil to cover a wide speed range at a single angle of attack. Pressures measured at various speeds as the carriage decelerated are shown in Figure 19. This test was run both with and without the spray deflecting strips; the first part of the test series without them, i.e., a bare parabolic strut, corresponds to the test condition of the parent foil.

The sudden cut-off of ventilation air above a certain speed, reflected in the lift curves of the parent foil (Figure 29), was not observed on the TAP-1 foil, although the angle of attack chosen most certainly corresponded to a fully cavitating flow over the TAP-1 foil. Rather, there was a gradual and linear decrease with speed of the strut base pressure from atmospheric, beginning at V_K = 40 knots which was the lowest test speed, and continuing up through the maximum tested speed of 90 knots. In interpreting these results, it must be remembered that the initial acceleration of the carriage (5 g's) is much faster than the fluid can accelerate under gravity, so the flow over the foil must be assumed initially ventilated.

To continue this part of the experiments, the spray strips were mounted in a full down position on the strut; that is, with the lower edge of the spray wedge resting against the top of the strut mounting stub, which is an integral part of the foil but extends somewhat behind the strut base itself. The lower edge of the spray strip is tapered to zero so that the juncture provides a smooth airflow path. In this condition full ventilation (here we define full ventilation as $\sigma_c < 0.01$) was observed over the entire speed range. A plume of water thrown high in the air behind the foil was observed.

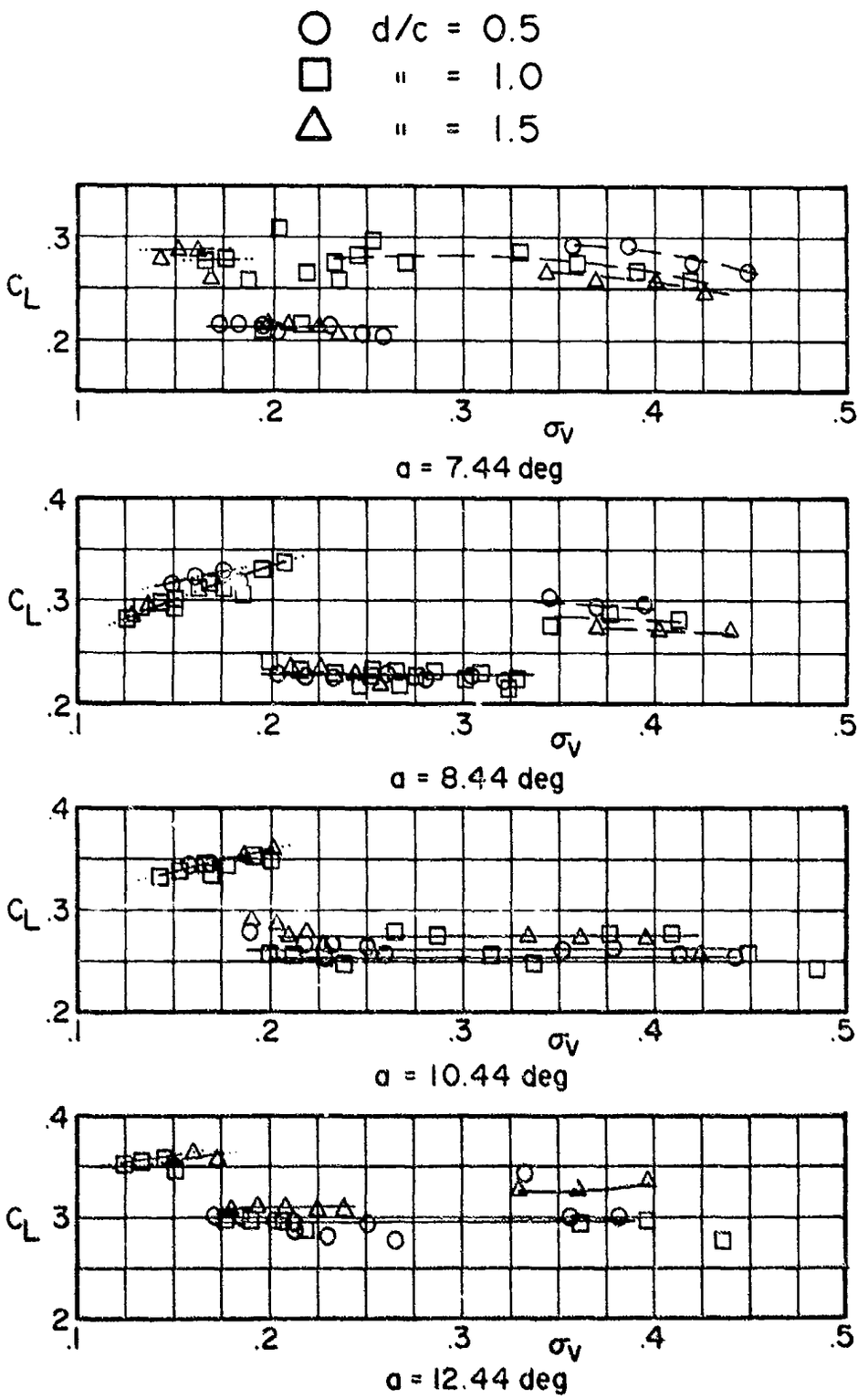

Figure 29 - Lift Coefficient of BuShips Parent Hydrofoil, Measured in NASA High-Speed Towing Carriage

The purpose of the spray wedges is to deflect outward the strut spray sheet which otherwise is drawn down the strut base cavity and blocks the air passage. Wadlin[7] suggests that the flow is choked in this air passage immediately behind the strut; if so, the airflow rate would depend only on the passage area.

The tapered spray wedges of TAP-1 can be mounted at various vertical positions along the strut base in 2-inch increments. Because the foil with the 18-percent strut and wedges fully lowered exhibited full ventilation at all speeds, runs were made only at 80 knots with the wedges in various up positions. Because of the taper, this means that the effective wedge angle at the strut-waterline intersection and the area of the air passage were reduced. Data are shown in Figure 20. Rather than a gradual decrease in ventilation, the σ_c value at the strut base rose suddenly as the wedge was raised above a certain position, 4 inches up from the foil. At that point, the bottom of the wedge was nearly level with the static waterline; of course, the strut spray sheet rises considerably above this, about one strut chordlength. Apparently the vent air flow is reduced almost immediately as the wedge is moved above this spray sheet, and the function of the wedge in enlarging the strut base cavity is not significant.

Taking advantage of this information, the 12-percent strut was built with adjustment holes only 1 inch apart. Tests showed that at the standard condition $\alpha = 8.4$ degrees of the foil, the wedges could be raised above the 4-inch setting while maintaining full ventilation; however, this was not maintained as the foil incidence angle was reduced, and the 4-inch up setting proved to be the amount of spray wedge necessary to maintain full ventilation over a range of angle of attack. This was then called the "optimum wedge location" for the remainder of the experiments for both struts.

During experiments with force ventilated hydrofoils in towing tanks,[11] the parameter

$$\kappa_V = \frac{Q_V}{AV},$$

is used to characterize the ventilation state, where Q_V is the volumetric amount of vent air supplied. Implicit in its use is the assumption that vent air demand is proportional to water speed V. Nothing in the present experiments contradicts this assumption. The measured pressure difference across the strut cavity air passage is generally linear with the water speed (Figure 19) and the thinner strut (t/c = 12 percent) shows a greater pressure drop than the larger one, which is consistent with the flow of air at low Mach number through a confined passageway.

Other Observations

The cavity appeared to cover the foil out to the wing tips in most of the photographs and to extend downstream out of camera range. Missing were the cavity oscillations observed for the parent foil, which are associated with flow at larger cavitation numbers, say $\sigma_c \geq 0.20$. These values did not occur for TAP-1 because of the use of spray strips. However it is unclear why these oscillations should not have occured for TAP-1 with the 12-percent strut (versus parent foil 15-percent) and no spray wedges (see Figure 30). In this case the foil area is the same, while TAP-1's structural rigidity is greater and its loading less than that of the parent foil. Yet no leading edge vibration was observed either, even at the maximum test speed of 92 knots. The leading edge thicknesses of TAP-1 and the parent foil are almost identical. Presumably the difference

[11] Dobay, G. F. and N. L. Ficken, "Supercavitating and Ventilated Performance of Three Hydrofoil Sections," NSRDC Report 1828, Jan 1964

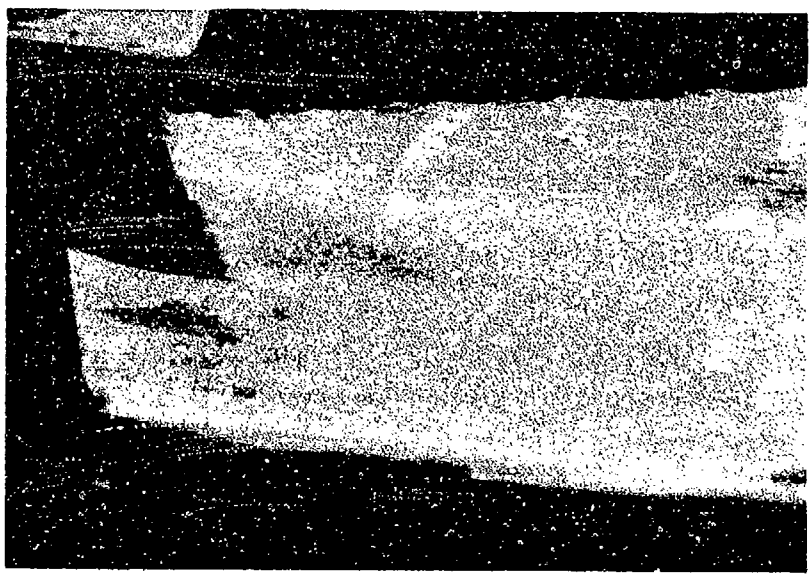

Without Spray Wedges

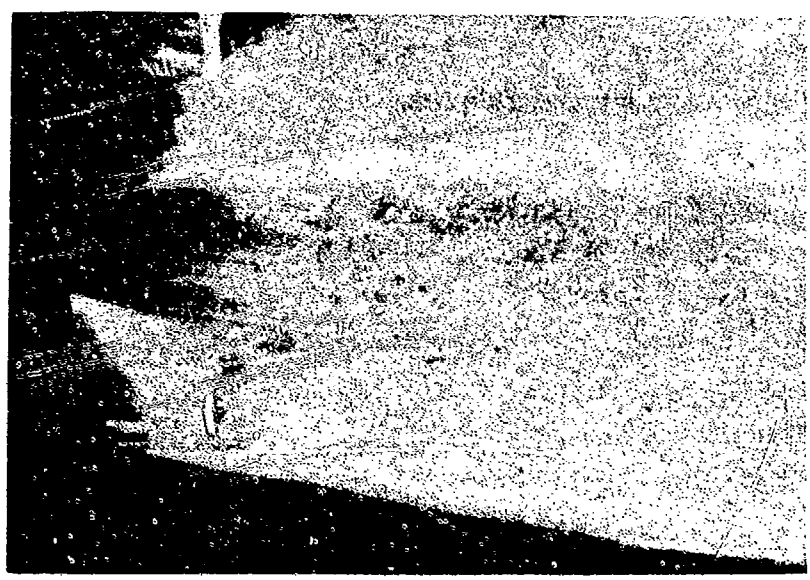

With Spray Wedges

Figure 30 - Photographs of Flow over TAP-1, V = 80 Knots, with and without Spray Wedges

comes from the leading edge sweepback angle, and possibly the reduced aspect ratio for TAP-1.

The ventilation airflow path could be observed visually in motion pictures of the TAP-1 foil during the carriage runs. Small droplets of water would be pushed along on the upper foil surface by the rush of air. A sketch is shown in Figure 31. From this it is clear that there is a beneficial effect on the air distribution from setting the strut ahead of the trailing edge of the foil. If the strut base is even with the foil trailing edge, such as with the parent foil, there could be an air distribution problem, since the foil might be wetted there by the strut downwash effect on the foil cavity roof and the air could not flow out to the foil cavity.

Although the simple pressure difference from atmospheric, as measured at the strut base, increased quite linearly with increasing water speed, the behavior of the pressure in coefficient form appears more complicated. Curves of the measured cavitation number at the strut base and in the wing cavities are shown in Figures 21 and 22, where the data are taken from runs with no spray deflecting strips. The asymptotic behavior of σ_c to zero at high speed without regard to ventilation is clearly shown. Yet for the 18-percent parabolic strut especially, it appears that strut thickness alone, without spray wedges, can achieve ventilation for speeds in the 40-knot range. When the spray wedges were mounted on the 18-percent strut in the full down position, the result was full ventilation over the entire speed range as is shown in Figure 23.

The equivalent data for the cavitation numbers measured at the strut base, with and without spray wedges, are shown in Figures 24 and 25, as a function of vapor cavitation number. In the present case of towing basin testing at full water speed, the vapor cavitation

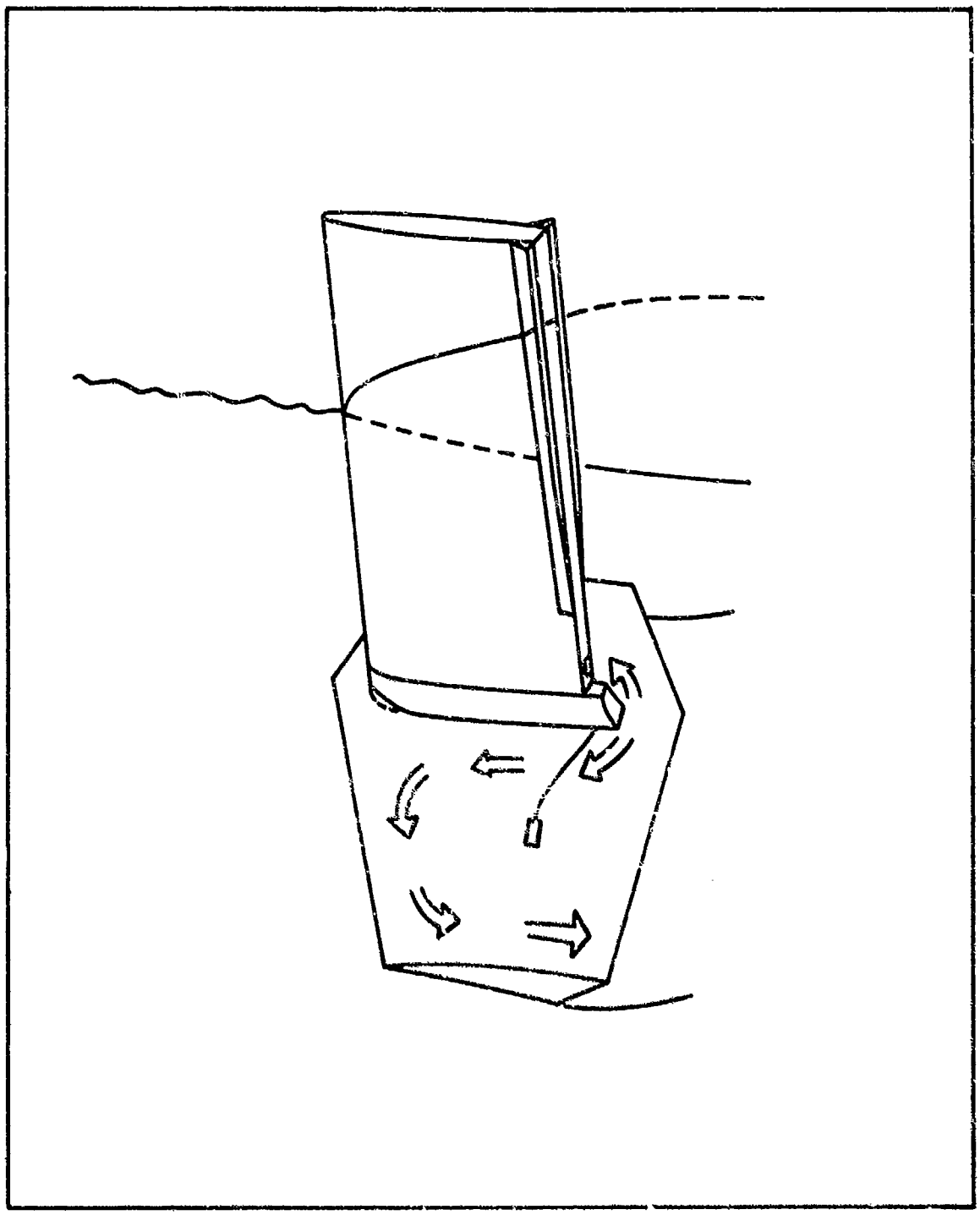

Figure 31 - Sketch of Air Flow Pattern

number σ_v is a function only of speed, water density (fresh water), water vapor pressure, and atmospheric pressure, which was taken daily from records maintained at Langley Air Force Base. Again, the asymptotic behavior of $\sigma_c \rightarrow \sigma_v$ is evident at large speeds and low values of σ_v. The amount of ventilation in qualitative terms may be given by the difference of σ_c and σ_v.

One purpose of using a variable spray wedge location was to minimize spray wedge drag yet provide the required ventilation. At the best location which could be found, there was full ventilation (as defined by $\sigma_c \leq 0.01$) over a wide range of speeds and angles of incidence. The measured lift-to-drag ratio of the entire strut and foil system, which includes strut drag, wave drag, friction drag, and spray drag, is shown in Figure 26. Because these drag components scale with different parameters (Froude, Reynolds, and cavitation number) and because the scaling of ventilation air supply rates is still a matter of some conjecture, it would not be necessarily meaningful to apply them to large-scale prototype craft whose structural requirements may be different from those of the TAP-1 foil, which as a solid foil at design lift has stresses in the 15 ksi range.

The depth of submergence was measured above the leading edge of the 40-percent spanwise foil section in relation to its chord at static water conditions. Its effect on measured lift coefficient is shown in Figure 27 for the best position of the spray wedges. Besides the theoretical effect of C_L increasing at small submergences and constant cavitation number, the measured cavitation number varies somewhat along this graph because of the varying submergence of the spray deflection wedges. The limited amount of data on lift-to-drag ratio at a depth-to-chord ratio of 0.5 are shown in Figure 28, where most of the improvement shown is due to the reduction of the strut drag at the decreased submergence.

Sudden Strut Side Ventilation

A typical plot of the base-vented strut/foil side force as a function of sideslip angle for all other conditions fixed is shown in Figure 32. The figure illustrates the phenomenon known as sudden strut side ventilation. As the sideslip angle β is increased up to some value β_{vent}, the side force increases linearly. For $\beta = \beta_{vent}$ the entire low pressure side of the strut fills with air at or near atmospheric pressure, causing the side force to reduce suddenly. The side ventilation cannot be "washed off" simply by reducing the sideslip angle to a value less than β_{vent}. The ventilated cavity can be removed only by decreasing β to some lower value known as the closure angle, $\beta_{closure}$. Side ventilation is generally an undesirable phenomenon on high-speed craft, not only because it causes a reduction in the side force, but also because it introduces nonlinearities and double-valued functions into the control system.

The present experiments determined the sudden strut side ventilation angle β_{vent} but did not determine the closure angle because the strut sideslip angle β could not be varied while the carriage was moving.

Succeeding frames of motion pictures taken on board the carriage showing the inception of side ventilation are shown in Figure 33. The frames are 0.002 seconds apart in time. Notice the almost instantaneous replacement of the leading edge cavity with a relatively large ventilated cavity at inception.

Data Analysis

The strut side force data were averaged for each value of β where more than one data point existed, and a least-squares fit

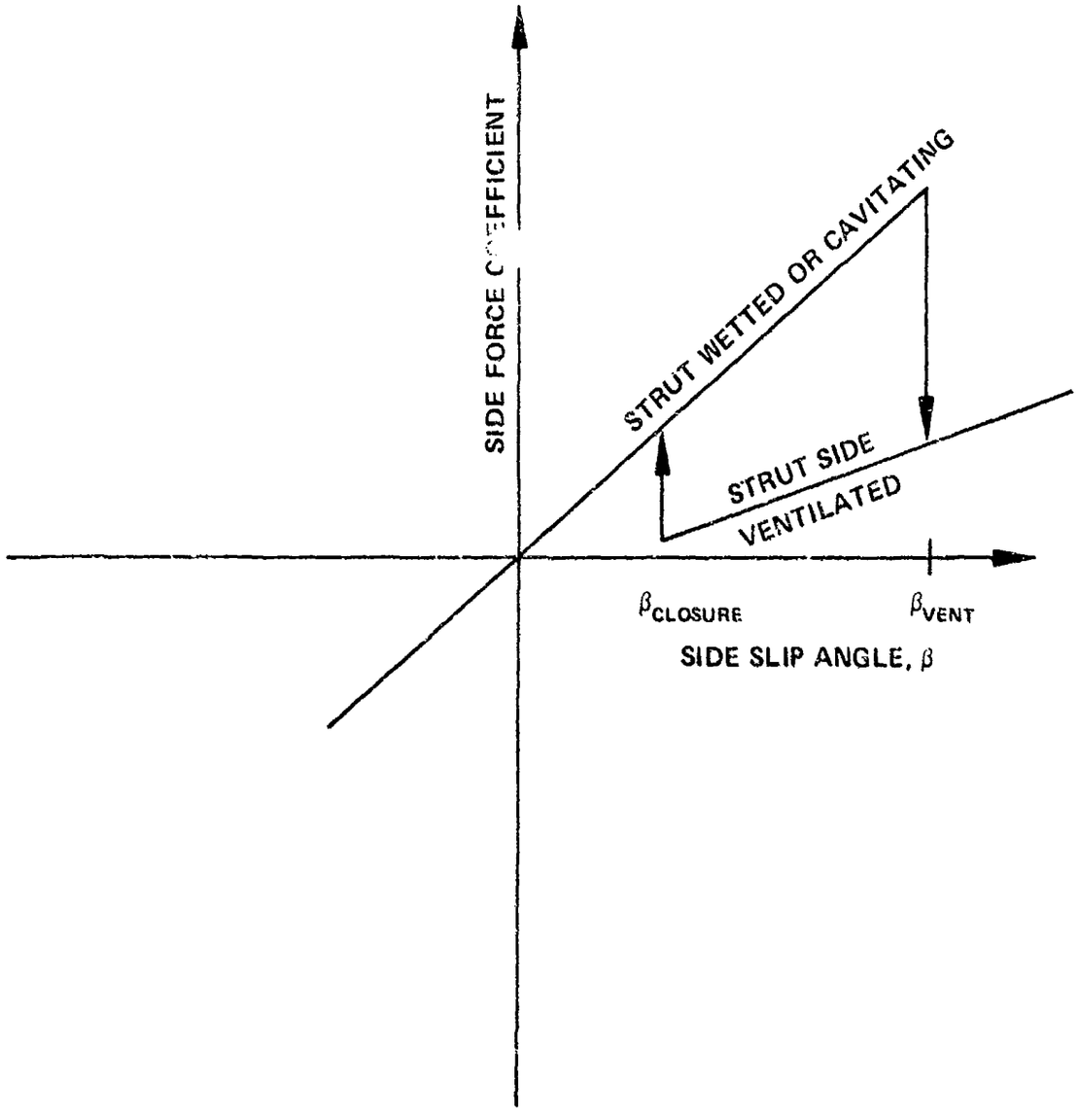

Figure 32 - Schematic Illustrating Side Force Ventilation Hysteresis for a Base-Vented Strut

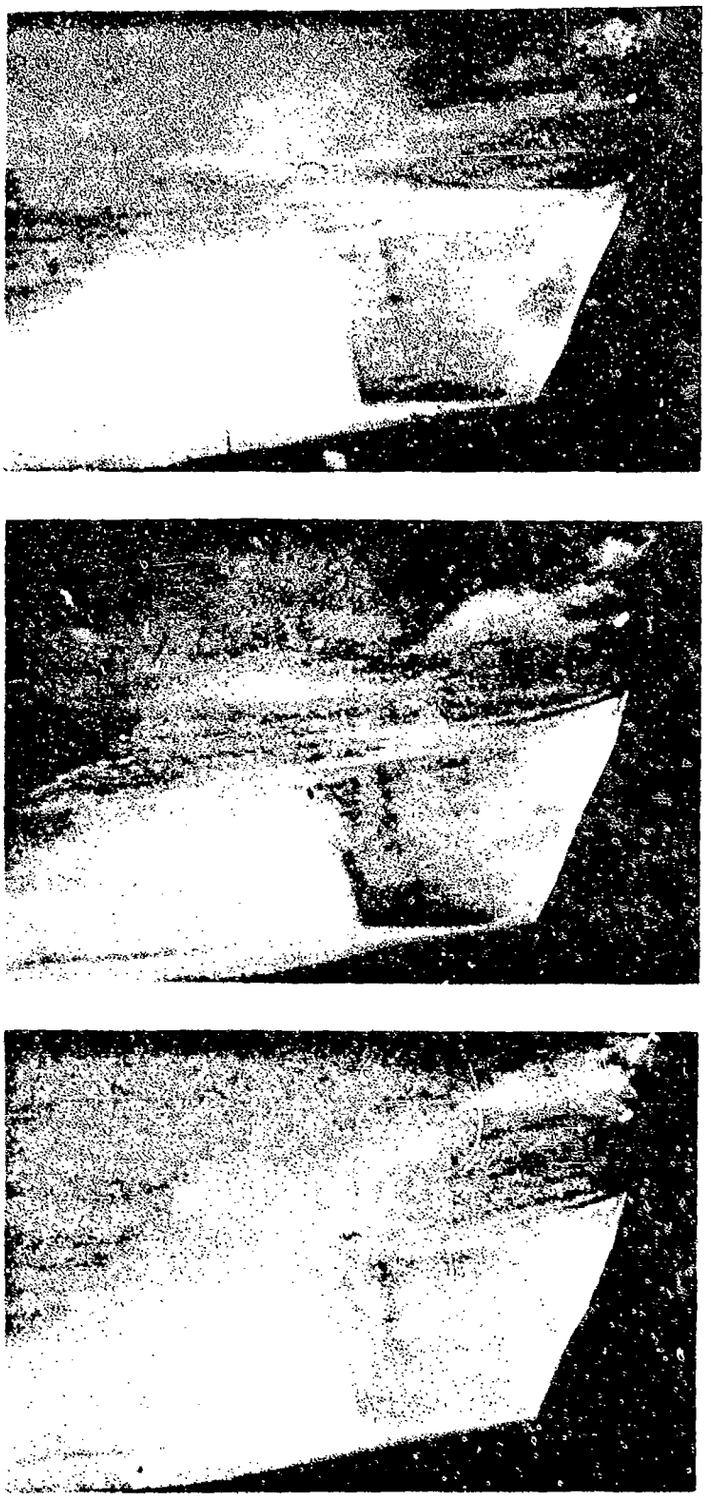

Figure 33 - Sequential Photographs Showing Occurrence of Side Ventilation

was made through the data as shown by solid lines in each figure. For some speeds the data were obtained after deceleration from higher speeds. For these cases the actual ventilation inception angles are not known, although the pre- and post-ventilation inception forces are valid.

STRUT SIDE FORCE

Side force coefficients are presented as functions of the sideslip angle in Figures 34 through 38. Figure 39 compares the strut with wedges to the strut without wedges. Crossplots of the data are presented in Figures 40 through 45. In these figures the value of the cavitation number, σ, may be approximated by $(2100/V^2)$ where V is in fps. Figure 40 demonstrates the effects of σ on the ventilation inception angle β_{vent}, while Figure 41 demonstrates the effects of d/c, the depth-to-foil chord ratio, on the ventilation inception angle. Figure 42 illustrates the effects of d/c and foil hydrodynamic flow (wetted or ventilated) on the side force coefficient slope prior to side ventilation. Figures 43 and 44 show the loading on the strut in the neighborhood of ventilation. Figure 45 shows the required sideslip angle as a function of the loading for the unventilated strut.

There are two important questions to be answered concerning strut side forces and sudden side ventilation. First, what are the critical parameters affecting the ventilation incention angle and the side force coefficient slope? And second, what is the optimum strut for an 80-knot hydrofoil craft?

During the experiments it was established that the side force coefficient slope and strut sudden side ventilation angle for parabolic struts depend on:

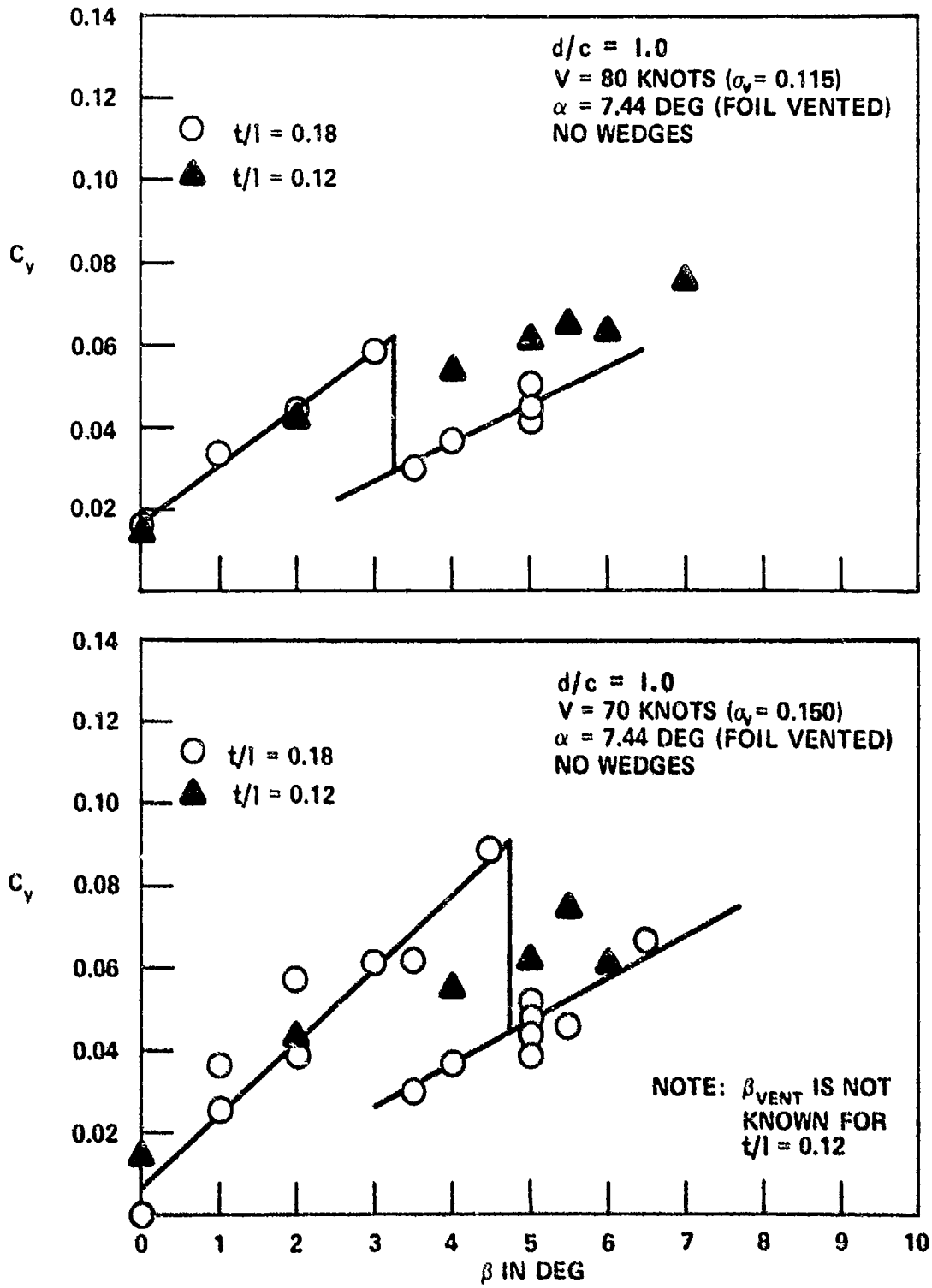

Figure 34 - Side Force Coefficient C_y for the 12- and 18- Percent Thick Struts as a Function of Sideslip Angle β for Speeds V of 80, 70, 50 and 40 Knots and a Depth-to-Foil Chord Ratio d/c of 1 for the Ventilated Foil

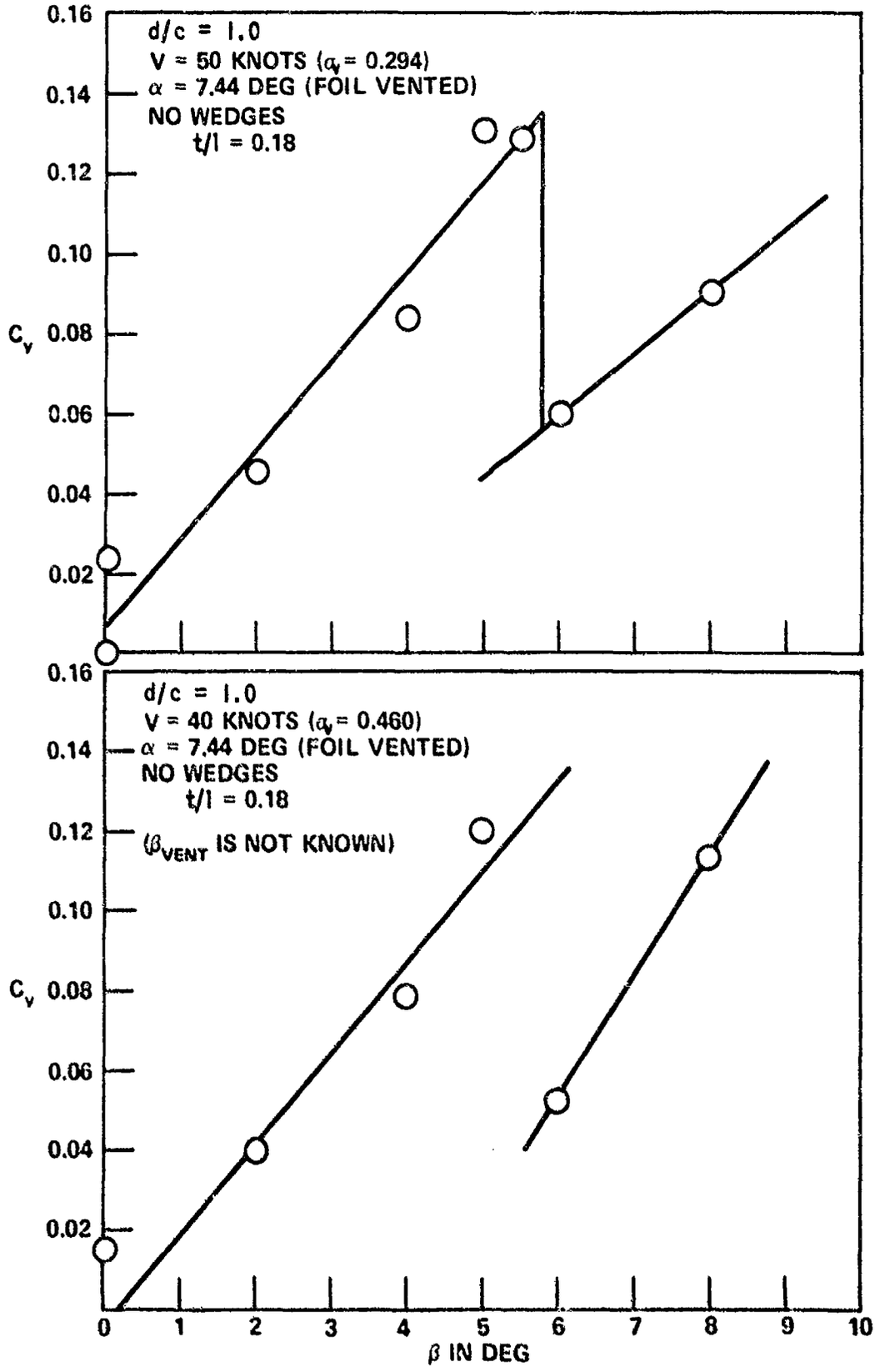

Figure 34 (continued)

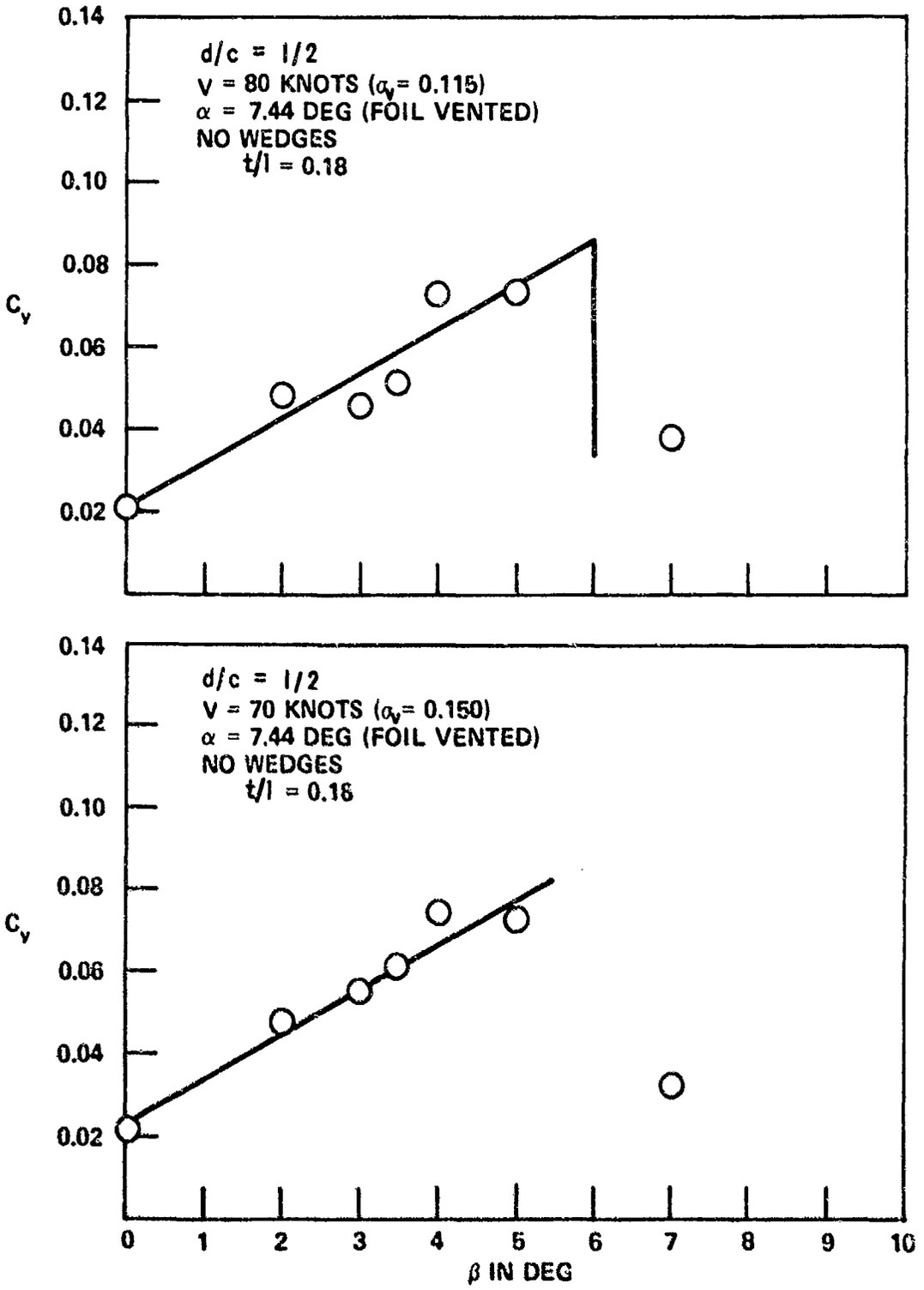

Figure 35 - Side Force Coefficient C_y as a Function of Sideslip Angle β for Speeds V of 80 and 70 Knots for a Depth-to-Foil Chord Ratio d/c of 1/2 for the Ventilated Foil

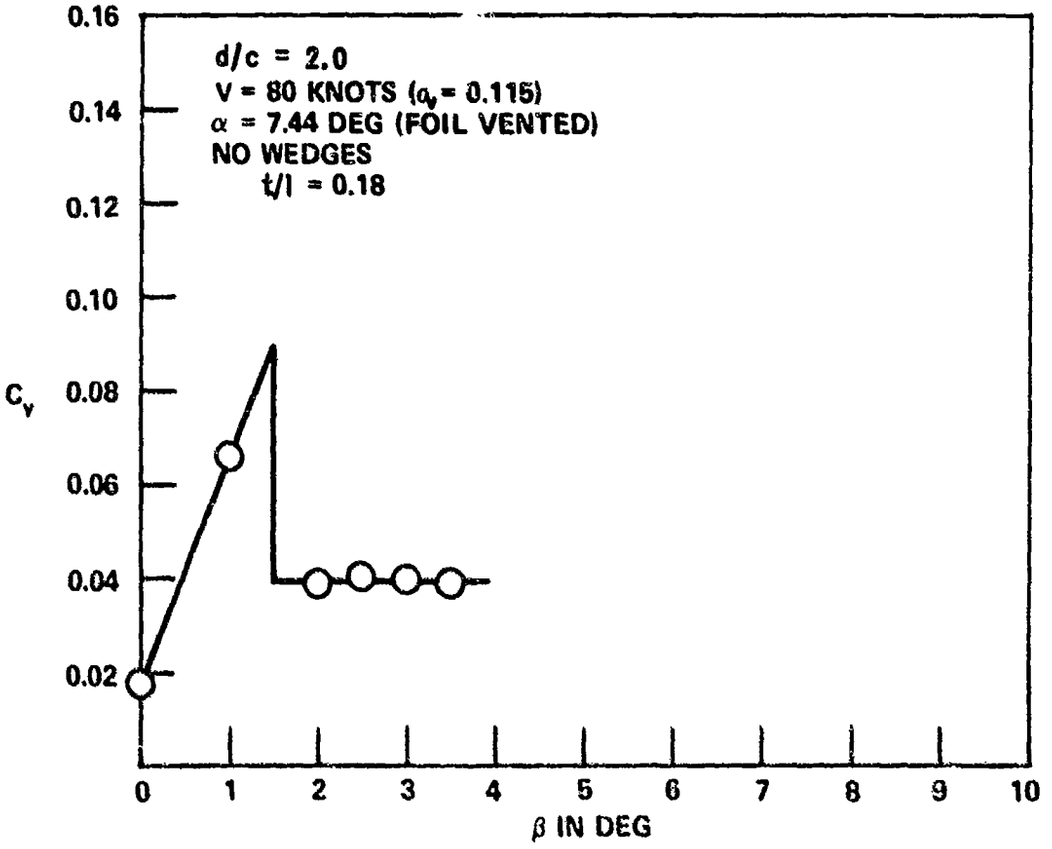

Figure 36 - Side Force Coefficient C_y as a Function of Sideslip Angle β for a Speed of 80 Knots for a Depth-to-Foil Chord Ratio d/c of 2 for the Ventilated Foil

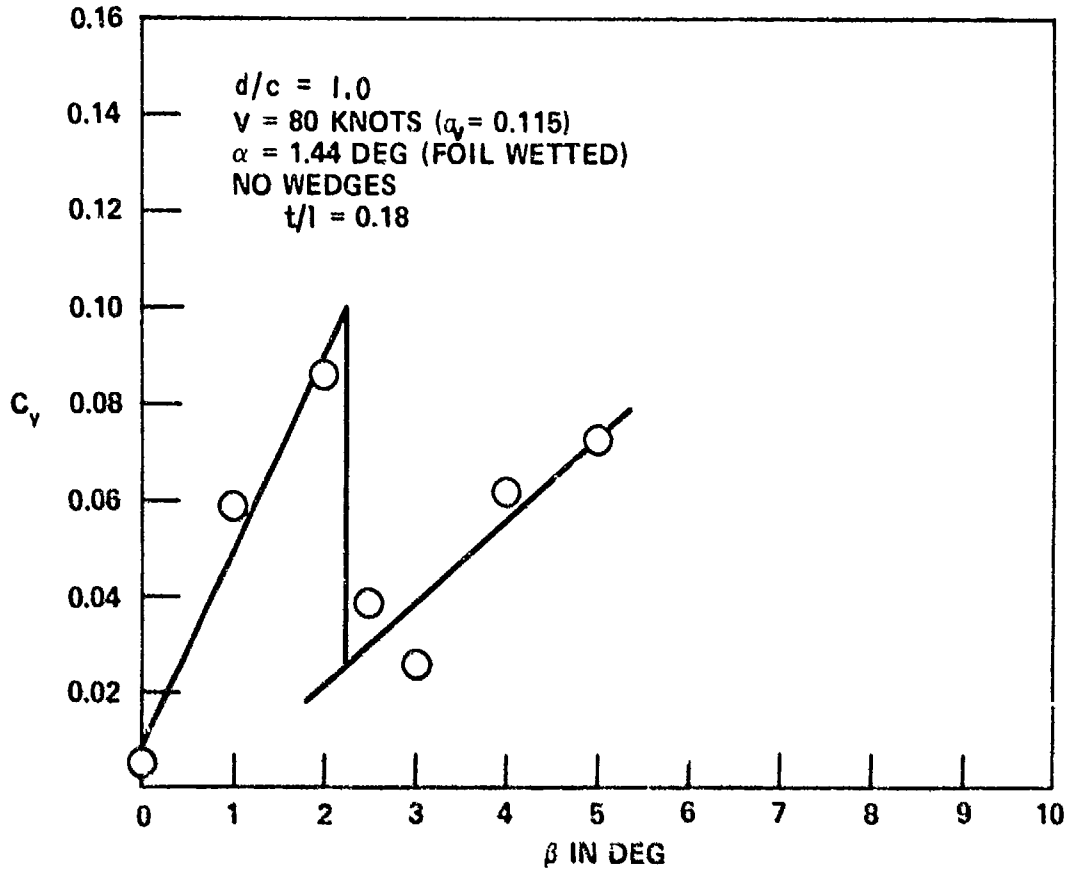

Figure 37 - Side Force Coefficient C_y as a Function of Sideslip Angle β for a Speed V of 80 Knots for a Depth-to-Foil Chord Ratio d/c of 1 for the Wetted Foil

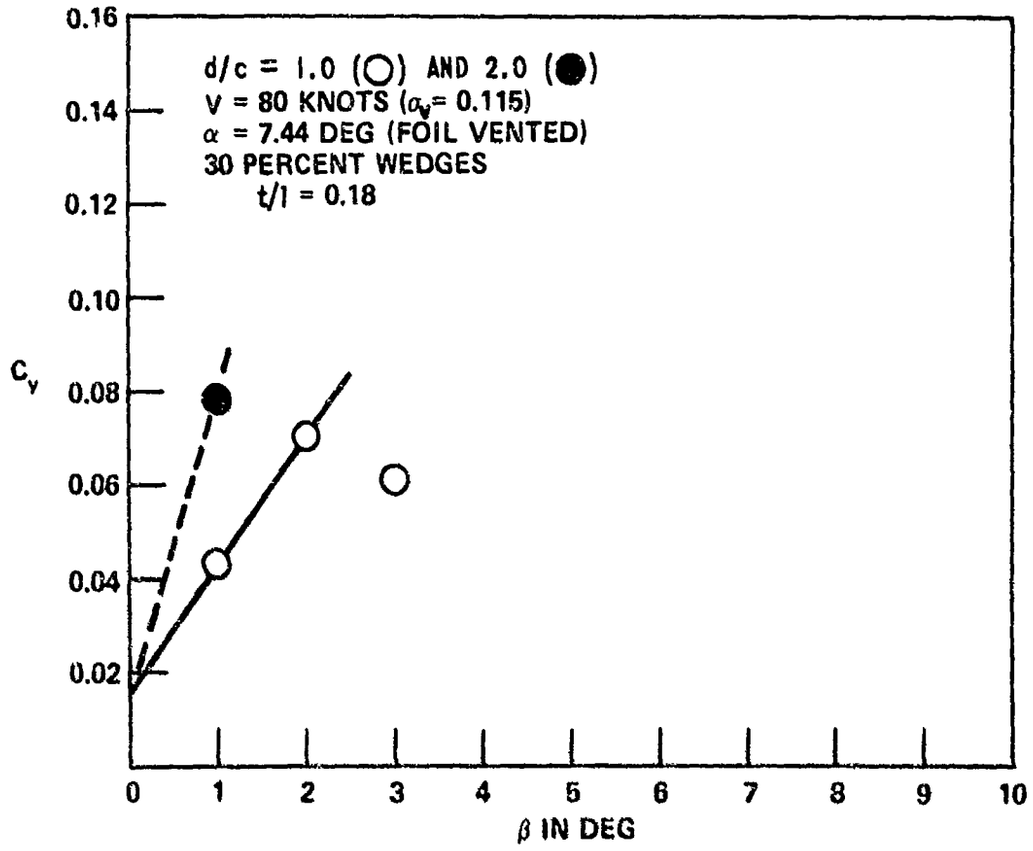

Figure 38 - Side Force Coefficient C_y as a Function of Sideslip Angle β for a Speed V of 80 Knots for a Depth-to-Foil Chord Ratio d/c of 1 and 2 for the 18-Percent Thick Strut with Wedges and a Ventilated Foil

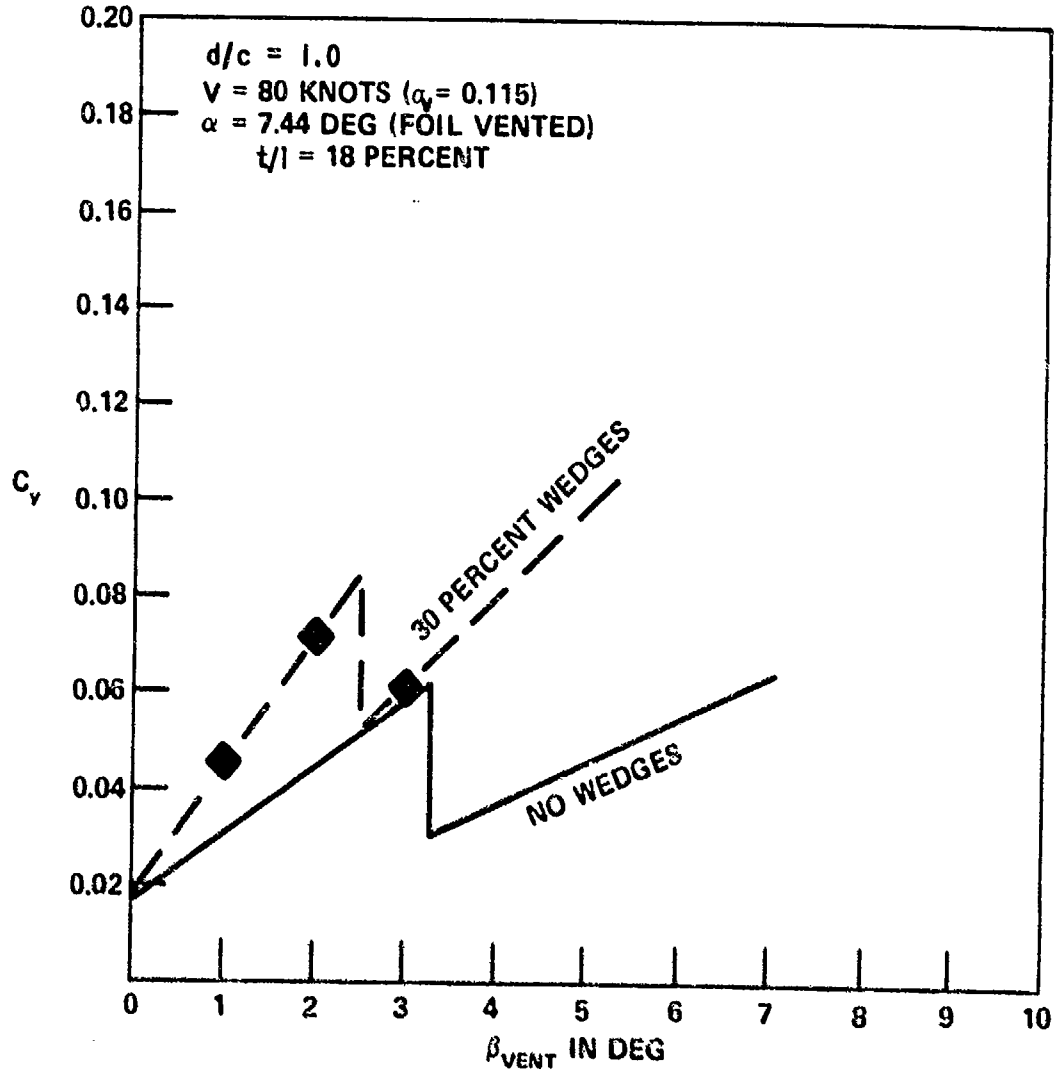

Figure 39 - The Effect of 30-Percent Trailing Edge Wedges on the Ventilation Inception Angle β_{VENT} for the 18-Percent Thick Strut

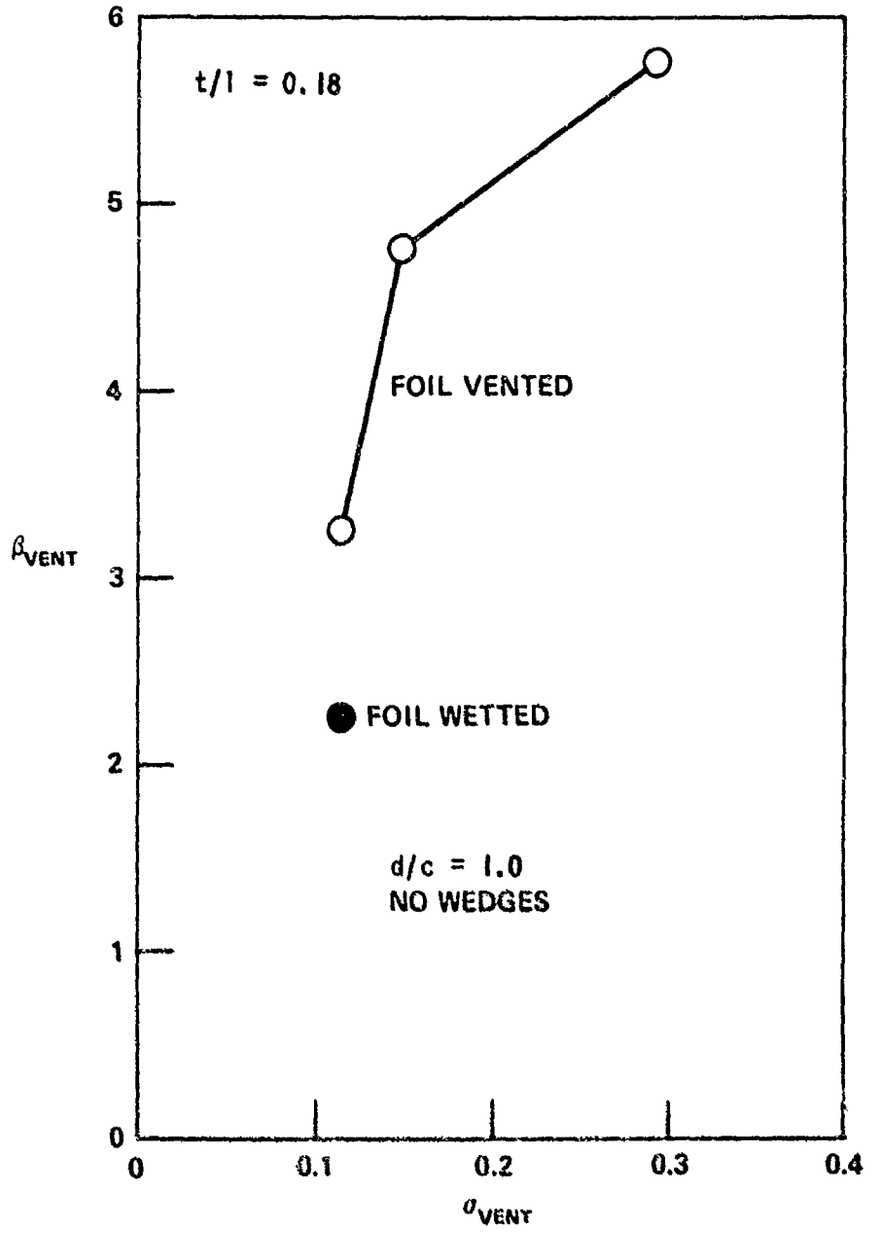

Figure 40 - Ventilation Inception Angle β_{VENT} as a Function of Cavitation Number σ for the Ventilated and Wetted Foil Chord Ratio d/c of 1 for the 18-Percent Thick Strut without Wedges

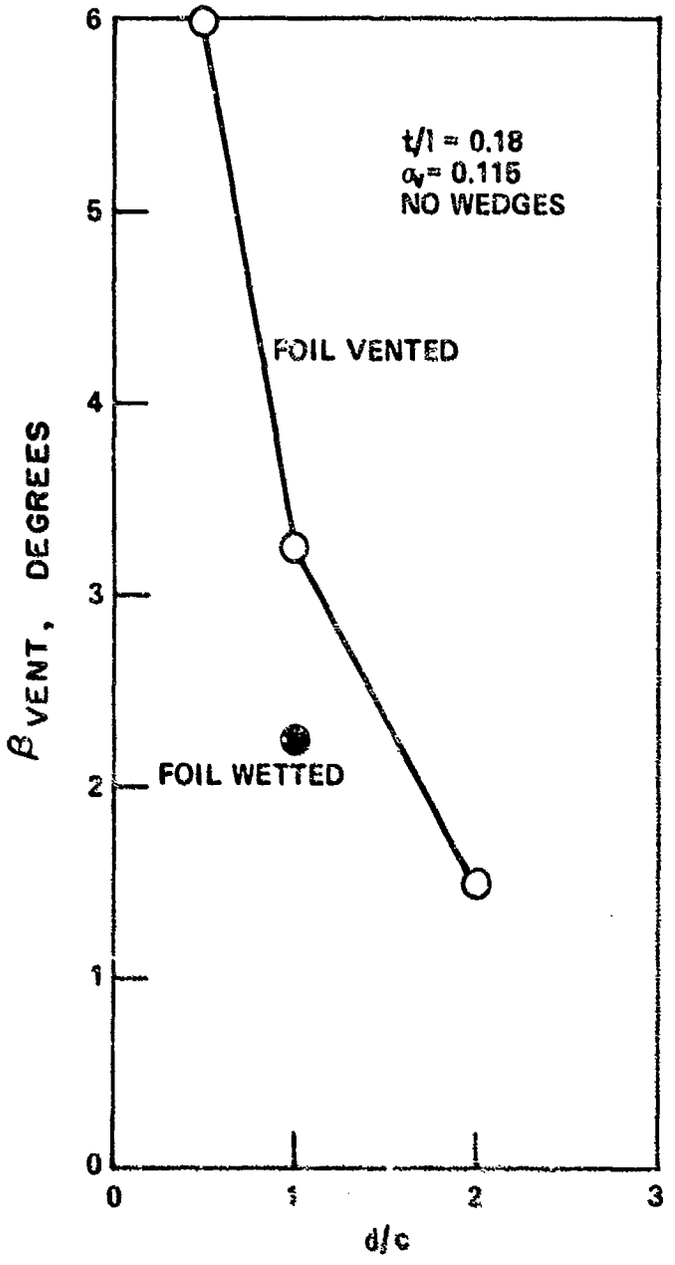

Figure 41 - Ventilation Inception Angle β_{VENT} as a Function of Depth-to-Foil Chord Ratio d/c for the Ventilated and Wetted Conditions for a Cavitation Number of 0.115 for the 18-Percent Thick Strut without Wedges

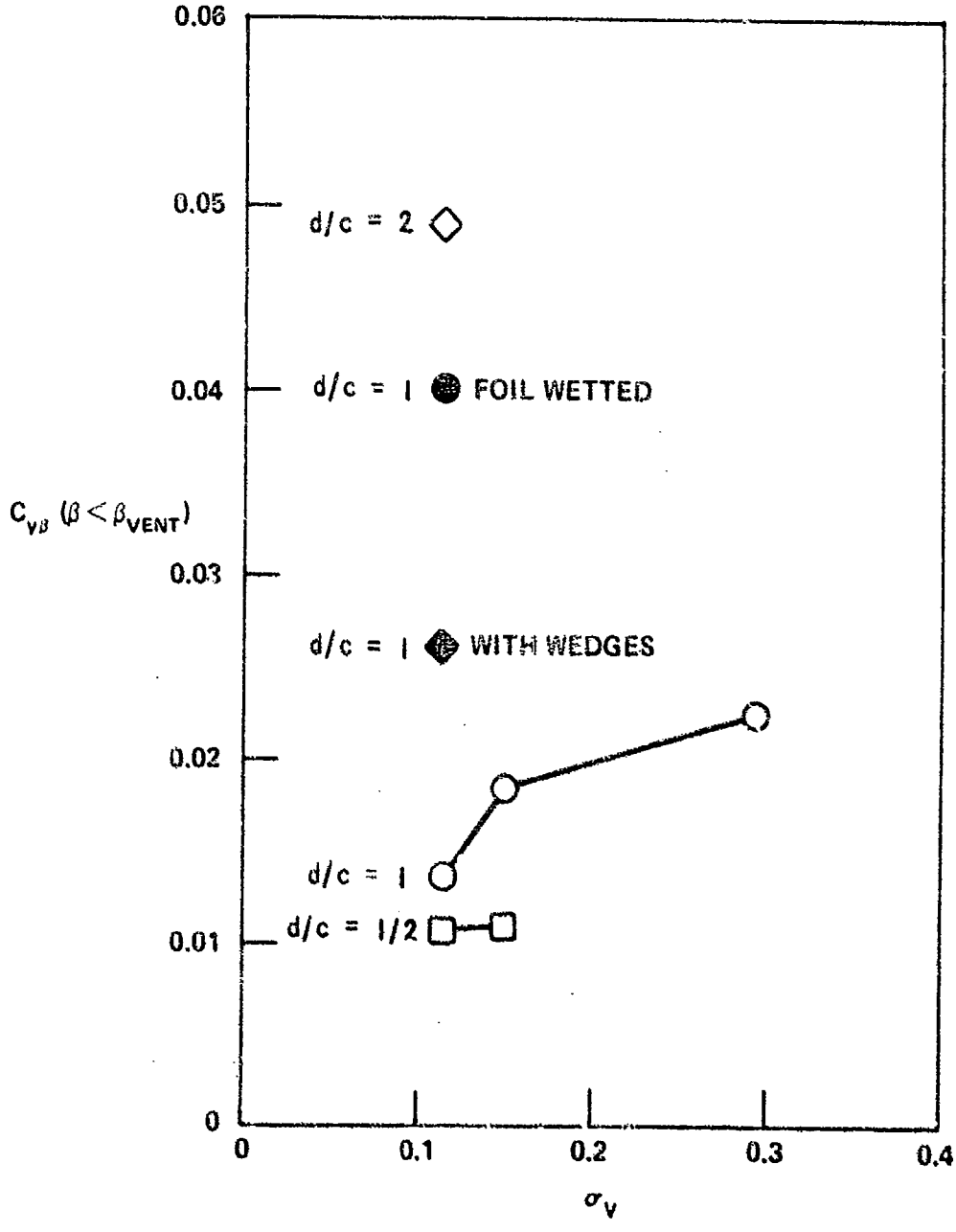

Figure 42 - Side Force Coefficient Slope $C_{y\beta}$ for the Unventilated Strut with and without Wedges as a Function of Cavitation Number σ_v

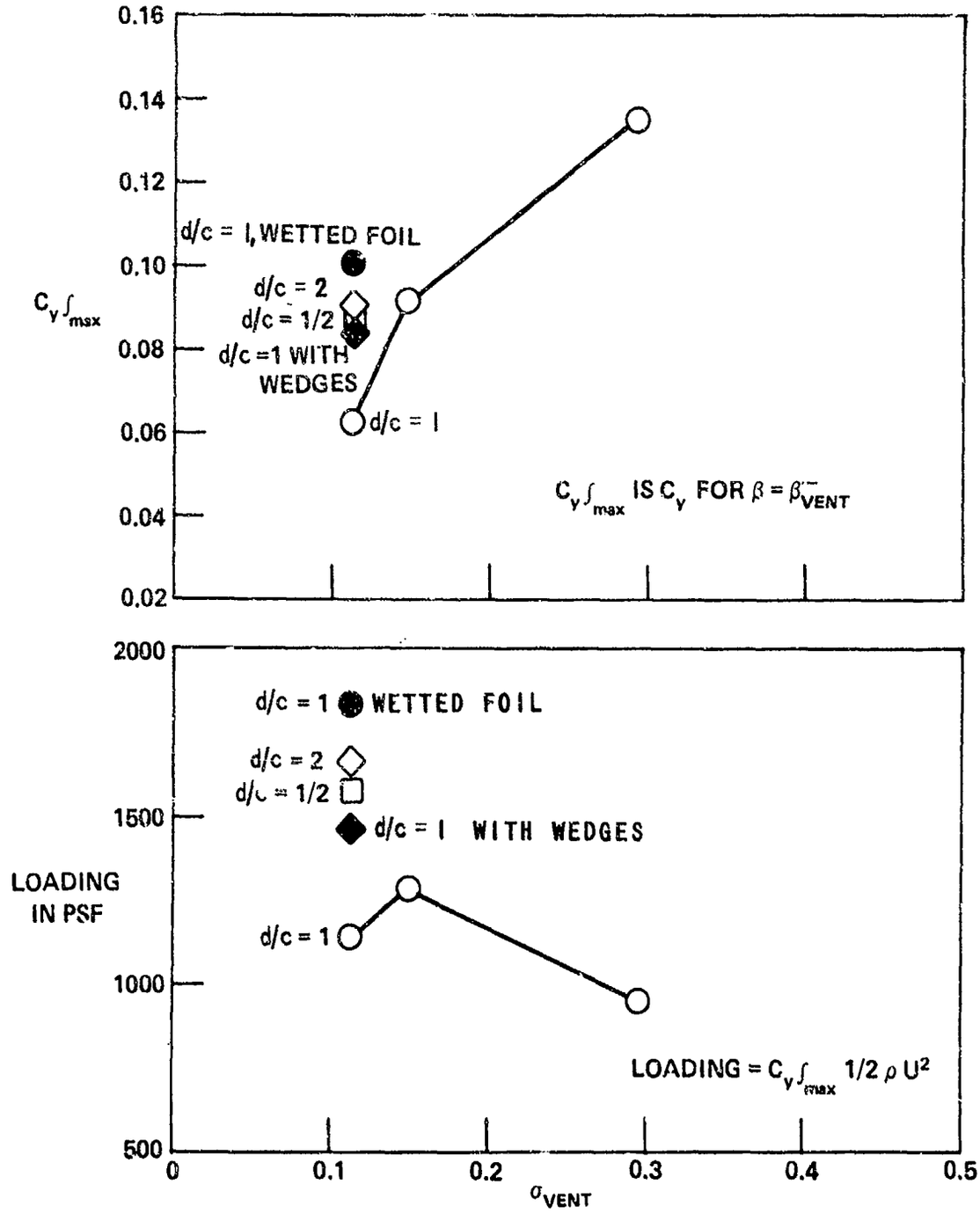

Figure 43 - Maximum Side Force $C_y \int_{max}$ and Side Force Loading at Ventilation Inception as a Function of Cavitation Number σ with and without Wedges on the Strut

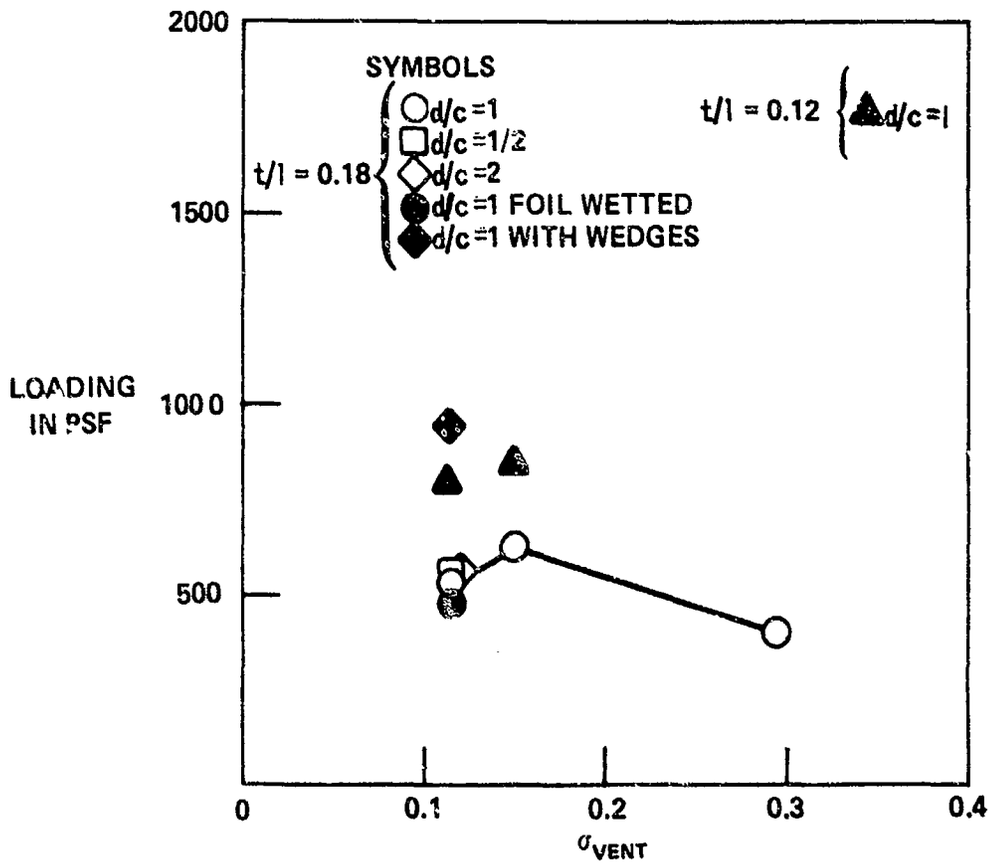

Figure 44 - Immediate Post Ventilation Side Force Loading as a Function of Cavitation Number at Ventilation Inception σ_{VENT} for the Strut with and without Wedges

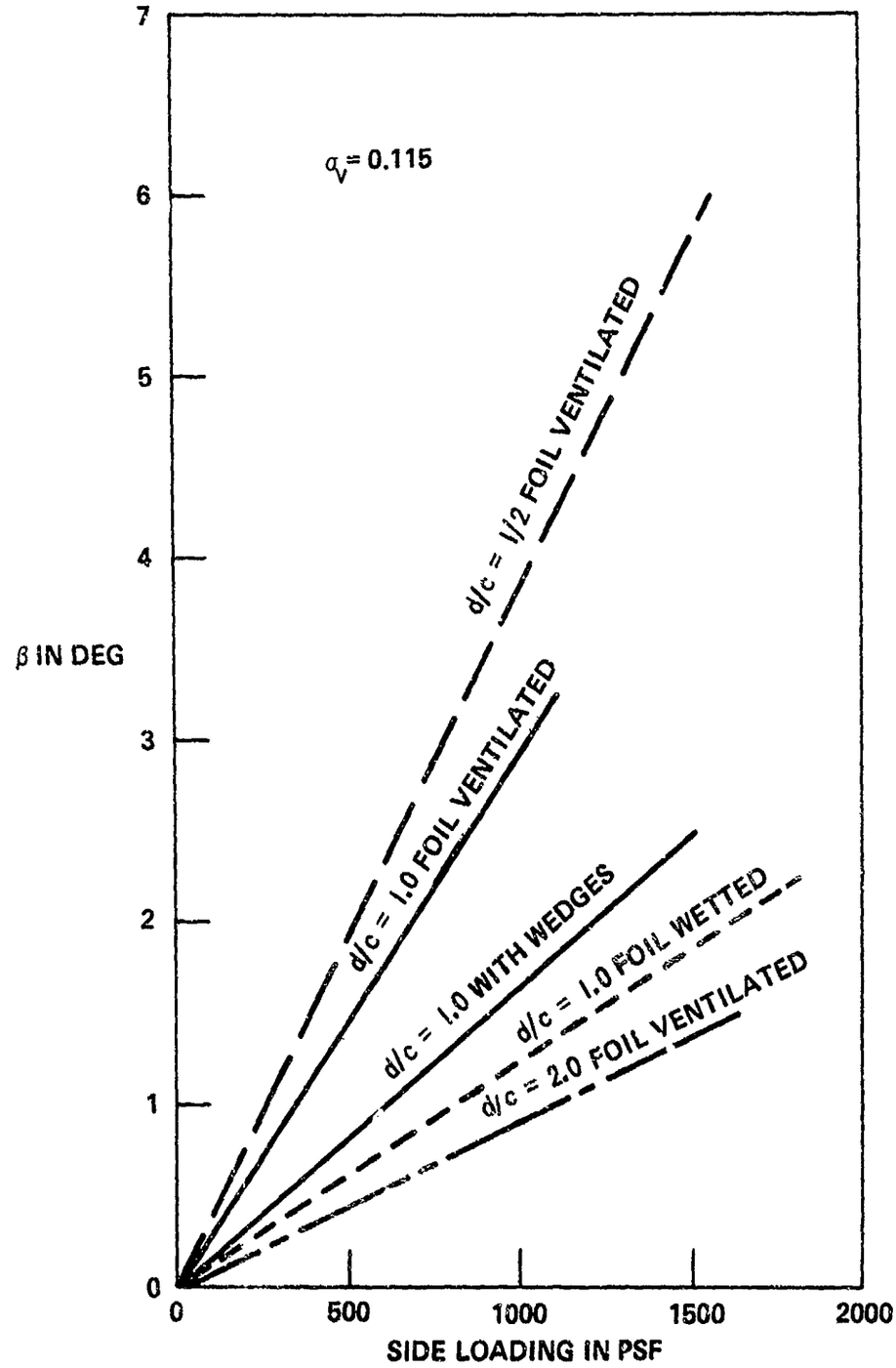

Figure 45 - Sideslip Angle β as a Function of Side Force Loading for Several Conditions

1. the cavitation number (or speed),
2. the foil hydrodynamics (ventilated or wetted),
3. the strut depth of submergence, and
4. the presence of trailing edge wedges.

The remaining parameter, the thickness-to-chord ratio, was shown to have no significant effect between values of 0.12 and 0.18, although it may affect other values outside of this range. Increasing the ratio decreases the tendency for cavitation along the side of the strut for non-zero sideslip angles, but increases the tendency for leading edge cavitation because it increases the nose radius. In the present study, the two effects may have cancelled each other out. Additional study of the photographic data would perhaps clarify the effects of thickness ratio.

The ventilation inception angle and the pre-ventilation side force coefficient slope both increased with increasing cavitation number (decreasing speed). However, the ventilation inception angle was decreased by fully wetting the foil (removing the ventilation cavity), by adding wedges, or by increasing the strut submergence. In each of these cases, the side force coefficient slope was increased in addition to the fact that the action was destabilizing with respect to side ventilation (see Figures 39 through 42). In other words, those characteristics favorable for providing side force for blunt-based, high-speed struts are unfavorable for avoiding sudden strut side ventilation, with the exception of slowing the craft speed which increased the ventilation inception angle as well as the side force coefficient slope (see Figures 40 and 42). Therefore the designer, requiring a certain side force, must balance those strut characteristics that increase the side force slope with those characteristics that decrease the ventilation inception angle. If the designer wants the strut to

produce minimal side force in the absence of side ventilation, the foil should be ventilated, the strut depth-th-chord ratio should be as small as possible, and the strut trailing edge should be faired streamwise.

Assuming that maximum side force is desired without risking strut side ventilation, the second question posed above will now be discussed. An optimum strut attains the required side force at a low value for the sideslip angle without incurring a high probability for the occurrence of sudden strut side ventilation. The work "probability" refers to the statistical nature of a seaway and its influence on the effective strut sideslip angle. For present purposes the effects of the seaway will be ignored.

The study of optimum strut characteristics can concentrate on the loading in the vicinity of strut side ventilation inception. Figure 44 shows the maximum side force loading occurring before side ventilation as a function of the cavitation number. Note that the loading has a peak at $\sigma = 0.15$ (70 knots). Also note from the figure that increasing d/c or wetting the foil (both destabilizing with respect to side ventilation) do, in fact, increase the available side loading. It has already been shown that those changes increase the side force coefficient slope.

Figure 44 shows the side loading on the strut immediately following side ventilation inception. This loading is of interest to the designer studying the effects of side ventilation on craft performance. The figure shows that the effect of d/c or of the foil hydrodynamics is insignificant. However, the loading can be increased by decreasing the thickness or by adding wedges. The percentage reduction in side loading at ventilation inception increases as the thickness increases and as the foil is changed from ventilated to wetted flow. The effect of adding wedges is to

decrease the percentage reduction in the side force. Therefore, the percentage reduction is decreased with thin struts with wedges and a ventilated foil.

Methods of increasing side force at the risk of incurring strut side ventilation are evident in Figure 45, which shows the yaw angle β as a function of the required loading for $\sigma = 0.115$ (80 knots). Each line in the figure represents a different condition and terminates at strut side ventilation.

Given the angle β, which must include the effects of a seaway, a designer can immediately determine from Figure 45 whether or not the strut is ventilated. If the strut is not ventilated, the side loading on the strut can be determined from Figure 45. For example, given $d/c = 2$ and $\beta = 2$, there is strut side ventilation if the foil is ventilated, while for $\beta = 1$ the strut is not ventilated. Note that $d/c = 2$ will occur for a craft making its way through waves despite a design $d/c = 1$. Conversely, the side loading for a strut with a ventilated foil attached is limited to 800 psf for $d/c \leq 1$.

Also note from Figure 45 that the presence of wedges provides 50 percent more loading than without wedges while decreasing the ventilation inception angle only 25 percent. Therefore, the strut with the wedges is superior to the strut without the wedges as far as side force is concerned. There are other factors involved in the design, however, such as a 10-percent drag penalty and the requirement for the wedges to provide an air path for ventilation of the foils, as well as the need for the strut to survive induced sideslip angles in a seaway.

Apparently an optimum strut would be as thin as feasible and would be equipped with trailing edge wedges. Such a strut would have large side force for a relatively low sideslip angle. However,

if the seaway introduces effective strut sideslip angles in excess of the ventilation inception angle, it will be necessary to remove the wedges to increase the ventilation inception angle at the expense of the available side force.

CONCLUSIONS

The important conclusions from the experiments of interest to the designer of an 80-knot craft with superventilated foils are:

1. A parabolic strut will side ventilate for a sideslip angle of 3 1/4 degrees, suffering at least a 50-percent loss in side force.

2. The ventilation inception sideslip angle decreases to 1 1/2 degrees and the side force slope increases dramatically with increasing foil submergence depth. The side force at ventilation inception increases with increasing depth.

3. The side force will increase substantially as the foil becomes fully wetted or chokes and becomes supercavitating.

4. The washing off of the foil ventilation is destabilizing with respect to strut side ventilation, reducing the ventilation inception angle perhaps by a degree.

5. The addition of trailing edge wedges decreases the ventilation angle but greatly increases the side force. The overall effect is to increase the maximum side force prior to side ventilation.

6. Decreasing the strut thickness does not affect the ventilation inception angle, although it substantially decreases the side force loss at ventilation.

7. The designers of a high-speed craft must consider the effective sideslip angles on a strut in a seaway in relation to the ventilation inception angle as well as the maximum available side force for a given strut.

8. The overall performance of the TAP-1 system, even without the spray deflecting wedges, was comparable to that of the parent hydrofoil. The maximum lift-to-drag ratio recorded in full cavity flow was 6.6, as compared to 6.9 for the parent foil. No structural vibrations were observed even at the maximum speed of 92 knots, and the cavity appeared to cover the top of the wing completely, including the wing tips, unlike the case with the parent foil.

9. The foil ventilation behavior was smooth and gradual over a wide speed range, which was probably the result of setting the strut base forward of the foil trailing edge, which visually appeared to improve the air distribution in the cavity.

10. The cavity air demand of the strut and foil assembly varied linearly with speed (or Froude number) if it is assumed that the airflow rate is proportional to the pressure difference along the strut. Sudden choking at zero yaw at high speeds was not observed, nor were vortex shedding or leading edge vibration.

11. The spanwise twist built into the model was successful in maintaining a full cavity above the foil out to the wing tips at low angles of attack, but the sectional lift coefficients were not obtained by twisting the foil.

12. The strut spray strips were required to maintain full ventilation of the foil (arbitrarily defined here as $\sigma_c \leq 0.01$). However, in their best position on the model they added about 10 percent to the drag.

13. The 33 percent wetted chordlength of the annex allowed a range of angle of attack of 3 1/2 degrees between the minimum angle of attack for full cavity flow and the maximum angle of attack at which the annex would not interfere with the lower cavity wall.

14. The TAP-1 foil is possibly conservative in its design. The annex could have been made larger, and the absence of the vibration observed on the parent foil indicates that the main body could have been made thinner.

RECOMMENDATIONS

The general hydrodynamic forces produced by supercavitating hydrofoils are much more sensitive to the structural criteria of foil design than those designed for subcavitating operation. The thinness of the body of the foil allows a lower angle of attack to be achieved and consequently a larger lift-to-drag ratio. And while the shape of the leading edge itself may not be critical, the thinness of the leading edge region (first 20 percent of chord) is very critical for reducing foil section drag. In this respect, the design of supercavitating hydrofoils is a very strongly related hydrodynamic and structural problem.

The use of full water speed experimentation is necessary when ventilation is being investigated because cavity air demand seems to depend heavily on the rate of air withdrawal in the bubbly froth at the end of the cavity. A future set of experiments on the TAP-1 foil are planned in which vapor cavitation number may be preset while Froude number is varied. This should clarify some of the scaling procedures involved in prototype design, for it is

by no means certain that those are the only important parameters. Certainly the high water speed data presented here represent the most difficult conditions for achieving natural ventilation of the foil.

In addition to the above, future experiments would be valuable to:

a) measure the cavity location. This is very desirable in order to correlate theoretically predicted lift-to-drag ratios with experimental evidence.

b) measure the flutter speed. This is the ultimate structural limit, and marks the transition from static design to dynamic design.

ACKNOWLEDGMENTS

The authors appreciate the help and encouragement of Mr. Douglas Gregory, and also thank Miss Pat Rooney for the preparation of the manuscript.

REFERENCES

1. Wu, T. Y., "A Free Streamline Theory for Two-Dimensional Fully Cavitating Hydrofoils," Journal Mat. Phys. Vol. 35, No. 3, 1956, pp. 236-265

2. Dobay, G. F. and E. S. Baker, "Special Problems in the Design of Supercavitating Hydrofoils," AIAA Paper No. 74-309 presented at the AIAA/SNAME Advanced Marine Vehicles Conference, Feb 1974

3. Schiebe, F. R. and J. M. Wetzel, "Ventilated Cavities on Submerged Three-Dimensional Hydrofoils," University of Minnesota, St. Anthony Falls Hydraulic Laboratory, Technical Paper No. 36, Series B, Dec 1961

4. Christopher, K. W. and V. E. Johnson, Jr., "Experimental Investigation of Two Low-Drag Supercavitating Hydrofoils at Speeds up to 200 Feet per Second," NASA TN D-436, Aug 1960

5. Johnson, V. E., Jr. and T. A. Rasnick, "Investigation of a High-Speed Hydrofoil with Parabolic Thickness Distribution," NASA TN D-119, Nov 1959

6. Spangler, P. K., "Performance and Correlation Studies of the BuShips Parent Hydrofoil at Speeds from 40 to 75 Knots," NSRDC Report 2353, Dec 1966

7. Wadlin, K. L., "Ventilated Flows with Hydrofoils," Presented at the 12th General Meeting of the American Towing Tank Conference, University of California, Aug 1959

8. Gornstein, R. J. and T. A. Holgate, "Depth Effects on Hydrodynamic Characteristics of the Annex Foil at 80 Knots," Boeing Company Report Number D2-82505-1, Feb 1965

9. McGehee, J. R. and V. E. Johnson, Jr., "Hydrodynamic Characteristics of Two Low-Drag Supercavitating Hydrofoils," NASA Memo 5-9-59L, Jun 1959

10. Dobay, G. F., "Performance Characteristics of the BuShips Parent Foil," NSRDC Report 2084, Aug 1965

11. Dobay, G. F. and N. L. Ficken, "Supercavitating and Ventilated Performance of Three Hydrofoil Sections," NSRDC Report 1828, Jan 1964

INITIAL DISTRIBUTION

Copies	
2	Chief Naval Material Command (MAT 033)
1	Naval Sea Systems Command (SEA 03412)
1	Naval Sea Systems Command (PMS-303)
1	Naval Ship Engineering Center (6110)
1	Naval Ship Engineering Center (6136)
12	DDC
1	California Institute of Technology (A.J. Acosta)
1	University of Michigan (T.F. Ogilvie)
3	Boeing Aerospace Company (C.T. Ray)
1	Grumman Aircraft (H.R. Wright)

CENTER DISTRIBUTION

Copies	Code
1	115
1	15
1	152
1	1524, Shen
25	1532, Baker
1	1542
2	1556
2	1572
1	1576
30	5214.1
1	5221
1	5222